LITHUANIAN ENERGY INSTITUTE

NOURA RAGAB ABDELATY ELSALAMOUNY

NUMERICAL INVESTIGATION OF SEVERE ACCIDENT PHENOMENA BASED ON EXPERIMENTAL INVESTIGATIONS APPLYING BEPU APPROACH

Doctoral Dissertation
Technological Sciences, Energetics and Power Engineering (T 006)

2025, Kaunas

The dissertation has been prepared at the Laboratory of Nuclear Safety Installations of Lithuanian Energy Institute in 2020–2024.

The doctoral right has been granted to Kaunas University of Technology together with the Lithuanian Energy Institute.

Scientific Supervisor:
Chief Researcher Dr. Tadas KALIATKA (Lithuania Energy Institute, Technological Sciences, Energetics and Power Engineering, T 006).

Edited by: English language editor Lina Abraitienė (UAB Bella Verba), Lithuanian language editor Irma Urbonavičienė (No. 670485).

The dissertation defence will be held on 24 October 2025, at 10 a.m. in a public meeting of the Dissertation Defence Board of Energetics and Power Engineering Science Field in the Conference room at the Lithuanian Energy Institute.

Address: Breslaujos 3-202, LT-44403 Kaunas, Lithuania.
Phone: +370 37 401801; e-mail studijos@lei.lt

The dissertation was sent out on 24 Septemebr 2025.
The dissertation is available on the website http://ktu.edu and at the libraries of Kaunas University of Technology (Gedimino 50, LT-44239 Kaunas, Lithuania) and Lithuanian Energy Institute (Breslaujos 3, LT-44403 Kaunas, Lithuania).

LIETUVOS ENERGETIKOS INSTITUTAS

NOURA RAGAB ABDELATY ELSALAMOUNY

SUNKIŲJŲ AVARIJŲ SKAITINIS TYRIMAS, REMIANTIS GERIAUSIO ĮVERČIO METODIKOS TAIKYMU EKSPERIMENTŲ MODELIAVIMUI

Daktaro disertacija
Technologijos mokslai, energetika ir termoinžinerija (T 006)

Kaunas, 2025

Disertacija rengta 2020–2024 metais Lietuvos energetikos instituto Branduolinių įrenginių saugos laboratorijoje.

Doktorantūros teisė Kauno technologijos universitetui suteikta kartu su Lietuvos energetikos institutu.

Mokslinis vadovas:
vyr. m. d. dr. Tadas Kaliatka (Lietuvos energetikos institutas, technologijos mokslai, energetika ir termoinžinerija, T 006).

Redagavo: anglų kalbos redaktorė Lina Abraitienė (UAB Bella Verba) , lietuvių kalbos redaktorė Irma Urbonavičienė (IDV veiklos pažyma Nr. 670485).

Energetikos ir termoinžinerijos mokslo krypties disertacijos gynimo taryba:
vyr. m. d. dr. Viktorija GRIGAITIENĖ (Lietuvos energetikos institutas, technologijos mokslai, energetika ir termoinžinerija, T 006) – **pirmininkė**;
doc. dr. Linas PAUKŠTAITIS (Kauno technologijos universitetas, technologijos mokslai, energetika ir termoinžinerija, T 006);
dr. Davide PIZZOCRI (Milano politechnikos universitetas, Italija, technologijos mokslai, energetika ir termoinžinerija, T 006);
doc. dr. Giedrė STRECKIENĖ (Vilniaus Gedimino technikos universitetas, technologijos mokslai, energetika ir termoinžinerija, T 006);
dr. Andrius TAMOŠIŪNAS (Lietuvos energetikos institutas, technologijos mokslai, energetika ir termoinžinerija, T 006).

Disertacija bus ginama viešame Energetikos ir termoinžinerijos mokslo krypties disertacijos gynimo tarybos posėdyje 2025 m. spalio 24 d. 10 val. Lietuvos energetikos instituto posėdžių salėje.

Adresas: Breslaujos g. 3-202, LT-44403 Kaunas, Lietuva.
Tel. +370 37 401801; el. paštas studijos@lei.lt

Disertacija išsiųsta 2025 m. rugsėjo 24 d.
Su disertacija galima susipažinti interneto svetainėje http://ktu.edu, Kauno technologijos universiteto bibliotekoje (Gedimino g. 50, LT-44239 Kaunas, Lietuva) ir Lietuvos energetikos instituto skaitykloje (Breslaujos g. 3, LT-44403 Kaunas, Lietuva).

CONTENT

LIST OF TABLES

LIST OF FIGURES

ABBREVIATIONS

LWR	Light Water Reactor
PWR	Pressurised Water Reactor
BWR	Boiling Water Reactor
VVER	Water-Cooled and Water-Moderated Nuclear Energy Reactor
NPP	Nuclear Power Plant
CSAU	Code Scaling, Applicability, and Uncertainty
GRS	Gesellschaft für Anlagen- und Reaktorsicherheit (German Nuclear Safety Organisation)
IPSN	Institut de Protection et de Sûreté Nucléaire (French Institute for Nuclear Safety)
ENUSA	Empresa Nacional del Uranio SA (Spain's Uranium Company)
GSUAM	General Statistical Uncertainty Analysis Method
BEAU	Best Estimate Analysis Uncertainty
BEPU	Best Estimate Plus Uncertainty
ASTEC	Accident Source Term Evaluation Code
RELAP	Reactor Excursion and Leak Analysis Program
SCDAP	Severe Core Damage Analysis Package
MELCOR	Methods for Estimation of Leakages and Consequences of Releases. Severe accident modelling code
MAAP	Modular Accident Analysis Program
SAMG	Severe Accident Management Guidelines
SA	Severe Accident
BE	Best Estimate
LOCA	Loss of Coolant Accident
LOFA	Loss of Flow Accident
SBO	Station Blackout
SS	Stainless Steel
PDF	Probability Distribution Function
TC	Thermocouple
FOM	Figures of Merit
DBA	Design-Based Accident
AEKI	Atomic Energy Research Institute (AEKI) in Hungary
CO	Carbon Monoxide
CO2	Carbon Dioxide
B4C	Boron Carbide
CH4	Methane
Cs/I	Caesium/Iodine

INTRODUCTION

Nuclear energy can significantly contribute to the solution of the current energy problems in the EU and Lithuania [1], as it would positively contribute to the security of supply, stability of energy prices, and the achievement of carbon dioxide reduction goals [2], [3], [4]. However, the catastrophic events at Three Mile Island [5], Chernobyl [6], and Fukushima Daiichi [7] nuclear power plants highlighted the devastating consequences of severe nuclear accidents. These severe accidents showed the importance of improving safety measures, enhancing accident management strategies, and developing numerical tools to predict accident scenarios accurately [8]. Therefore, research related to the safety of existing and new nuclear power plants remains relevant. Severe accidents, particularly those leading to partial core melting, involve complex physical phenomena, such as fuel rod degradation, hydrogen production, and fission product release. These events are influenced by numerous factors such as thermal-hydraulic conditions, chemical reactions, and material behaviour under high temperatures [9]. Better understanding and accurately modelling these physical phenomena are essential for improving reactor safety and mitigating the risks associated with severe accidents.

This dissertation focuses on analysing severe accident phenomena based on experimental investigations, specifically the PHEBUS [10] and QUENCH experimental programs [11]. These experiments provide valuable insights into fuel rod behaviour, hydrogen generation, and fission product release under severe accident conditions. The PHEBUS tests [10], which are in-pile tests, offer a detailed investigation of fuel degradation, hydrogen production and fission product release. The QUENCH tests [11] (out of pile tests) focus on the behaviour of fuel assembly overheating and reflooding processes. In such tests, fuel degradation and hydrogen production, especially during the reflooding scenario, are investigated in detail.

For modelling the above-mentioned complex phenomena, computer tools based on the best estimate (BE) approach are used [12], [13]. These computer tools are constantly improved and validated against experimental results. However, numerical analysis of severe accidents can meet significant uncertainties, which could give an inaccurate numerical prognosis. Thus, uncertainty quantifications of the received results are needed. Best Estimate + Uncertainty (BEPU) approach, which was developed for the analysis of design-based accidents, could also be applied to severe accidents [14], [15]. One of the first international attempts was the HORIZON 2020 MUSA [16] project and the IAEA CRP [17] Advancing the State-of-Practice in Uncertainty and Sensitivity Methodologies for Severe Accident Analysis in Water-Cooled Reactors. However, application of BEPU to the calculations of severe accident conditions needs further investigations (which are presented in this dissertation). Another observed point which raises difficulties for numerical investigations is the modelling of nuclear facilities with asymmetric geometries. Most of the computational tools rely on symmetric models. Thus, in this work, the application limits of such codes were investigated, and a methodology to evaluate physical processes in nuclear facilities with asymmetric geometry was developed.

Relevance and Impact of Work

Severe accidents at Three Mile Island, Chernobyl, and Fukushima highlighted the need for further investigation into severe accident conditions in nuclear reactors and the review of safety guidelines. Experimental programs such as PHEBUS, QUENCH, and CORA have been conducted to study these phenomena, alongside numerical simulations using tools like ASTEC, AC2, MELCOR, and RELAP/SCDAPSIM. Initially, conservative approaches were used for the modelling. However, such an approach could give too many conservative values and/or some vital safety issues may be masked. To improve accuracy, modern analyses employ Best Estimate (BE) methods, which are validated against experimental data. However, severe accident modelling still faces significant uncertainties, necessitating uncertainty quantification. The Best Estimate + Uncertainty (BEPU) approach, initially developed for design-basis accident analysis, is being extended to severe accident scenarios. International projects, such as HORIZON 2020 MUSA and IAEA CRP, have pioneered this application, but further research is still required. Another challenge in numerical analysis is the modelling of nuclear facilities with asymmetric geometries, as most computational tools assume symmetry. Defining the limits of such models and exploring alternative methods for analysing asymmetric configurations is crucial.

Object of the Thesis

This dissertation focuses on analysing severe accidents leading to partial fuel bundle melting using experimental data by applying the RELAP/SCDAPSIM code and the BEPU approach.

Aim of the Thesis

To propose a research methodology based on experimental data and apply the BEPU approach for the numerical investigation of physical processes in nuclear facilities with both symmetric and asymmetric geometries.

Tasks of the Thesis

1. Develop numerical models of experimental facilities simulating severe accidents that lead to partial fuel bundle meltdown, overcoming RELAP/SCDAPSIM's limitations in fission product release calculations via the integration of the CORSOR-M model.
2. Apply the BEPU approach and perform uncertainty quantification to assess the sensitivity of initial conditions, boundary conditions, and model parameters on the simulation results.
3. Analyse the physical processes occurring during severe accidents in facilities with asymmetric geometry.

Novelty of the Thesis

The integration of the BEPU approach to analyse severe accidents leading to partial fuel bundle melting for experimental facilities with symmetric and asymmetric geometry structures represents a first-of-its-kind methodology, extending the applicability and accuracy of severe accident analysis tools.

Practical Value

The developed methodology, based on the BEPU approach, allowed the analysis of severe accidents in facilities with symmetric and asymmetric geometry. Developed recommendations for the numerical investigation.

Defensive Statements

1. RELAP/SCDAPSIM system computer code, together with CORSOR-M model, is appropriate for the evaluation of Cs/I release fraction in early degradation phases.
2. The evaluation of numerical modelling uncertainties applying the BEPU approach improves the understanding and confidence levels of severe accident simulations.
3. Using the pseudo-symmetrical model (developed using experience gained from simulating PHEBUS and QUENCH tests) for asymmetric geometry, it is capable of evaluating processes in the fuel bundle only at the pre-oxidation and transient phases. For the better numerical evaluation of the intensive oxidation processes according to the experimental data of the asymmetric geometry test, component-level modelling is required.

1 REVIEW OF RESEARCH

1.1 The Severe Accidents in LWRs

A severe accident refers to an event that occurs in a nuclear power plant when multiple safety systems fail or are overwhelmed, leading to the release of radioactive materials and potentially causing significant damage to the reactor core and surrounding environment [9]. Severe accidents are rare but can have substantial consequences for both human health and the environment. Severe accidents are considered as extended design basis accidents. The first accident, which was defined as a severe accident, was Three Mile Island. The Three Mile Island accident occurred in 1979 in the USA [5]. The Chernobyl accident occurred in 1986 [6] and the Fukushima accident in 2011 [7]. These three major severe accidents led to a core meltdown. There are many scenarios or events that could lead to severe accidents in LWRS, such as LOCA and SBO, among others [9], [13].

Loss of coolant accident (LOCA) is initiated when breaks occur in the reactor coolant system (RCS) or any of the connecting circuits. Without sufficient coolant, the reactor core would heat up and potentially melt the zirconium fuel cladding, causing a potential reaction between zirconium and steam, which produces hydrogen in addition to a significant release of radioactivity [9], [18]. The steam generator rupture accidents (SGTR) have ranged from major leaks to complete rupture of one or more steam generator tubes, in addition to the secondary line breaks, water or steam. Leakages or ruptures of steam generator tubes will cause a drop in the reactor cooling system pressure. The Steam generator rupture accidents (one tube or two tubes) could lead to core melting in addition to total loss of coolant from the secondary loop [9]. Station blackouts refer to a scenario in which a nuclear power plant experiences a loss of offsite power, resulting in the loss of all electrical power to the plant. This means that the plant is unable to operate its safety systems, including the pumps that provide cooling to the reactor core. As a result, the reactor core can become uncovered, leading to overheating and potential damage to the fuel rods [18], [19].

1.2 Severe Accident Phenomena Overview

- **Fuel damage**

Fuel damage could occur either due to overpower, such as that brought on by a reactivity excursion, or a reduction in reactor cooling: loss of flow or loss of coolant accidents (LOFA or LOCA). In LWRs, overpower or reactivity excursion conditions are countered by reactivity insertion rate constraints and by negative reactivity feedbacks such as negative void and temperature feedback coefficients intrinsic to the design (contrary to the RBMK reactor accident in Chernobyl) [6], [9]. The analysis and investigations that were conducted for LWRs demonstrate that accidents involving undercooling (as was the case in the TMI-2 accident) are the more likely bring to severe fuel damage [9].

- **Accident progression stages**

Every severe accident has its unique progression and features, but LWR scenarios typically progress in the following manner [9], [18], [19]:

1. An event is initiated wherein some safety system failures lead to inadequate cooling of the fuel, causing a reactor trip and SCRAM of the core (control rods are fully inserted), but heat continues to be generated through the decay of fission products in the nuclear fuel.
2. The coolant (light water) level begins to drop in the reactor vessel, this could lead to the uncovering the core and causing a rapid fuel temperature increase .
3. Exothermic reactions occur between steam and overheated zircaloy cladding, which leads to an oxide layer forming on the Zr cladding surface (further inhibiting cooling of the fuel claddings), ultimately resulting in hydrogen generation and accelerating the heat-up of the fuel assembly.
4. The Zr cladding and UO_2 form a molten solution of U-Zr-O, which is commonly referred to as core corium.
5. Due to the loss of the integrity of fuel assembly and failures of the fuel claddings, various fission products are released.
6. The corium slumps towards the lower head, after which a burst of steam is produced, which enhances oxidation, embrittlement, and shattering of remaining tight fuel rods.
7. The corium continues to migrate towards the concrete floor underneath the vessel. Corium starts to erode the concreate. Depending on the thickness of the concrete basement, the corium may potentially penetrate the ground and contaminate the soil and groundwater, triggering serious ramifications on the safety of the public and the habitability of the region where the reactor is located.

Depending on the series of events leading to the accident, the initiation of core uncovering would vary from <1 than minute to a full day, and the accident progression could vary from several hours to days. A brief explanation of the different severe accident phenomenology is presented in Fig. 1, which is discussed below.

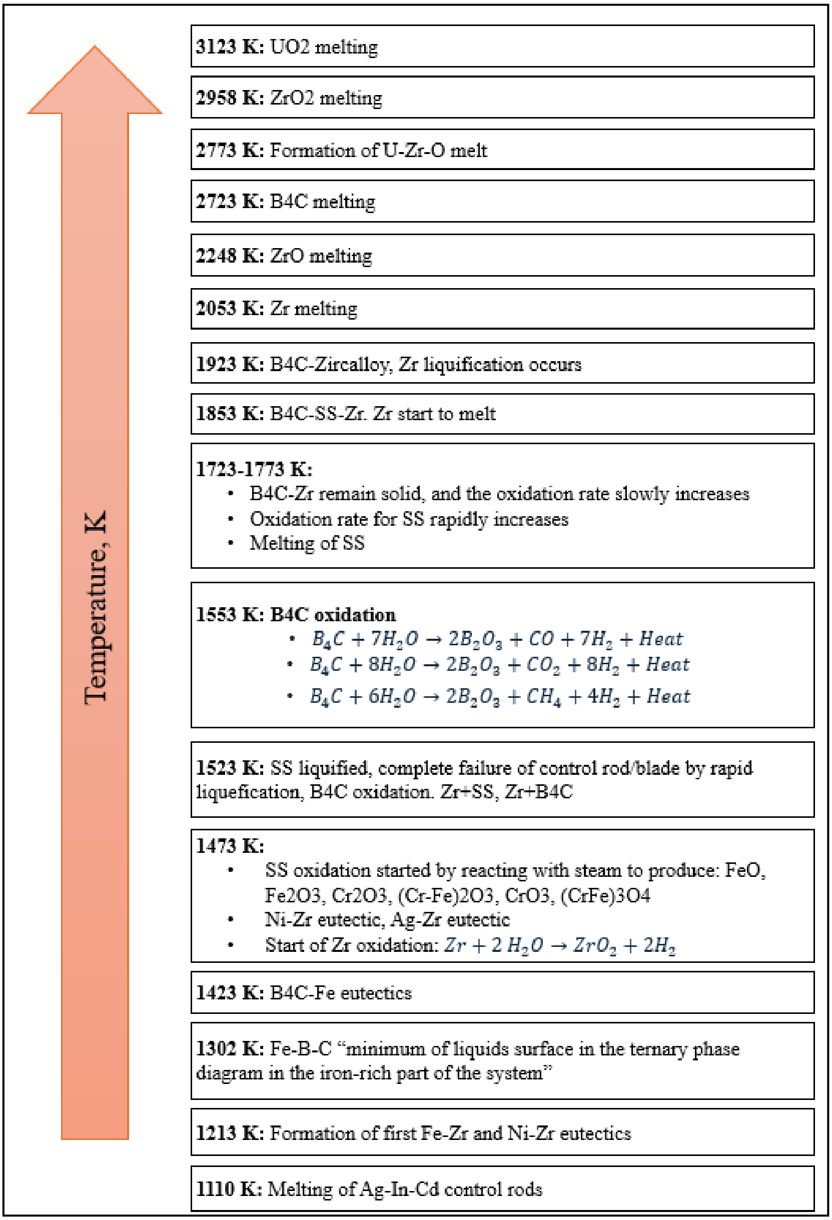

Fig. 1. Core degradation processes with temperature [9]

Once a part of the nuclear fuel is exposed, the coolant is no longer able to extract the residual heat generated by the nuclear fuel entirely. As a result, the uncovered parts of the fuel rods begin to heat up, the temperature is ascending. The zircaloy cladding, which surrounds the nuclear fuel pellets (UO_2), operates at regular temperatures, reaching a maximum of 623 K. The degradation of the mechanical properties of Zr, which takes place within the temperature range of 973 to 1 173 K, triggers the cladding deformation [9], [19]. The pressure inside the vessel may be either higher or lower than that within the fuel rod gap (pressure of the inert gases, usually helium, filling the gap between the fuel pellets and the cladding). If the pressure in the gap is lower than the pressure inside vessel, the cladding will deform and come into contact with the fuel pellets, resulting in the formation of UO_2-Zr eutectic with a melting point ranging from 1473 to 1 673 K, significantly lower than the fusion point of uranium dioxide (see Fig. 2). Conversely, if the pressure in the gap exceeds the pressure inside the vessel, the cladding will expand until it ruptures (see Fig. 3). When the integrity of the cladding structure fails, it leads to a breach of the initial barrier that contains radioactive materials. This results in the release of irradiated fuel particles and fission products, including highly volatile substances and noble gases.

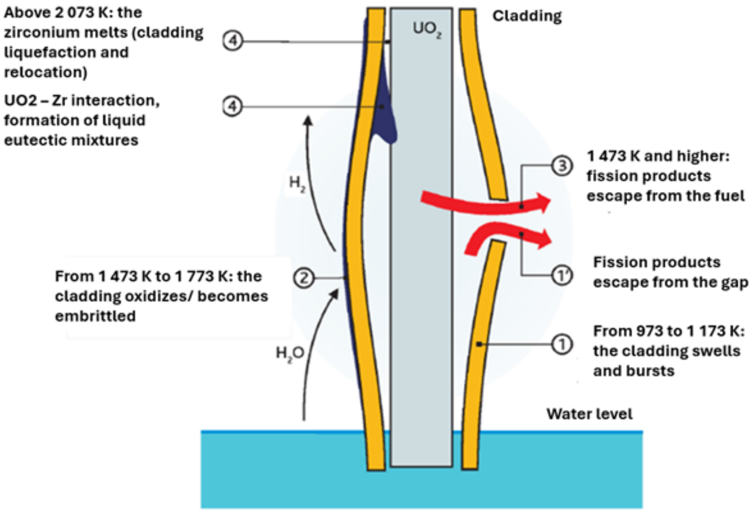

Fig. 2. Cladding Failure at Low Pressure [9]

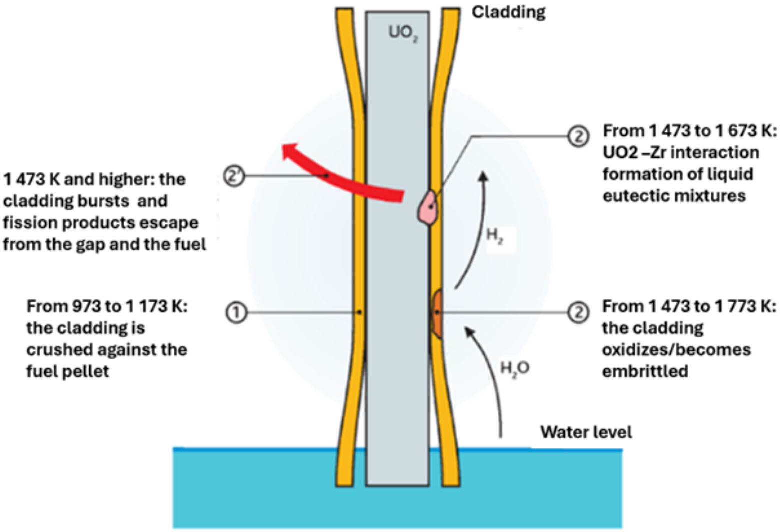

Fig. 3. Cladding Failure at High Pressure [9]

The oxidation of zirconium is considered one of the main phenomena which has a key role in increasing the degradation of the fuel rods and reactor core [9], [19], [20]. The oxidation reaction occurs when Zr reacts with superheated steam (see Fig. 4). The chemical reaction of Zr oxidation is given in (Equation 1-1):

$$Zr + 2\,H_2O \rightarrow ZrO_2 + 2H_2 \qquad \textit{(Equation 1-1)}$$

The reaction initiates at around 1473 K and is characterised by an exothermic chemical process. The energy released during this reaction ranges from 600 to 700 kJ per mole of Zr undergoing the reaction. At a temperature of around 1773 K, the thermal energy transferred to the cladding cannot be dissipated. The presence of convection with the steam causes the reaction to speed up, resulting in a rapid increase in the core temperature [18]. The heat emitted during this period can exceed the residual heat power, reaching higher peaks. According to the chemical equation, molecular hydrogen is produced and discharged into the core. Then it is transported through the RCS to the containment. In this scenario, the presence of air can initiate ignitions that result in deflagration. Under specific circumstances, this deflagration might escalate into an explosion, potentially causing the breakdown of the containment system, as observed in particular units during the Fukushima Daiichi accident. During the oxidation process, the Zr cladding undergoes a progressive substitution by a ZrO_2 layer, which is more fragile but has a higher melting point compared to Zr [19], [21].

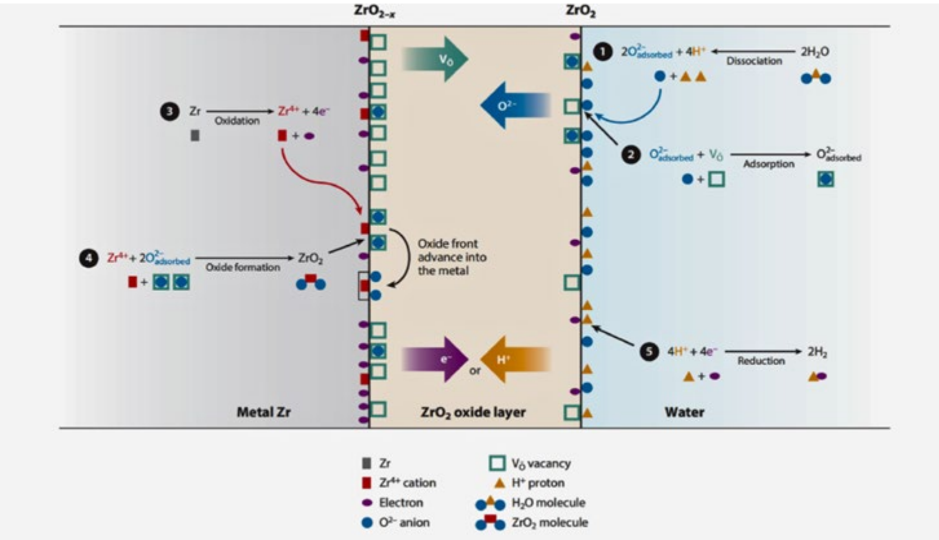

Fig. 4. Zr Oxidation and the Formation of the Oxide Layer [21]

The oxidation of B_4C is an important contributor to the production of hydrogen and other combustible gases during reflood of the reactor core. In addition, the methane generated by the oxidation of B_4C may react with the iodine released from the fuel to form organic iodine and thus influence the source term considerably. However, it should be noted that the amount of B_4C is relatively small compared to the amount of zircaloy in typical NPPs, so that the consequences of B_4C will be less critical [9], [22], [23]. Although the oxidation of B_4C during the standard heating and melting of the core could also be necessary because of the reaction of B_4C with steam. The experiments conducted without reflooding have not clearly shown any significant difference in the hydrogen production in assemblies with and without B_4C [23]. Reflooding includes injecting coolant water into the reactor core to cool the fuel rods and prevent further damage. The oxidation of B_4C with steam is presented in Equation 1-2, Equation 1-3 and Equation 1-4:

$$B_4C + 7H_2O \rightarrow 2B_2O_3 + CO + 7H_2 + Heat \qquad \text{(Equation 1-2)}$$

$$B_4C + 8H_2O \rightarrow 2B_2O_3 + CO_2 + 8H_2 + Heat \qquad \text{(Equation 1-3)}$$

$$B_4C + 6H_2O \rightarrow 2B_2O_3 + CH_4 + 4H_2 + Heat \qquad \text{(Equation 1-4)}$$

The dissolution of steel structural components by eutectic mixtures occurs before the steel melting temperature is reached, often below 1 473 K. Once the temperature reaches the melting point (~2 033 K), the fuel UO_2 begins to dissolve partially due to its contact with the liquid metal, resulting in the creation of UO_2-Zr eutectic [9].

At temperatures over 2 073 K, the core components that are currently in solid form, primarily composed of oxides, initiate the process of melting. This degradation process leads to the localised degradation of the mechanical strength of the fuel rods, causing a change in their geometry, loss of integrity, and resulting in the formation of partially solid fragments of core materials. If coolant flow is restored, the blockage and obstruction of core zones may be caused by the loss of core geometry and the relocation of damaged materials (see Fig. 1). The UO_2 reaches its maximum melting point at around 3 073 K. At these temperatures, all the volatile and semi-volatile fuel particles evaporate entirely. The corium mass progresses as it moves and solidifies in colder surroundings and stays solid until the point of liquefaction and subsequent collapse is reached. Thus, the molten pool grows both in the axial and radial directions until it reaches the core support plate [18].

Fission products (FPs) are generated as a result of neutron interactions with fuel during fission processes. During cladding failure, gaseous materials (Kr, Xe) are released. A similar phenomenon occurs with the fraction of fission products (FPs) that were initially trapped within the fuel pellets. As the temperature rises and the core is melting down partially, volatile FPs are gradually released from the pellets. Almost all of the volatile and semi-volatile fuel molecules will evaporate before the fuel begins to melt [9], [18], [19]. The FPs transport to containment and then outflow to the environment varies depending on how they change physically and chemically as they travel through the system. Their transport is mainly influenced by their phase (gases or aerosols), their chemical composition, and the thermohydraulic and chemical conditions inside the reactor.

The primary chemical and physical components present in the containment's atmosphere include gaseous iodine (I_2), molecular iodine in aerosol form (e.g., caesium, iodine, Cs, and I), and organic iodine gases (such as methyl iodide, CH_3I). Among these, organic iodine poses the highest level of threat because it is difficult to capture by current filtration techniques. Quite simply, after a severe accident (SA), iodine is emitted as gas and aerosol particles (molecular iodine) into the reactor cooling system (RCS) and then into the containment area. At this point, the iodine molecule in its gaseous state may undergo various phenomena: the material is absorbed by the coating on the containment walls. It reacts with it to release organic iodine in gas form. If the containment spray system is activated, some iodine dissolves into the spray water and water basins in the containment. Regardless of those barriers, a portion of gaseous iodine can still escape into the environment [18]. Table 1 Shows the groups of radioactive fission products released during a severe accident, their produced isotopes and their half-life.

Table 1. Representative Groupings of Radioactive Fission Products [19]

Group	Isotope	Half-life	Isotope	Half-life

Nobel gases	Kr−85	10.72 y	Kr−88	2.54 h
	Kr−85m	4.48 h	Xe−133	5.245 d
	Kr−87	1.27 h	Xe−135	9.09 h
Halogens	I−131	8.04 d	I−134	52.6 m
	I−132	2.3 h	I−135	6.61 h
	I−133	20.8 h		
Alkali metals	Cs−134	2.062 y	Cs−138	30.17 y
	Cs−136	13.16 d	Rb−86	18.66 d
Tellurium group	Sb−127	3.85 d	Te−129	1.16 h
	Sb−129	4.40 h	Te−129m	33.6 d
	Te−127	9.35 h	Te−131m	30 h
	Te−127m	109 d	Te−132	3.26 d
Barium, strontium	Ba−139	1.396 h	Sr−90	29.1 y
	Ba−140	12.746 d	Sr−91	9.5 h
	Sr−89	50.52 d	Sr−92	2.71 h

1.3 Overview of Severe Accident Numerical Codes

Various severe accident experiments address specific phenomena or aspects of severe accident progression. For the numerically evaluate these physical processes the several computer codes have been developed and validated by the limited scope experiments available. Several of those computer codes addressing some specific severe accident phenomena are discussed and compared in Table 2. However, to investigate and simulate these phenomena interactively in assessing reactor safety, it is necessary to perform analyses with integral severe accident codes (ASTEC, RELAP/SCDAPSIM, MELCOR, etc.) that simulate severe accident progression, including hydrogen generation, degradation of fuel, and the FPs releases.

- ASTEC Code

The ASTEC (Accident Source Term Evaluation Code) software system simulates all phenomena that occur during a water-cooled reactor meltdown accident, from the initial event to the discharge of radioactive material (called source term) outside containment [24]. This includes, in particular, Western-designed pressurised water reactors (PWRs) [25] such as those used for nuclear power supply in France, Russian-designed pressurised water reactors (VVERs) [26], boiling water reactors (BWRs) [27], and CANDU [28] heavy water reactors. ASTEC is currently maintained and developed by IRSN [24], [29]. The main applications of the software package are safety analyses of nuclear reactors (e.g., European Pressurised Reactor – EPR), source term assessments in accident cases, and development of guidelines for the management of serious accidents. ASTEC is widely used in IRSN Level 2 Probabilistic Safety Assessments (PSA2) of French reactors. It is also used to prepare and interpret experimental programs related to phenomena inside or outside the ship that can occur during breakage incidents. Moreover, ASTEC is also sometimes used to prepare crisis exercises (nuclear or radiological accident simulation exercises) in the IRSN Technical Crisis Centre, training different players and the organisation itself. ASTEC is the European reference program within the European Commission’s Network of Excellence SARNET (Severe Accidents Research Network). It is also used by many organisations outside Europe (Canada, Russian Federation, India, Singapore, Ukraine, etc.) (see Fig. 5).

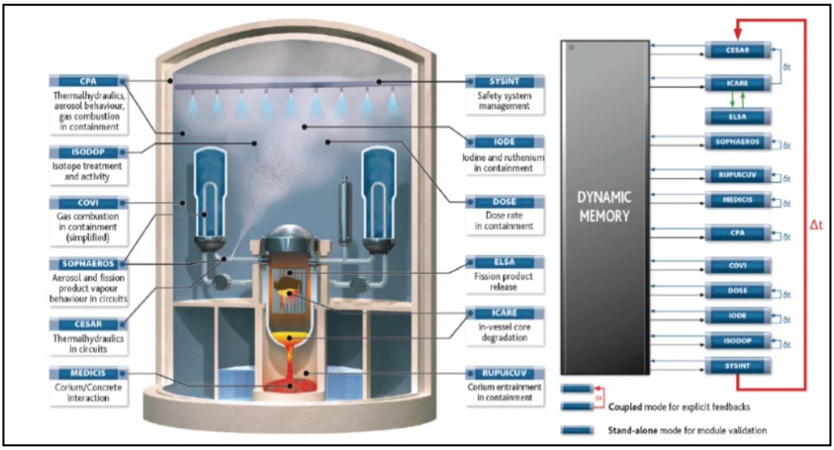

Fig. 5. ASTEC Code Structure [29]

- RELAP/SCDAPSIM code

RELAP/SCDAPSIM is a computer code designed specifically for the prediction of the total thermal-hydraulic reactor cooling system response and basic behaviour during normal operation conditions as well as under design basis or severe circumstances of the accident [30], [31]. RELAP/SCDAPSIM uses publicly available RELAP/MOD3.3 as well as SCDAP/RELAP5/MOD3.2 models. It is developed by the US Nuclear Regulatory Commission (NRC) in conjunction with Special Advanced Programming Numerical methods, user options, and models. RELAP/SCDAPSIM is developed within the international SCDAP development framework and training program (SDTP) [31]. DTP software and the main developer of specific RELAP/SCDAPSIM forms is a limited liability company, Innovative Systems Software (ISS). Its optimisations allow the code to run faster and more reliably than the original US NRC codes.

In the RELAP/SCDAPSIM/MOD3.5 comprehensive thermal-hydraulic components reactor cooling system, control system behaviour, Reactor kinetics, as well as the behaviour of special reactor system components such as valves and pumps, are calculated by the RELAP5 part of the code and its models. On the other hand, the basic structure and ship, under both normal and accident conditions, are calculated by SCDAP. SCDAP is a part of the code that includes user-definable reactor component models for LWR, B_4C, and Ag-In-Cd control rods, channel boxes/BWR control blades, as well as electrically heated rods, general vessels, and core structures. SCDAP also has models to address later stages of severe accidents with the formation of debris and molten cores, debris-vessel interactions, and structural failure (creep rupture) of the vessel and its structures (see Fig. 6).

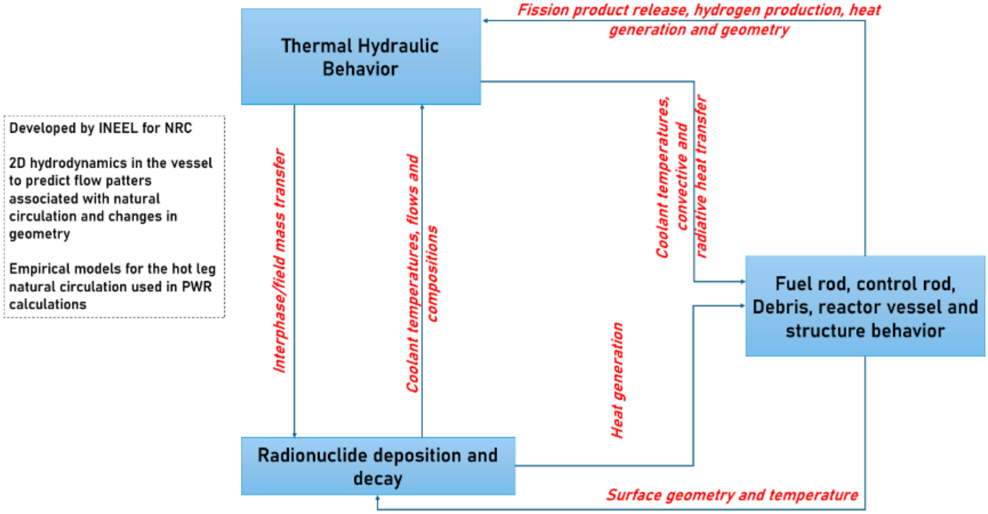

Fig. 6. RELAP/SCDAPSIM Code Structure

- MELCOR code

The MELCOR code was developed at Sandia National Laboratories for the U.S. Nuclear Regulatory Commission (NRC) [32]. The purpose of the MELCOR code is to simulate and model the accident progression of light water reactors. The project of developing the MELCOR code was started in 1982 after the occurrence of the Three Mile Island accident. It has undergone continuous development to address emerging issues, process new experimental information that emerged following the TMI-2 accident and create a repository of knowledge on severe accident phenomena. CORCON, VANESSA, and CONTAIN codes were integrated into the MELCOR core to expand its capabilities. MELCOR code can perform probabilistic risk analysis and evaluate the complete reactor accident sequence.

MELCOR can simulate severe accident phenomena in light-water reactors, including coolant system thermal-hydraulic response, reactor cavity, containment and confinement buildings, core heat-up, degradation, and relocation, core-concrete attack, hydrogen production, transport, and combustion fission-product release, transport behaviour [32] (see Fig. 7).

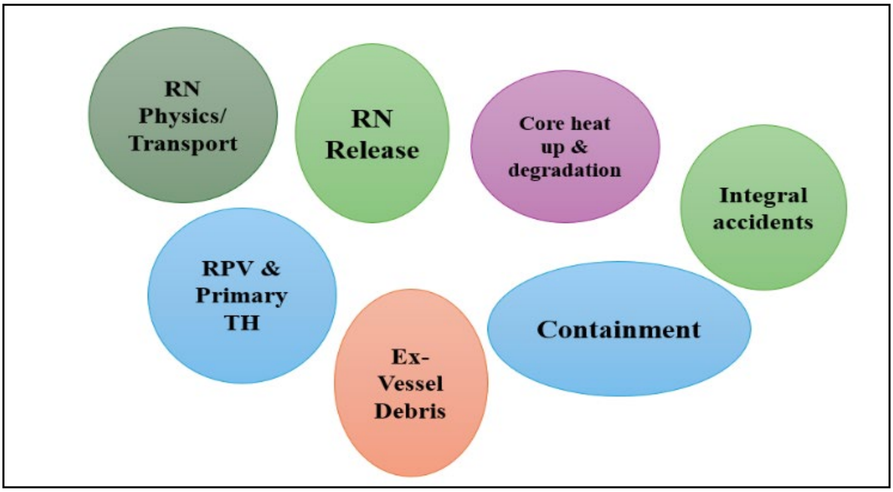

Fig. 7. MELCOR Code Structure

- ICARE/CATHARE code

The ICARE/CATHARE code was developed by IRSN within the framework of PWR safety analyses. The code is the result of the coupling of the two mechanical severe accident codes ICARE2 (developed by IRSN since 1988) with the French best-estimate system code CATHARE2 (co-developed by the CEA, EDF, FRAMATOME-ANP, and IRSN since 1979). The code allows for the simulation of severe accident events in the whole RCS of PWR, VVER, and EPR reactors. The ICARE/CATHARE first version was validated against a vast experiment conducted by IRSN on PWR 900 MWe. In ICARE/CATHARE V1, the ICARE2 code calculates all known phenomena occurring inside the core during both the early and late degradation phases, while the CATHARE2 code computes the thermal hydraulics in the lower and upper plena as well as the rest of the system circuit [33] (see Fig. 8).

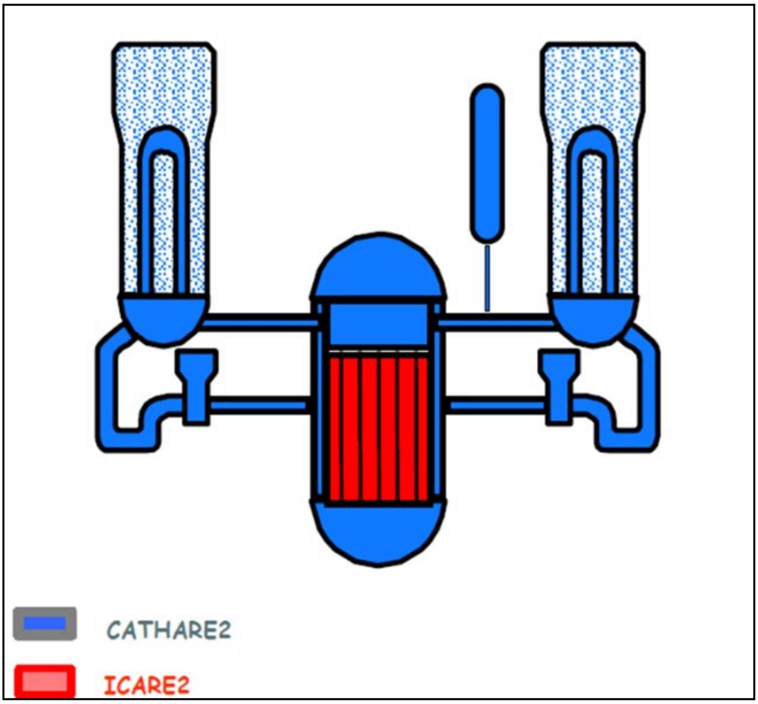

Fig. 8. ICARE/CATHARE Code Structure [33]

- MAAP code

The Modular Accident Analysis Program (MAAP) is owned by the Electric Power Research Institute (EPRI). MAAP simulates the response of light-water and heavy-water moderated nuclear power plants for both current and Advanced Light Water Reactor (ALWR) designs. It can simulate Loss-Of-Coolant Accident (LOCA) and non-LOCA transients for Probabilistic Risk Analysis (PRA) applications as well as severe accident sequences, including actions taken as part of the Severe Accident Management Guidelines (SAMGs). There are several parallel versions of MAAP for BWRs, PWRs, CANDU designs, FUGEN designs, and the Russian VVER design [34]. The original MAAP code was developed in the 1990s by Fauske & Associates, LLC (FAI) as part of the Industry Degraded Core Rulemaking (IDCOR) program. FAI continues to support the code owner EPRI and their MAAP customers for software updates, maintenance, and training, drawing on decades of experience in modelling severe accidents at nuclear power plants. FAI also has extensive experience in implementing MAAP into nuclear training simulators.

Table 2. Main Features of Severe Accident Codes

Phenomenon	ASTEC [24], [34]	MAAP [34]	MELCOR [32]	ICARE/ CATHARE [29]	RELAP/ SCDAPSIM [31]
Thermal hydraulic part	Simplified	Simplified	Simplified	Detail	Detail
Severe accident part	Detail	Simplified	Detail	Detail	Detail
Ballooning	✓	✓	-	✓	✓
Cladding degradation	✓	✓	✓	✓	✓
Spacer grid deformation	✓	✓	✓	✓	✓
SS, Zr, B_4C oxidation	✓	✓	✓	✓	✓
Hydrogen generation	Detailed, comprehensive and integrated modelling	Simplified models	Detailed models	Detailed models	Detailed models
Absorber blades modelling	Oxidation, mechanical degradation, fission product release models	Oxidation models	Oxidation, mechanical degradation, fission product release models	Oxidation and mechanical degradation models	Oxidation and mechanical degradation models
Fission product release	Detailed, comprehensive and integrated modelling. Fission product release, transport and deposition	Simplified fission product release using phenomenological models	Detailed modelling of fission product release, transport, and chemical interaction	Advanced models for fission product release and transport	Only fission product release from the gap as a sum of (Xe+Kr+He) and a sum of (CsI+CsOH). Additional models could be implemented

1.4 Overview of Severe Accident Research Programs

After the occurrence of the Three Mile Island accident [5], many international experimental programs have been conducted to investigate the physical phenomena that cause severe accidents in Light water reactors. These experimental programs are divided into two different categories: in-pile and out-of-pile. The in-pile experiments in which real fuel rods are used, such as PHEBUS tests [10]. An out-of-pile experiment where electrically heated rod emitters are used, such as CORA [35], and QUENCH tests [11]. In this part, a brief description of each program will be provided. These experimental programs were selected because they were conducted to analyse and investigate the physical phenomena occurring during the first phase of the accident. In addition to understanding the fuel behaviour under extreme conditions, hydrogen production, initial damage to the core and partial meltdown of the core.

- CORA experiment

The CORA test facility operated (see Fig. 9) at Kernforschungszentrum Karlsruhe studies the behaviour of PWR and BWR fuel elements under severe accident conditions [35]. The CORA facility includes a 2-meter-high fuel rod package with a 1-meter electrically heated area that simulates the force of decay; PWR and BWR configurations. The CORA test package consists of heated simulation rods, unheated fuel rods, and control materials. Ag-In-Cd (silver, indium, cadmium) control rods or B_4C (boron carbide) control blades enclosed in an insulating jacket. The insulating shroud consists of zirconia and zirconia [35]. The objectives were: analysis of heating and fusion stages of fuel elements at the CORA test facility and special focus on the reliability and accuracy of computer codes for critical incidents; investigate the thermal and mechanical behaviour of the fuel pack at high temperatures (e.g., formation of blockages, breakage of rods); study of the physical and chemical processes during primary decomposition (e.g., oxidation of cladding and other metallic components, hydrogen formation) and post-test analysis.

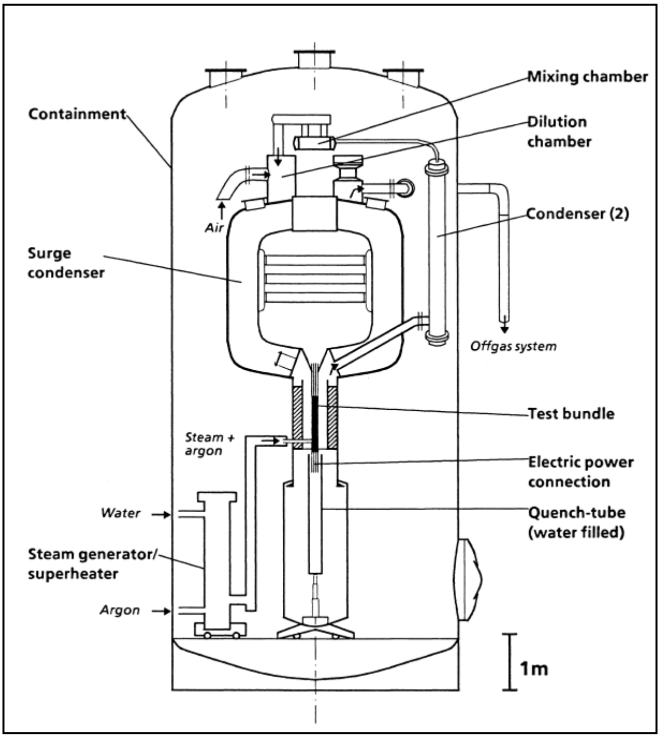

Fig. 9. CORA Test Facility [35]

- The QUENCH program

QUENCH experimental program was conducted at the QUENCH facility (Fig. 10) at the Forschungszentrum Karlsruhe Institute to study and determine the source of hydrogen [11]. The QUENCH program began with small-scale experiments using ZIRCALOY's fuel rod segments. Based on the results presented at the QUENCH facility at KIT, a large-scale package containing fuel rod simulators and well devices is being implemented under adiabatic conditions. Large-scale bundle experiments provide more representative conditions for reactor accident models than single-rod experiments. The test package contains some critical parameters, which are steam, water flow injection rate, cladding oxide layer thickness, initial flood temperature, and cooling medium [11]. According to the QUENCH matrix, more than 20 experiments have been conducted with different severe accident scenarios, as well as a series of 7 DBA LOCA experiments.

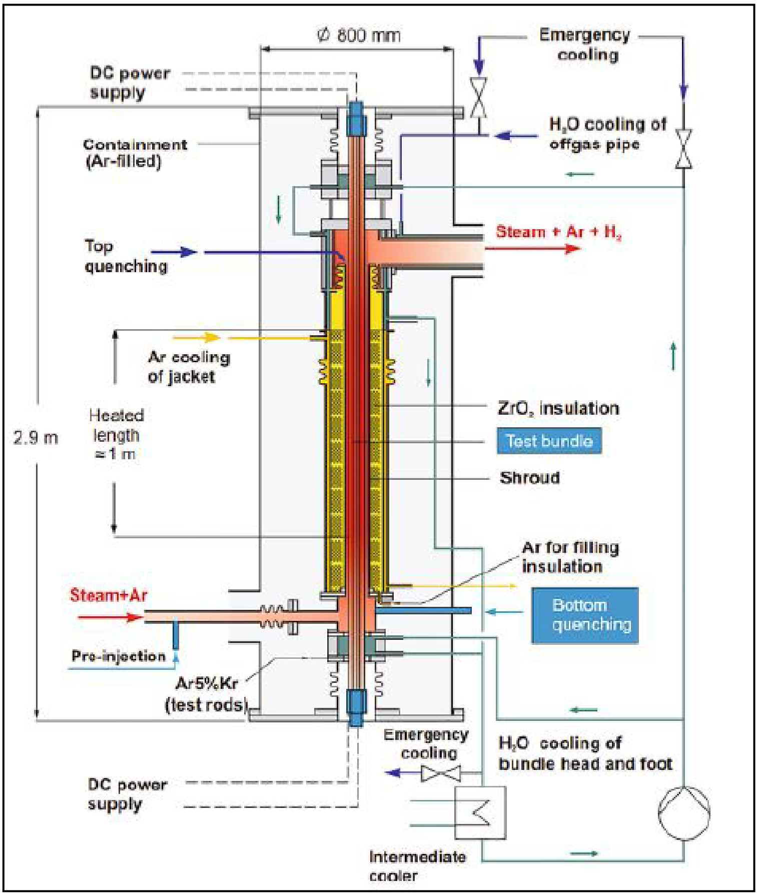

Fig. 10. QUENCH Test Facility [11]

- The CODEX program

The CODEX (Core Decay Experiment) facility (see Fig. 11) was initially established for studies of severe accidents [36]. Several experiments have been performed using the VVER and PWR fuel bundles. The behaviour of fuel rods in high-temperature steam, high-temperature cooling, phenomena related to air entry scenarios, and the role of control rods have been addressed in different CODEX tests. At AEKI, an experimental program focusing on the high-temperature behaviour of VVER fuels and base materials has been initiated. The interactions of the Zr1%Nb cladding with uranium dioxide grains, a stainless-steel spacer, and a boron steel absorber were studied in separate small-scale impact tests. Based on the experience gained in these tests, the CODEX Integrated Test Facility was established to continue this work under more typical conditions.

First, the facility's capabilities were demonstrated by conducting a CODEX-1 experiment using Al_2O_3 pellets. The test section was heated with argon, and then the electrical power was increased. When beam degradation was indicated by temperature measurements, the power was turned off, and the section was cooled by argon. Post-test inspection showed that the package was partially damaged, and further melting was stopped in time. Therefore, the facility has been proven to be applicable to experimental modelling of controlled fundamental decomposition processes [36].

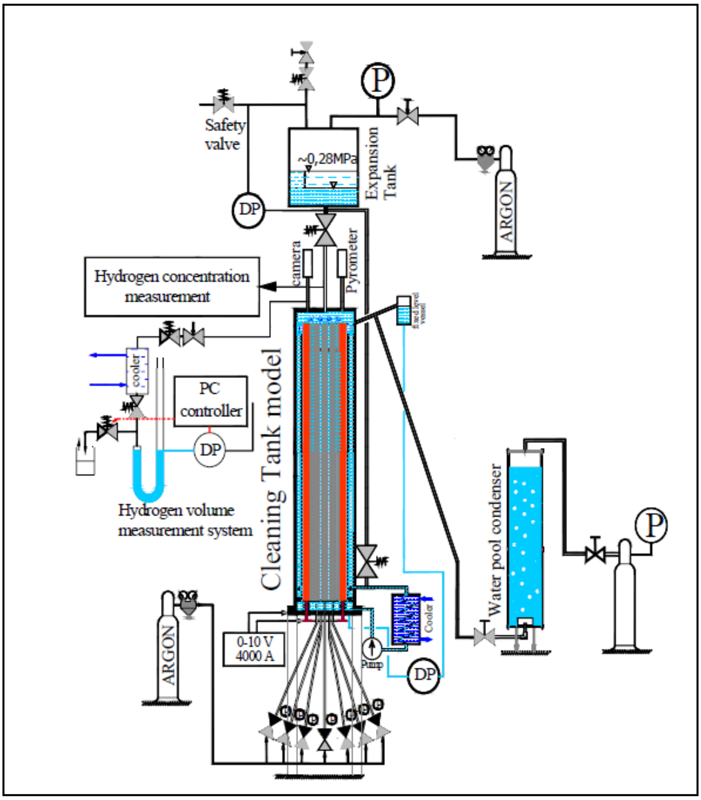

Fig. 11. CODEX Test Facility [36]

- The PHEBUS program

The PHEBUS Fission Program (FP) was initiated in 1988 after the occurrence of severe accidents at nuclear reactors (Three Mile Island (TMI), USA, in 1979 and at Chernobyl, Ukraine, in 1986). The main objective of the program is to study the release, transfer, and retention of fission products in an in-pile facility under severe accident conditions in light water reactor (LWR) [10] (see Fig. 12). The Institute for Nuclear Protection and Security (IPSN) of the Atomic Energy Commission (CEA) and the Commission of the European Communities (CEC) have agreed to cooperate

in carrying out a series of six tests in cooperation with others. The international partners are the US Nuclear Regulatory Commission (NRC), Japan Nuclear Power

Engineering Corporation (NUPEC), Japan Atomic Energy Research Institute (JAERI), Canadian Kando Owners Group (COG), and the Korea Atomic Energy Research Institute. (KAERI) and later the Swiss Paul Scherrer Institute (PSI) and the Swiss Federal Nuclear Safety Board (HSK). The program is managed by the Département de Recherche en Sécurité (DRS) of CEA-Cadarache and the Joint Research Centre (JRC) of the CEA. The first test of the pilot program (FPT0) was successfully conducted on 2 December 1993. The second test of the program (FPT1) was performed on 26 July 1996 [10].

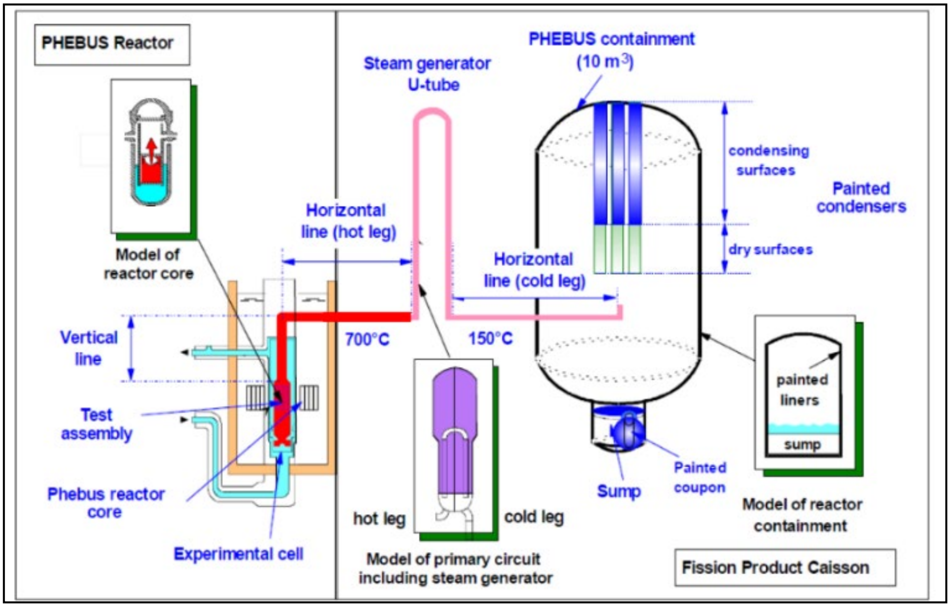

Fig. 12. PHEBUS Test Facility [10]

1.5 Best Estimate Approaches and Tools

Over the past few decades, safety analysis has evolved various approaches, including the quality of material data available and the nature of computer codes associated with initial and boundary conditions. The studies have been performed over the years under different assumptions [37].

1. Conservative approach

During the early development of nuclear power plants, computer codes for design, analysis, and licensing were primarily developed based on conservative assumptions to produce *conservative results*. This conservative approach arose from the challenges of accurately modelling complex physical phenomena, given the limited capabilities of early computational tools and the scarcity of reliable experimental data (see Fig. 13).

In this approach, initial and boundary conditions were intentionally selected to yield pessimistic estimates of safety margins relative to established acceptance criteria. These estimates also account for parameter measurement and prediction uncertainties, whether derived from experiments or theoretical models. Conservative codes played a significant role in the design and analysis of second-generation (GEN II) nuclear power plants, with their accuracy and efficiency constrained by the computational power and technology available at the time [14], [39].

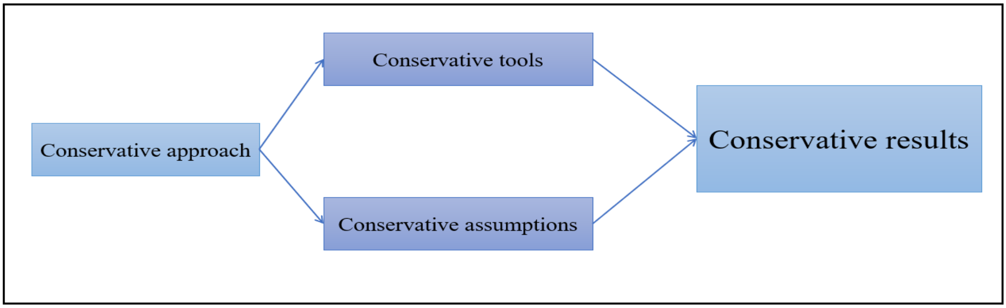

Fig. 13. Conservative approach scheme

2. Best estimate approach

The history of the best-estimate approach in safety analysis dates back to the 1970s. The USNRC [38] issued a regulatory guide in 1974 that allowed the use of best estimate methods in safety analyses, however, with conservative assumptions and safety margins [39], [40]. In the late 1970s and early 1980s, the USNRC initiated the Best Estimate Methods Program (BEM) to develop and validate best-estimate computer codes. In 1988, the USNRC revised the ECCS rule and allowed the use of best estimate codes with uncertainty estimation [41].

The best estimate approach in severe accident analysis is a method that uses realistic, or *best estimate*, methods and input data to predict the behaviour of fuel rods and reactor cores during severe accidents, considering both deterministic and probabilistic methods [12], [38]. The BE approach contrasts with the conservative approach, which employs deterministic and pessimistic assumptions and methods to ensure that the predicted consequences of an accident are more severe than what would actually occur. The BE uses detailed models that account for the physical phenomena that occur under severe accident conditions. These models are based on a combination of experimental data, theoretical analysis, and computational simulations. The input data reflect the most expected conditions in the reactor during a severe accident, including the reactor's initial state and the progression of the accident. A key aspect of the best estimate approach is applying uncertainty and sensitivity analysis. To quantify the uncertainties in the models and input data and provide a measure of confidence and probability in the predicted results [38], [39], [40].

3. Best estimate approach plus uncertainty

The goal is to provide a credible capability for comprehensive and sophisticated modelling and simulation methodologies by integrating information from multiple sources, historical databases, experimental measurements, numerical simulations, and expert judgment. The main components of this methodology are verification, validation, calibration, and uncertainty quantification. The uncertainty quantification effect is considered in multiple modules of the system, the challenge being to combine data available from different sources and in different formats and model predictions of various physical phenomena such as hydrogen generation, cladding degradation, fuel degradation, etc. The model uncertainties are quantified by comparing model predictions with experimental measurements. The model uncertainties in predictions are quantified by considering the sensitivity analysis, propagation of uncertainty analysis, discretisation uncertainty quantification, and truncation uncertainty (residual) quantification (see Fig. 14). The measurement uncertainty is propagated for predicting the output parameter. Such error may be approximated by first-order sensitivity analysis, which could then allow for the quantification of the model's error. This process is previously demonstrated in the works of IAEA [42].

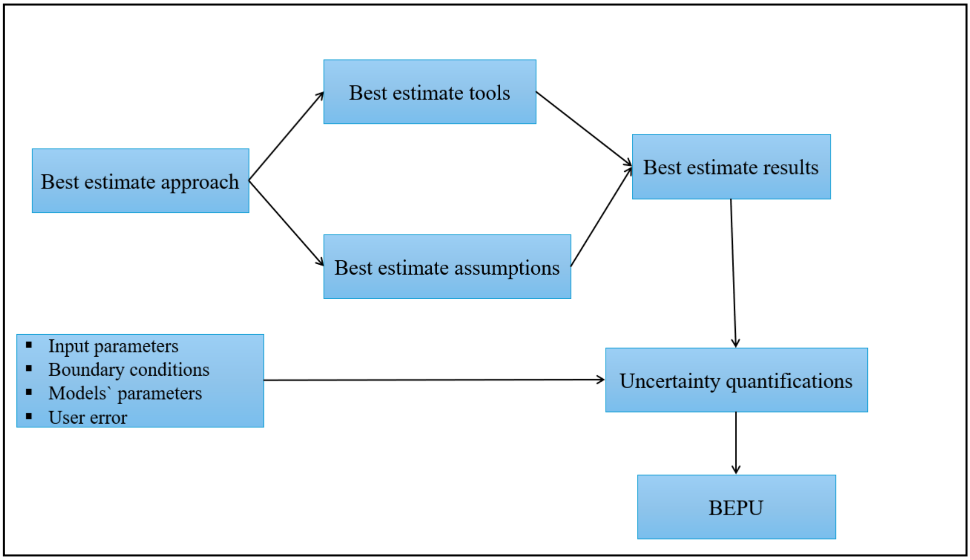

Fig. 14. Best Estimate Approach and Plus Uncertainty Scheme

Best Estimate Methods

The best estimate methods aim to model physical processes with higher accuracy. These methods provide a deeper understanding of complex phenomena by reducing conservative assumptions and offering more precise insights into the progression of severe accidents [12]. These BE methods are generally divided into either deterministic or probabilistic methods. Deterministic methods focus on developed scenarios and establish conservative constraint limits to calculate uncertainties, relying on experimental data and engineering judgments to ensure safety limits under the potential conditions. In deterministic methods, uncertainties are evaluated by selecting the most conservative assumptions without quantifying their likelihood [41]. The deterministic methods are AEAW and EDF-Framatome, which define the uncertainty ranges to cover extreme scenarios, ensuring that the reactor is safe and within operational limits. On the other hand, probabilistic methods employ a comprehensive approach that identifies and quantifies uncertainties using probability distributions. The probabilistic methods enable a more comprehensive analysis of their potential and the impact of various accident scenarios. Probabilistic methods provide insight into the probability of specific events occurring, in addition to offering a reliable risk assessment that enhances the conservative, deterministic methods' scenario-based approach [12]. The most commonly used BEPU methods are presented below.

1. CSAU Method

The CSAU (Code Scaling, Applicability, and Uncertainty) method is a probabilistic methodology which was developed by the U.S. Nuclear Regulatory Commission (NRC) for evaluating and improving the accuracy of different computer codes used in nuclear reactor safety analysis, specifically the severe accident computer codes [13]. The CSAU focuses on the identification and quantification of the uncertainties associated with numerical analyses to apply the BE approach to the reactor's behaviour during accidents. The CSAU method provides a comprehensive study for systematically evaluating uncertainties in predicting the accident progression of core damage, hydrogen generation, fission product release, and other physical phenomena during severe accidents in LWRs.

The CSAU (Code Scaling, Applicability, and Uncertainty) method comprises three main phases: code scaling, applicability, and uncertainty quantification. Code scaling ensures that the mathematical models employed in the severe accident simulation code appropriately scale from experimental data or small-scale systems to full-scale reactor systems. This involves verifying that the physical phenomena are accurately modelled and consistently represented across different scales (e.g., from laboratory scale to reactor scale) [43]. Applicability assesses the relevance of the code to the specific severe accident scenarios under investigation. The objective is to confirm that the physical models implemented in the code are capable of accurately simulating the severe accident conditions of interest, such as cladding temperature evolution, core melting, fuel degradation, and thermal-hydraulic phenomena during core uncovering. Uncertainty quantification focuses on identifying and quantifying uncertainties associated with the code inputs, physical models, and boundary conditions. These uncertainties pertain to thermal-hydraulic properties, material behaviour, and reactor-specific parameters under severe accident conditions. The method evaluates how these uncertainties propagate through simulations and affect the modelling outcomes.

2. GRS Method

The GRS Method (Gesellschaft fur anlagen- und reaktorsicherheit method) is a best estimate systematic method which is used in severe accident analysis to calculate uncertainties and evaluate safety margins in NPPs. The GRS method was developed by a German research organisation specialising in nuclear safety. This method is widely used in Europe for evaluating nuclear reactor behaviour under severe accident conditions [44], [45]. The GRS method is similar to the CSAU method, providing a structured framework for analysing severe accident scenarios through model validation and uncertainty quantification. The application of the GRS method involves the following steps: the GRS method begins with the identification of the most significant phenomena that influence the progression of severe accidents. This includes reactor core melting, hydrogen generation, cladding oxidation, and the release of fission products. A better understanding of these physical phenomena is crucial for the accurate modelling of severe accidents. Model development and validation: The GRS method utilises well-validated computer codes specifically designed for severe accident scenarios. These computer codes are extensively validated against experimental data to ensure their applicability to real reactor conditions, and uncertainty and sensitivity analysis: the GRS method places a significant emphasis on uncertainty and sensitivity analysis. The uncertainties are quantified in model parameters, initial, and boundary conditions, which allows for a comprehensive understanding of how these parameters influence the modelling results of severe accidents. The sensitivity analysis is performed to identify which uncertain parameters have the highest influence on the modelling results [46].

3. IPSN Method

The IPSN Method was developed by the Institute de Protection et de Surete Nucleaire (IPSN), which is a French institute responsible for nuclear safety and radiation protection. At the current time, it is integrated into the Institute de Radioprotection et de Surete Nucleaire (IRSN). The IPSN method is the best estimate method, which focuses on a detailed and comprehensive analysis of severe accidents [47], [48]. The IPSN method emphasises improving reactor safety through both deterministic and probabilistic assessments. This method is used to validate severe accident models and enhance accident management strategies, with a strong focus on core melting, hydrogen generation, and fission product release. The IPSN method is characterised by several key features that contribute to a comprehensive assessment of severe accident scenarios. It combines both deterministic and probabilistic analyses, allowing for a more robust evaluation of accident progression and system behaviour. A central aspect of the method is the identification and modelling of key phenomena likely to occur during a severe accident, including core melting, hydrogen generation, and the release of fission products.

These phenomena are simulated using validated severe accident codes to ensure accurate representation under relevant conditions. Additionally, the IPSN method places significant emphasis on the quantification of uncertainties and the execution of sensitivity analyses. It systematically evaluates uncertainties related to model parameters, initial conditions, and boundary conditions, thereby enhancing the reliability and credibility of the simulation outcomes.

4. ENUSA Method

The ENUSA method, developed by Empresa Nacional del Uranio SA in Spain, is considered a probabilistic method similar to the GRS method and the CSAU framework. The ENUSA method utilises the Wilks formula. In the ENUSA method application, the number of uncertain parameters input was limited to 26, determined through a PIRT process. This limitation was intended to improve the process of determining uncertainty distributions and reducing the complexity for the analysis [13], [38].

5. GSUAM Method

The general statistical uncertainty analysis method (GSUAM), developed by Siemens (Framatome ANP), is a specialised method for the licensing process for the Angra 2 Nuclear Power Plant. The GSUAM method focuses on evaluating point values, such as PCT, and does not quantify uncertainty in time-dependent code results. The method identifies three main factors contributing to uncertainty: the code, the NNPs conditions, and the fuel conditions. The code represents the largest source of uncertainty. The GSUAM method uses a statistical approach to integrate uncertainty data from the given sources, providing a comprehensive uncertainty analysis [37], [42].

6. BEAU Method

The best estimate analysis uncertainty (BEAU) method was developed in Canada by Ontario Power Generation and Atomic Energy of Canada. It is similar to the CSAU framework and has been applied to evaluate the first energy pulse during a large break LOCA (LB LOCA) in CANDU reactors. The BEAU method includes a PIRT process and performs numerous simulations, ultimately providing a probabilistic uncertainty analysis. This method has been verified and validated by a broad international group of experts to establish its usage in the field of nuclear safety analysis [42].

Table 3 presents the advantages and disadvantages of different BE methods.

Table 3. Comparison of BE Methods

Method	Advantages	Disadvantages
GRS	▪ Well validated using different severe accident computer codes like ATHLET-CD, etc. ▪ Strong emphasis on evaluating uncertainty and sensitivity analysis. ▪ Can be used for both deterministic and probabilistic assessments. ▪ Can identify a large number of parameters ▪ Applicable for a wide range of accident scenarios.	▪ More computational resources might be needed for handling multiple accident scenarios. ▪ Limited international application usage compared to some other methods.
IPSN	▪ Combines both deterministic and probabilistic methods for comprehensive analysis. ▪ Strong experimental validation, especially for PHEBUS international program.	▪ Highly dependent on complex experiments and detailed validation, which may limit its flexibility in some severe accident scenarios. ▪ Requires access to detailed experimental data (which might not be available)

CSAU	▪ Using a systematic approach to code scaling and its applicability. ▪ Comprehensive uncertainty quantification ▪ Established in the U.S. and internationally recognised.	▪ Time-consuming due to its intensive scaling and uncertainty quantification process. ▪ Relying on expert judgments in defining conservative estimates.
ENUSA	▪ Focuses on detailed severe accident modelling specific to the Spanish nuclear field. ▪ Wide experience with European nuclear power plants.	▪ Limited application outside Spain ▪ Comparatively narrow scope in international benchmarking for severe accident analysis.
GSUAM	▪ Provides an uncertainty analysis framework for severe accidents. ▪ Strong ability to handle complex physical phenomena under severe accident conditions with probabilistic methods.	▪ The method can become computationally intensive. ▪ It requires extensive data inputs for accurate results.
BEAU	▪ Gives realistic best-estimate predictions with uncertainty analysis. ▪ Improves the understanding of accident progression.	▪ Relatively new compared to other BE methods ▪ Its usage requires significant validation against experimental data (which needs more time and data)

BEPU Tools

The BE tools are developed to quantify and address uncertainties, combined with models, and provide more realistic predictions of modelling results. This section presents an overview of the BE statistical tools used in severe accident analysis.

- SUSA

SUSA is a software for uncertainty and sensitivity analysis, developed by GRS (Gesellschaft für Anlagen- und Reaktorsicherheit) in Germany. SUSA is a statistical tool designed to perform comprehensive uncertainty and sensitivity analysis. The SUSA tool is commonly used to evaluate the influence of uncertain parameters on the prediction results of severe accident simulations [49], [50]. The SUSA tool has many features. The SUSA is used to perform uncertainty quantification, which enables users to assess the uncertainty in model predictions by varying the input uncertain parameters and analysing how these parameters would affect the simulation results. Additionally, the SUSA tool is used to perform sensitivity analysis by identifying which input uncertain parameters most influence the simulation results, as well as applying statistical random sampling techniques (e.g., Monte Carlo simulations) to explore the variability in model outputs and results. Moreover, the SUSA tool could be coupled with different severe accident analysis codes like MELCOR, MAAP, RELAP/SCDAPSIM or ASTEC [51]. The SUSA tool helps to analyse uncertainties in partial core melting, hydrogen generation, containment behaviour, and other severe accident phenomena. SUSA has a graphical user interface (GUI) that allows the visualisation of the calculation results. GUI provides a wide range of input and output options, such as importing and exporting data, parameter selection, and plot generation.

- RAVEN

The Idaho National Laboratory (INL) designed the RAVEN (Risk Analysis Virtual Environment) tool for evaluating uncertainty quantification, sensitivity analysis, and probabilistic risk of severe accident analysis. The features of the RAVEN tool include its ability to perform uncertainty quantification through stochastic sampling techniques, such as Monte Carlo and Latin Hypercube S [52].

RAVEN could assess the impact of uncertain input parameters on the simulation results of severe accidents. Moreover, the RAVEN tool is used to perform sensitivity analysis by identifying which uncertain input parameters most affect the simulation results and prioritising the uncertain parameters that have the highest influence on accident progression (e.g., core melt, hydrogen production, containment failure). Additionally, the RAVEN tool is often used in conjunction with severe accident simulation codes (e.g., MELCOR, MAAP) and thermal-hydraulic codes (e.g., RELAP-5, RELAP-7) [53].

- SUNSET

The SUNSET tool, used for severe accident analysis, was developed by the Institut de Radioprotection et de Sûreté Nucléaire (IRSN) to perform uncertainty and sensitivity analyses for severe accident analysis. The SUNSET helps to assess the effect of uncertain input parameters on simulation result [54], [55]. SUNSET tool is especially coupled with severe accident codes such as ASTEC. The features of the SUNSET tool are as follows: it helps evaluate the uncertainty of various uncertain parameters that influence the FOMs, such as core melting, hydrogen generation, and containment breach. It quantifies the uncertainties affecting the simulation results. The SUNSET tool can determine which input uncertain parameters have the most significant influence on the simulation results through sensitivity analysis. Additionally, the SUNSET tool can be coupled with severe accident codes, specifically ASTEC. The SUNSET tool provides a visualisation of the results of uncertainty and sensitivity analyses.

- DAKYOTA

DAKOTA (Design Analysis Kit for Optimisation and Terascale Applications) is a tool developed by Sandia National Laboratories for evaluating uncertainty quantification and sensitivity analysis. The DAKOTA tool integrates various simulations and analyses of severe accident applications [56], [57], [58]. The features of the DAKOTA tool include a range of optimisation and evaluation algorithms, such as gradient-based, derivative-free, and stochastic, which can be applied to various problems, including unconstrained, constrained, linear, nonlinear, and integer programming. Additionally, DAKOTA can assess uncertainties and sensitivity in computer models. These include Monte Carlo simulation, Latin hypercube sampling, polynomial chaos expansion, and global sensitivity analysis. These methods can help identify the sources and magnitudes of uncertainties.

Comparison between the BE tools is presented in Table 4. The comparison shows the developer of each tool, the methodologies used and the user interface.

Table 4. Best Estimate Tools

Feature / Tool	**SUSA** [49]	**SUNSET** [55]	**DAKOTA** [56]	**RAVEN** [52], [53]
Developer	GRS (Gesellschaft für Anlagen- und Reaktorsicherheit	IRSN (Institut de Radioprotection et de Sûreté Nucléaire)	Sandia National Laboratories	Idaho National Laboratory (INL)
Primary Focus	Uncertainty and sensitivity analysis in nuclear safety	Uncertainty and sensitivity analysis in nuclear safety	Design and analysis toolkit for optimisation and uncertainty quantification	Risk analysis and visualisation of environmental impacts
Application Area	Nuclear safety analysis	Nuclear safety analysis	Broad engineering applications, including aerospace, structural engineering, and nuclear	Nuclear safety, risk assessment, and environmental impact analysis
Methodologies	Statistical sampling, correlation analysis	Statistical sampling, variance-based methods	Optimisation, parameter estimation, uncertainty quantification	Probabilistic analysis, uncertainty quantification, risk assessment
Integration	Integrates with various nuclear safety codes (e.g., RELAP, MELCOR)	Integrates with various nuclear safety codes (e.g., ASTEC, CATHARE)	Interfaces with a wide range of simulation tools and models	Integrates with RELAP5-3D, MOOSE framework, and other INL tools
Output Analysis	Detailed statistical analysis, graphical plots	Statistical analysis, sensitivity indices	Comprehensive reporting, graphical visualisation	Advanced visualisation tools, detailed risk analysis reports

User Interface	Command-line and graphical user interface	Command-line interface	Command-line and graphical user interface	Graphical user interface, scripting support

1.6 Modelling of Overheating and Quenching Phenomena in Nuclear Fuel Rods based on experimental investigations

The PHEBUS FP program (Fission Product Program) was a large-scale international nuclear safety research initiative focused on understanding the behaviour of fission products during severe nuclear reactor accidents. The PHEBUS test facility and the PHEBUS FPT-1 test are described in detail in Section 2.4.1. The modelling and simulation of different PHEBUS tests (FPT0, FPT-1, FPT-2) were done using the ASTEC code [59]. The modelling results showed a good agreement with the experimental results for the containment gas pressure, cladding temperature, and fission product release. The detailed simulation also predicted phenomena such as partial core melting and hydrogen generation. Another simulation was done for PHEBUS FPT-1 using MELCOR severe accident code [60]. The focus is on partial core melting mechanisms during severe accidents in Light water reactors. The study evaluates the energy balance, mass distribution, and system pressure. It provides insight into the behaviour of the system under severe conditions. The research contributes to the understanding of the consequences of severe accidents and assists in the development of mitigation strategies to improve the safety of nuclear reactors. The results showed good agreement with the experimental results. PHEBUS FPT-1, which includes a test bundle representing a PWR fuel assembly, is simulated using the RELAP/SCDAPSIM models [61], [62]. The modelling results are compared with experimental data to validate the accuracy of the simulation. An uncertainty analysis and sensitivity analysis are performed for the evaluation of the impact of various parameters on the results.

The phenomena related to reflooding and quenching of the overheated fuel assemblies have been comprehensively investigated through the QUENCH program, which was conducted at Karlsruhe Institute of Technology (KIT). The QUENCH program has 22 different QUENCH tests to analyse various fuel bundle geometries and different severe accident phenomena. One of the famous tests is the QUENCH-06 test, which was equipped with a PWR fuel bundle [63]. It was conducted to investigate the PWR fuel behaviour under severe conditions. The QUENCH test facility and the QUENCH-06 test are described in detail in Section 2.4.2. Different severe accident codes were used for the modelling and analysis of the QUENCH-06 test, such as the ASTEC code. ASTEC obtained results were in good agreement with the experimental data for the selected FOMs [64]. The results showed the code's ability to simulate fuel behaviour under severe accident conditions, in addition to the evolution of hydrogen generation. This investigation showed that the code succeeded in evaluating the hydrogen production, cladding oxidation, and cladding temperature in addition to the oxide layer thickness. The MELCOR code was used for the validation of its new models [65]. The calculated results showed good agreement with the experimental data for the selected FOMs. The RELAP/SCDAPSIM code was used for modelling the QUENCH-06 test [17], [64]. The code showed its capabilities to model and investigate severe accident phenomena. Also, simulation results showed good agreement with the experimental data for the selected FOMs.

The RELAP/SCDAPSIM code successfully modelled various CORA and QUENCH tests, including CORA [35], [66], QUENCH-12 [67], and QUENCH-14 [68]. The scientists of Lithuanian Energy Institute (LEI) modelled the QUENCH-06 [64], QUENCH-03 [64], QUENCH-10 [69], [70], and QUENCH-18 [71] experiments using different severe accident codes, RELAP/SCDAPSIM and ASTEC. The QUENCH-03 and QUENCH-06 tests are related to the PWR fuel bundle with the oxidation phase in the water-steam ambient. This situation corresponds to the severe accident conditions in the reactor core. The specific QUENCH-10 and QUENCH-18 tests are the air ingress before the quenching phase. This corresponds to the severe accident conditions in the reactor core when the reactor cavity is not intact, or the processes in the spent fuel pools during loss of coolant. The analysis showed that the RELAP/SCDAPSIM and ASTEC SA codes succeeded in modelling the fuel rod simulators, and the results showed the codes' abilities to model and predict the different phenomena associated with the fuel rod degradation, cladding oxidation, oxide layer, and hydrogen generation.

In 2019, KIT conducted the first QUENCH test equipped with a BWR fuel bundle [72]. A detailed description of the QUENCH-20 test is presented in Section 2.5. The pre- and post-test of the QUENCH-20 test was performed by GRS experts using the AC^2 severe accident code. The results of the post-test computations showed that the predicted thermal behaviour was in good quantitative and qualitative agreement with the experimental data. However, there were some deviations during the reflooding and cooling phases, which appeared to be slower than in the experiment (which is identified in previous related works [1]). In addition, the oxidation of B_4C was underestimated. At KIT, the QUENCH-20 test was used for preliminary validation of ASTEC V.2.2.b [73]. The measured data of the QUENCH-20 test, such as fuel rod simulator and absorber blade temperatures, as well as hydrogen generation, were used for validation. The analysis performed with the detailed model for the study of severe accident phenomena showed that ASTEC can predict a total hydrogen generation value close to the experimental values. In addition, the code can predict the time evolution of the axial temperature distribution of most of the test structures in an acceptable manner. Overall, there is good agreement between the experimental data and the ASTEC calculation results. However, the non-symmetric behaviour of the test bundle cannot be reproduced by ASTEC due to the modelling approach based on cylindrical coordinates. The QUENCH-20 test was also modelled in Moscow at the Institute of Nuclear Safety (IBRAE) using the SOCRAT/V3 thermal-hydraulic and severe fuel damage best-estimated computer code. The modelling of the basic thermal-hydraulic, oxidation, and thermal-mechanical behaviour during all phases

[1] Elsalamouny N., Kaliatka T., Kaliatka A. "QUENCH-20 test analysis using RELAP/SCDAPSIM severe accident code". Nuclear Engineering and Design. Elsevier, 2024, Vol. 419, 112995, p. 1-12. ISSN 0029-5493. https://doi.org/10.1016/j.nucengdes.2024.112995.

was performed. As in the previous cases, the main challenge was the complicated geometry of the QUENCH-20 test bundle encountered in the modelling by the SOCRAT/V3 code. The calculated results were in good agreement with the experimental data, justifying the adequacy of the modelling capabilities of the SOCRAT code [74].

1.7 Author's Contribution to the Topic

Review of the literature showed that severe accidents, particularly those leading to partial core melting, involve complex physical phenomena, such as fuel rod degradation, hydrogen production, and fission product release, which are given great attention. Experimental investigations, combined with numerical tools, are used to study these processes. Numerical tools used for analysing severe accident conditions are always validated against experimental results; however, calculation results inevitably contain uncertainties. For the quantification of the uncertainties, the BEPU approach could be used. Still, the application of this method to the severe accident field is not widely used due to its complexity.

To solve this problem, the author proposed a methodology based on experimental data and applied the BEPU approach for numerical investigation of physical processes. The numerical models (for severe accident code RELAP/SCDAPSIM) of the PHEBUS FPT-1 and QUENCH-06 tests were renewed and updated according to the latest data. Numerical investigations were provided using the severe accident code RELAP/SCDAPSIM. For the uncertainty quantification of the received calculation results, the BEPU approach, based on the GRS methodology and utilising the SUSA statistical tool, was applied.

Another issue observed in the revised literature is the numerical investigation of physical processes in facilities with asymmetric geometry. This is because most severe accident codes are developed to evaluate symmetric geometries, leading to potential inaccuracies when applied to asymmetric geometry configurations (such as some experimental facilities and spent fuel pools).

The author utilises the experience gained from previous investigations conducted for symmetric geometry base experiments (PHEBUS-FPT1 and QUENCH-06) to develop numerical models and recommendations for the severe accident code RELAP/SCDAPSIM. This approach enables the investigation of processes in the QUENCH-20 test, which is based on asymmetric geometry.

2 THE METHODOLOGY OF INVESTIGATION

Fig. 15 introduces the research methodology of this work. The methodology begins with identifying the physical phenomena leading to partial core melting down, including fuel degradation, Zr oxidation, B_4C oxidation, hydrogen generation, cladding rupture, and fission product release. In the next step, the experiments which investigate the phenomena occurring at the severe accident conditions are selected. The experiments are divided into two categories: symmetric and asymmetric geometry. Computer codes are selected to model and simulate these experiments accurately. The analysis takes two paths: Model 1 development for symmetric geometry experiments. The reference calculation is performed for the selected FOMs. The Best Estimate (BE) approach is applied to refine the model predictions by performing uncertainty and sensitivity analyses.

The insights and experience gained from symmetric geometry analysis contribute to the analysis of asymmetric geometry experiments. Model 2 development of asymmetric geometry experiments involves developing a pseudo-symmetrical model and a component-level model to address complexities in asymmetric geometry. Recommendations are generated for the modelling of asymmetric facilities, contributing to improvements in accident analysis methodologies.

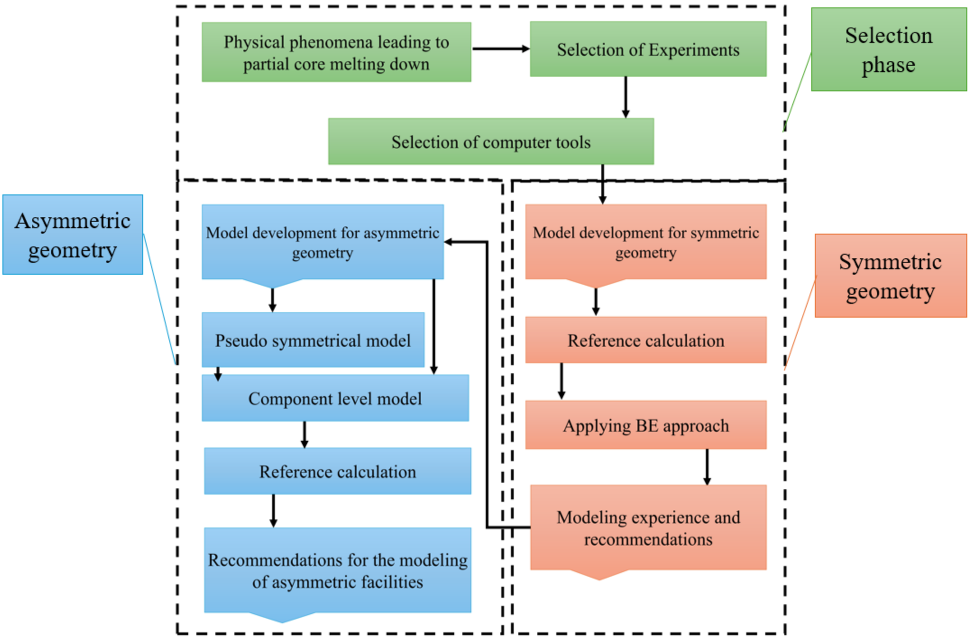

Fig. 15. Research Methodology

2.1 Selection of the Physical Phenomena Leading to Partial Core Meltdown

To investigate the physical phenomena leading to a partial core melting severe accident, specific physical phenomena were selected for detailed study (see Fig. 1). These phenomena are crucial for a deeper understanding of the progression of severe accidents, including the oxidation processes of core materials such as stainless steel (SS), zirconium (Zr), and boron carbide (B4C), as well as fuel rod degradation. This research focuses on the release of fission products, specifically those emanating from the gap between the fuel and cladding, which are crucial for assessing the radiological consequences of a severe accident on the environment and public health. Hydrogen generation is considered a key phenomenon for severe accident analysis, which is generated due to the high-temperature reactions between zirconium cladding and steam. Hydrogen is regarded as a highly flammable gas.

It ignites easily, even at low concentrations, and burns rapidly with an almost invisible flame. Because of its broad flammability limits in air (approximately 4% to 75% by volume), hydrogen can readily form explosive mixtures.

2.2 Selection of Computer Tools

Many computer codes have been developed following the occurrence of the TMI severe accident to simulate the physical phenomena that occur during severe nuclear accidents. These computer codes were well validated against experimental data. Based on the severe accident codes, a comparison is presented in Table 2. The RELAP/SCDAPSIM computer code was selected for the analysis in this research. The RELAP/SCDAPSIM code provides comprehensive modelling capabilities, which include thermal-hydraulic behaviour and partial core melting during different accident scenarios, leading to partial core meltdown. The RELAP/SCDAPSIM code integrates the RELAP5 and SCDAP models to allow detailed simulation of reactor cooling systems, core damage progression, and fission product release. The RELAP/SCDAPSIM has the capability to simulate a wide range of severe accident scenarios leading to partial core meltdown, including asymmetric geometries. Additionally, the RELAP/SCDAPSIM severe accident code supports uncertainty quantification, enhancing the accuracy of simulation results and enabling more realistic severe accident analysis.

2.3 Selection of the Experiments

This research involves two categories of experiments, distinguished by their geometrical structure into symmetric and asymmetric geometries. These experiments were selected to evaluate the effect of geometric structure on the progression of severe accidents leading to partial core melting. The variation in the geometric structure can lead to different physical phenomena and challenges in modelling. The selected experiments with a symmetric geometric structure are PHEBUS FPT-1 (Section 2.4.1) and QUENCH-06 (Section 2.4.2). The selection of symmetric geometry experiments is due to the fact that these experiments simulate different physical phenomena, leading to partial core melting in severe accidents. Additionally, these experiments are widely recognised and well-validated against experimental data using various severe accident codes. Also, the availability of the data for assessment and analysis should be considered. The selected experiment with asymmetric geometric structure is QUENCH-20 (Section 2.5). The QUENCH-20 test is selected as it is the first QUENCH program test with a BWR asymmetric fuel bundle, and it simulates the phenomena leading to partial core meltdown. Moreover, the boundary conditions (operation phases) of QUENCH-06 and QUENCH-20 are similar; however, the test bundles differ, allowing for a comparison of the results and an examination of the influence of bundle differences, as well as symmetric and asymmetric geometry differences.

Physical phenomena which were analysed, as well as the experimental phases vs reactor operation phases in the selected experiments, are presented in Table 5.

Table 5. Selection of Experiments and Physical Phenomena Analysed

Experiments	Exp. phases	Exp. phases vs reactor operation	Physical phenomena analysed
PHEBUS FPT-1 ***For PWR type fuel. In the test, irradiated and fresh fuel were used.***	Pre-oxidation Oxidation Power plateau Heat up Cooling down (with steam)	Pre-oxidation and Oxidation phases are needed to generate the oxide layer, which exists in the reactor core due to its operation time. Power plateau and Heat up phases imitate the accident situation – fuel dry out. Cooling down phase is only for experimental tests	Heat transfer within the reactor core and the surrounding structures. Oxidation of fuel cladding and structural materials. Oxidation is an exothermic reaction which contributes to additional heat generation and hydrogen generation. Deformation of fuel rod claddings and surrounding structures. Fission Product Release Transport of fission products
QUENCH-06 ***For PWR type fuel. In the test, fuel rod imitators were used.***	Pre-oxidation Transient Quenching with water	Pre-oxidation phase is needed to generate an oxide layer that exists in the reactor core due to its operation time.	Heat transfer within the reactor core and the surrounding structures. Oxidation of fuel cladding and structural materials and absorber blades (in the case of

QUENCH-20 ***For BWR type fuel. In the test, fuel rod imitators were used.***		The Transient phase imitates the accident event – fuel dry-out. Quenching phases imitate the application of safety measures (attempting to restore the reactor's coolability) – specifically, water injection into the hot core.	QUENCH-20). Oxidation is an exothermic reaction which contributes to additional heat generation and also hydrogen generation. Deformation of fuel rod claddings and surrounding structures and absorber blades (in the case of QUENCH-20). Partial melting of the fuel rod imitators and blades (in the case of QUENCH-20).

2.4 Symmetric Geometry Experiment

The selected experiments with symmetric geometry are PHEBUS FPT-1 [75] and QUENCH-06 [63] which are selected to investigate the physical phenomena leading to partial core meltdown. The RELAP/SCDAPSIM [31] severe accident code was used for the modelling and analysis of these experiments. Table 6 introduces the phenomena covered during model development using the RELAP/SCDAPSIM SA code.

Table 6. Phenomena Covered Symmetric Geometry Tests

Components	**Modelled phenomena**	**PHEBUS FPT-1 test**	**QUENCH-06 test**
Control rod (central rod)	Heat transfer between the central rod and the fuel rods. Degradation	Fuel component	Cora component
		All phenomena covered	All phenomena covered
Fuel rod (rod simulators)	Fuel rod degradation, cladding oxidation, hydrogen generation.	Fuel component	Cora component
		All phenomena covered	All phenomena covered

Corner rods	Heat transfer between fuel rods and corner rods. Zr oxidation. Degradation	NA	Fuel component
			All phenomena covered
Shroud	Heat transfer between fuel rods and shroud. Zr oxidation.	Shroud component	Shroud component
		All phenomena covered	All phenomena covered

2.4.1 PHEBUS FPT-1 Test

The PHEBUS FPT-1 is considered an experiment of the PHEBUS research program. The PHEBUS FPT-1 test was conducted to investigate severe accidents in light water reactors [75]. The PHEBUS FPT-1 is considered an in-pile test, which includes active fuel rods in the fuel bundle. The PHEBUS FPT-1 test was focused on in-core thermal hydraulics, partial core melting, and fission product (FP) release from the fuel. The PHEBUS FPT-1 test facility includes a pressurised water reactor core (PWR) with active fuel bundle, cooling circuit, water loop, an injection loop, steam generator, and containment vessel (see Fig. 12). The PHEBUS FPT-1 test fuel bundle is equipped with a total of 20 fuel rods (2 fresh and 18 irradiated) and a control rod (Ag-In-Cd) (see Fig. 16). Irradiated fuel rods have a different burn-up of approximately 23.4 GWd/tU. The PHEBUS FPT-1 is equal to 1/5000 scale factor to a PWR 900 MW. An insulating shroud with an inner thorium dioxide sleeve, an external Zirconium dioxide sleeve, and a pressure tube of Inconel coated on the internal face by flame-sprayed dense zirconium dioxide surrounds a fuel bundle of the PHEBUS FPT-1 test. The three annular structures are separated by two gaps under cold conditions; the gaps close at higher temperatures due to the metal's thermal expansion. An independent pressurised cooling circuit is used for cooling the outer pressure tube, with a large amount of water at a temperature of 438 K. The power of the PHEBUS FPT-1 test bundle during the test and the steam flow rate through the test bundle (measurement data) are presented in Fig. 17.

The PHEBUS FPT-1 test phases [75] are illustrated in Fig. 17, which includes calibration (0 to 7 900 s). The power of the bundle was increased in steps to assess the bundle's thermal response (from 0 to 3.19 kW). Meanwhile, the steam flow rate was first reduced from 1.8 to 0.5 g/s. The calibration phase exists only in the experiment, specifically during pre-oxidation (from 7 900 s to 11 060 s). At ~7 900 seconds, the nuclear power generated in the bundle increased at a rate of 5.3 W/s. At power equal to 7.75 kW (~9 000 seconds), the nuclear power stabilised for ~300 s (until ~9 300 seconds). The maximum measured temperature of ~1 603 K inside the bundle (limit of operating temperature for the K-type thermocouples). At ~7 900 seconds, the steam flow rate increased from 0.5 g/s to 2.2 g/s until ~10 160 seconds and then remained constant for ~5 220 s. It is necessary to generate the oxide layer that forms in the reactor core as a result of its operational time. Oxidation occurs between 11 060 s and 13 200 s. The power increases again at approximately 9 300 s, reaching 24 kW by 13 200 s, and remains stable at this level for about 1 380 s (until approximately 14 580 s).

The maximum temperature is ~2 003 K measured by TCs located inside the test bundle (TCW13 at the 0.5 m elevation). The temperature escalation started at ~11 060 seconds at the 600 mm elevation, and the cladding temperature exceeded 1 843 K in the upper part of the bundle. The total hydrogen generation increased very rapidly after 11 060 s; at 12 400 s, the measured hydrogen generation was ~70 g. The oxidation phase is required to generate the oxide layer that forms in the reactor core over the course of its operational lifetime. During the power plateau phase (13 200 s to 14 580 s), the maximum fuel temperature reached approximately 2 223 K and remained at this level for around 1380 seconds. The total duration of this period was ~3 500 seconds. This phase simulates the accident situation – fuel dry-out; heat-up (14 580 s to 17 039 s). The steam mass flow rate was reduced from 2.2 g/s to 1.5 g/s over a period of ~ 1 980 seconds. Fuel relocation was detected, characterised by a rapid increase in temperature at the lower levels of the shroud, accompanied by a cooling of the upper part. The second temperature peak in the lower part of the shroud led to the reactor being shut down and the end of the test for a maximum bundle power of 34.4 kW. The heat-up phase simulates the accident situation – fuel dry-out.

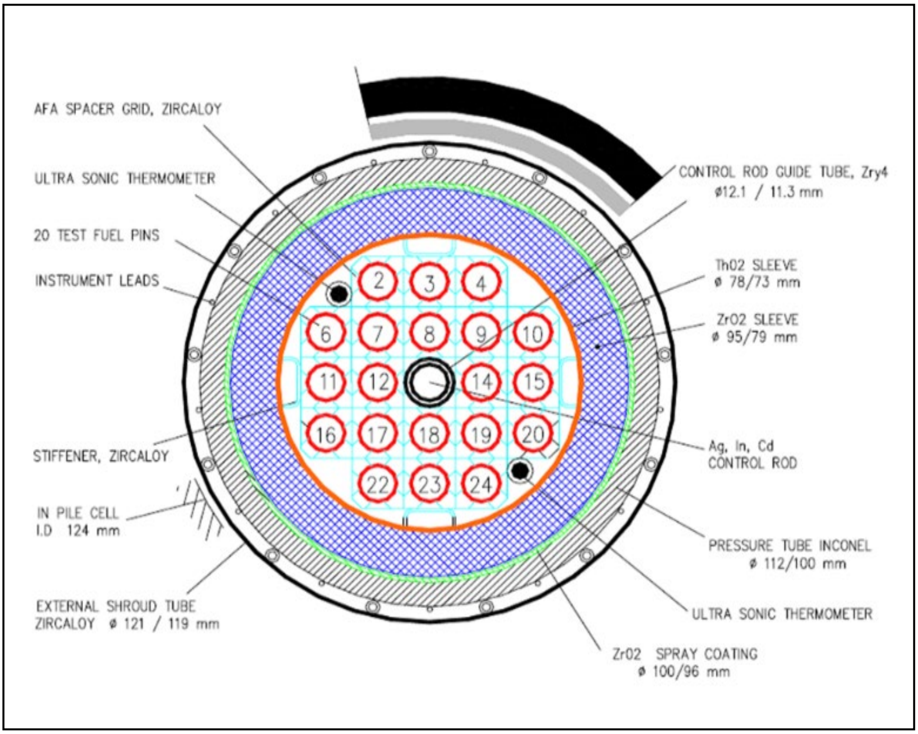

Fig. 16. PHEBUS FPT-1 Experiment Fuel Bundle [75]

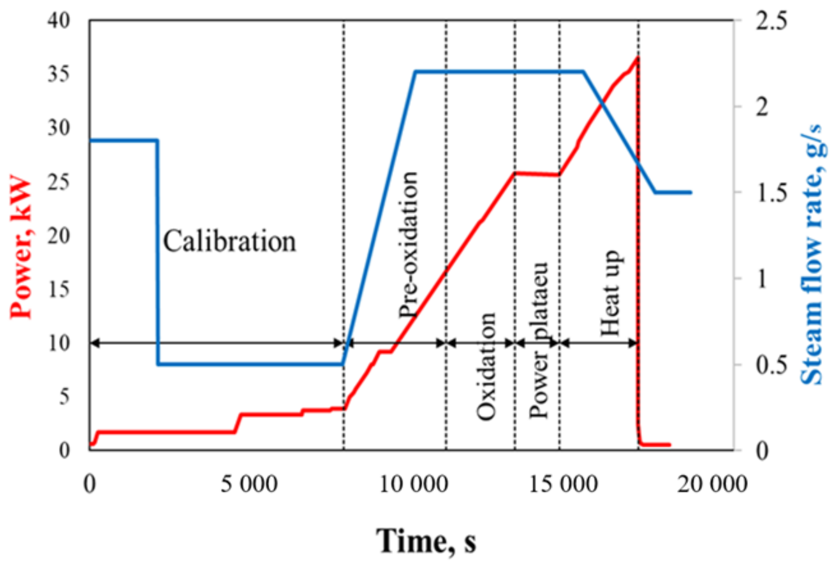

Fig. 17. Power and Steam Mass Flow Rate of PHEBUS FPT-1

Model Development

The RELAP/SCDAPSIM severe accident code was used for the development of the PHEBUS FPT-1 test model. The model focuses on simulating the physical phenomena that occur under severe accident conditions, which can lead to partial core melting. The developed model utilises a pre-existing model of the RELAP5/SCDAPSIM severe accident code, which incorporates the core and a U pipe that represents the steam generator.

In the RELAP part of the model (see Fig. 18), the boundary conditions were represented by time-dependent volumes 80 and 180, which facilitated the injection of steam and water into the system. Steam was introduced into the system through the branch component 90 via the time-dependent junction 85. The flow of steam from the branch to the pipe component 102 was regulated by the valve component 91, while the time-dependent junction 92 connected the branch component 90 with the pipe component 100, both of which represent the core. The two pipes 102 and 100 are connected through 11 single junctions (from 31 to 41), which served as crossflow junctions to manage the flow between the pipe components. The steam generator was modelled using pipe components 130, 140, and 141, connected by single junctions 131, 132, and 133, and further linked to the branch component 142. This structure was extended to include two additional pipe components 143 and 144, which were connected via a single junction 136 to the time-dependent volume 150 PDV. The surrounding shroud was modelled as a pipe component 200, with water being injected into this component through the time-dependent junction 185 and subsequently connected to the sink (time-dependent volume 230) via a single junction 186.

The SCDAP part of the PHEBUS FPT-1 test was modelled using five SCDAP components as presented in Fig. 19. These components included are: Component 1 shows the inner ring of eight irradiated fuel rods and was modelled as Fuel SCDAP component; Component 2 represents the control rod and was modelled as PWR control rod SCDAP component; Component 3 introduces the outer ring of ten irradiated fuel rods; Component 4 highlights two fresh fuel rods and was modelled as Fuel SCDAP components; and Component 5 represents the shroud and it was modelled as SCDAP Shroud component. The shroud has many different layers (see Fig. 19 (b)). This comprehensive modelling approach ensured that all the processes that occurred under severe accident conditions in the experiment were accurately captured.

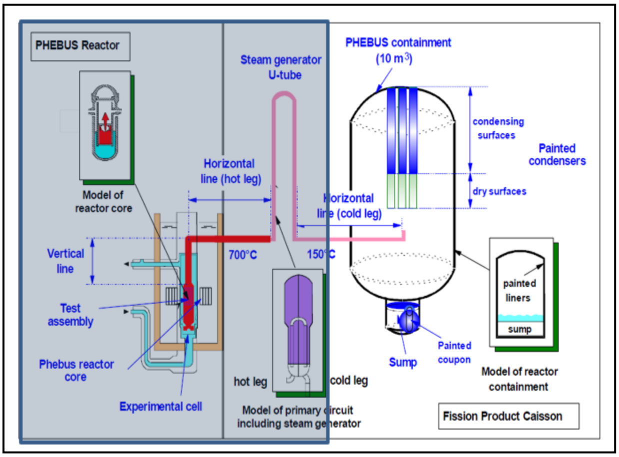

a)

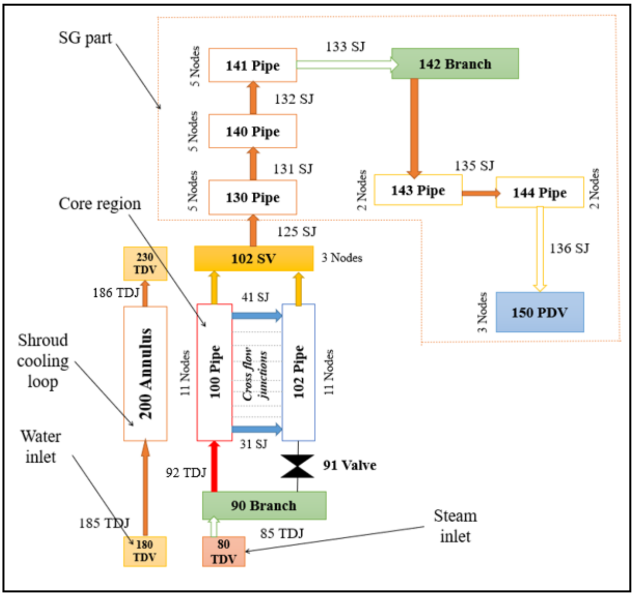

b)

Fig. 18. RELAP Part of PHEBUS FPT-1: a) The Modelled part is shaded; b) Nodalisation scheme

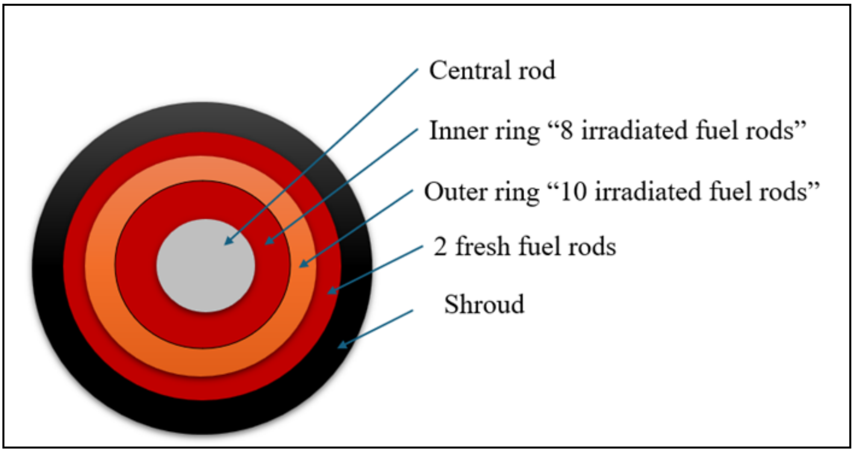

a)

Layer material	Explanation	Layer thickness, mm
12	Inconel	6
55	Coating	2
50	Gap	0.5
11	ZrO_2	8
50	Gap	0.5
10	ThO_2	2.5
51	Zr_4	0.2

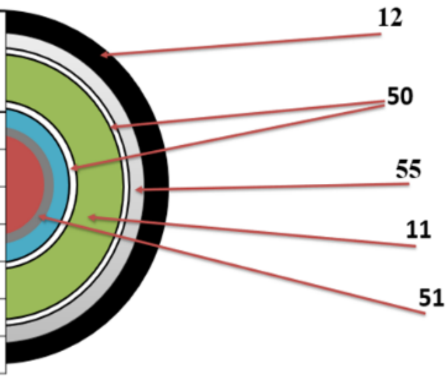

b)

Fig. 19. SCAP Part of PHEBUS FPT-1: a) Fuel bundle nodalisation, b) Shroud nodalisation

The RELAP/SCDAPSIM code has certain limitations that prevent it from evaluating the FP release to the containment and the processes in there. However, RELAP/SCDAPSIM can model FP release from the fuel-to-clad gap by grouping them into two categories: non-condensable gases (combination of all Xe, Kr and He gases) and soluble gases (combination of all CsI and CsOH gases). To overcome these limitations, the CORSOR-M model was selected for the analysis of fission product release. The CORSOR-M model is simple and is used for evaluating the release of fission products, which are produced solely from the fuel. The fission products released from the fuel are calculated according to the temperature of the fuel cladding. The CORSOR-M model uses the Arrhenius formula to calculate the fractional release rate coefficient [76].

$$k = k_0 \, exp\left(-\frac{Q}{RT}\right) \qquad \text{(Equation 2-1)}$$

Equation 2-1 allows for computation of the release rate coefficient (k) as a function of species-dependent constants k_0 and Q (min^{-1} and kcal/mol, respectively), the absolute temperature T in units of K, and the gas constant of R (1.987×10^{-3} kcal/mol-K). The k_0 and Q values have many different values depending on the species type, and they are based on modifications to the CORSOR-M model. For the evaluation of the fission products release of Cs and I using the CORSOR-M model in this work, these constant values are used ($k_0 = 2 \times 105\ min^{-1}$; $Q = 63.8$ kcal/mol).

The k can then be used in Equation 2-2 to calculate the mass of the fission product species released from the fuel:

$$FP_r = FP(1 - exp(-k\Delta t)) \qquad \text{(Equation 2-2)}$$

where FP presents the fission product species mass at the first time-step, and Δt presents the difference in time between the time steps. The CORSOR-M model is used to evaluate the release of fission products not only for RELAP/SCDAPSIM severe accident codes but also in different severe accident codes, such as MELCOR and ATHLET-CD [76].

Control system data can be integrated using the RELAP/SCDAPSIM code. Additional quantities can be calculated using this option in addition to the quantities typically calculated. A variety of control component types are available to choose from, including SUM, MULT, DIV, DIFFRENIT, INTEGRAL, FUNCTION, and others [76]. Taking advantage of these possibilities, the CORSOR-M model was implemented in the PHEBUS FPT-1 model (input deck). This allowed us to calculate fractional release rate coefficients via Equation 2-2 at each step of the calculation, using the temperatures calculated by RELAP/SCDAPSIM for the different components at the various nodes. The average fractional release rate coefficients calculated were determined by considering the number of pivot nodes and components incorporated in the PHEBUS FPT-1 modelling package. The initial mass of caesium and iodine was determined by IRSN. The release ratio was subsequently calculated. Thus, the caesium and iodine release ratio at each time step of the calculation was calculated using fuel rod shell temperatures calculated via RELAP/SCDAPSIM models.

2.4.2 QUENCH-06 Test

The QUENCH-06 test is conducted at KIT apart from the QUENCH program experiments to investigate fuel assembly behaviour under severe accident conditions [63]. The QUENCH-06 test is an out-of-pile test, in which fuel rod simulators are used for the investigation instead of actual fuel rods. The test is equipped with 21 fuel rod simulators, each ~2.5 m in length, and four corner rods (see Fig. 20). The fuel rod simulators are held in position by five grid spacers. The grid spacers are made of zircaloy and inconel in the lower bundle zone (Fig. 21). The fuel rod simulator cladding material is identical to that used in PWRs, in terms of material and dimensions, i.e., Zircaloy-4, with an outside diameter of 10.75 mm and a wall thickness of 0.725 mm. The fuel rod simulators are maintained at a pressure of 0.22 MPa with a mixture of 95% argon and 5% krypton. The krypton additive enables the detection of fuel rod failure during the experiment using the mass spectrometer. The QUENCH-06 test bundle is surrounded by a shroud and cooling jacket. The shroud material is Zircaloy-04, and the shroud is insulated with ZrO_2 material. The cooling jacket material is from Inconel [63]. The QUENCH-06 test consists of three distinct operational phases (see Fig. 22): pre-oxidation (from 1 965 to 5 965 seconds), transient (from 5 965 to 7 179 seconds), and quenching, which begins at 7 179 seconds. The pre-oxidation phase is crucial for forming an oxide layer comparable to that present in the reactor core during normal operation. The transient phase simulates the accident scenario, specifically the fuel drying out. Finally, the quenching phase replicates the safety measures taken to restore the reactor's coolability, such as injecting water into the overheated core.

Throughout the experiment, argon is injected at a constant flow rate of 3 g/s, maintaining it until the end of the test. Steam is also injected at a constant flow rate of 3 g/s, continuing until the conclusion of the transient phase. Water injections commenced 16 seconds prior to the start of the quenching phase, with a constant flow rate of 40 g/s and were maintained until the experiment concluded. The total amount of hydrogen generated during the QUENCH-06 test was 36 g, with 32 g produced before quenching and an additional 4 g generated during the quenching phase [63], [64].

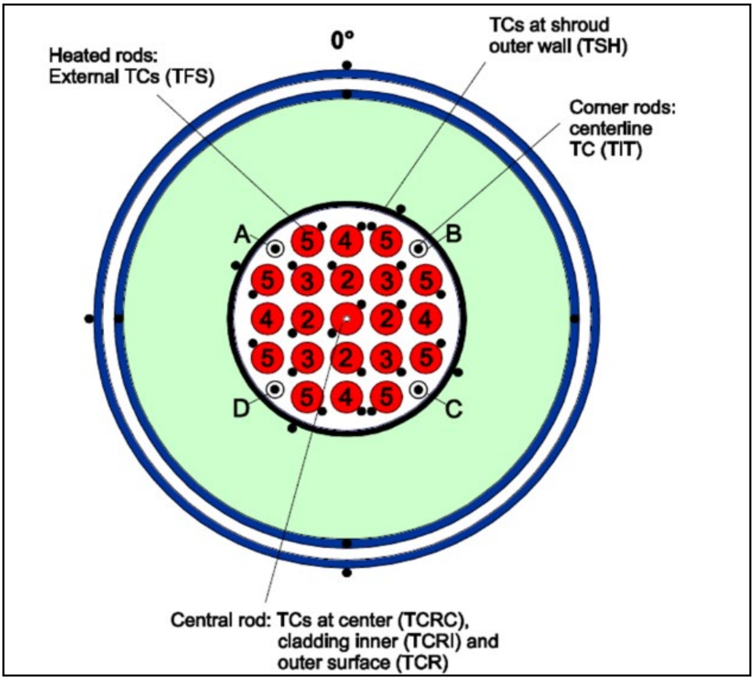

Fig. 20. QUENCH-06 Test Fuel Bundle [63]

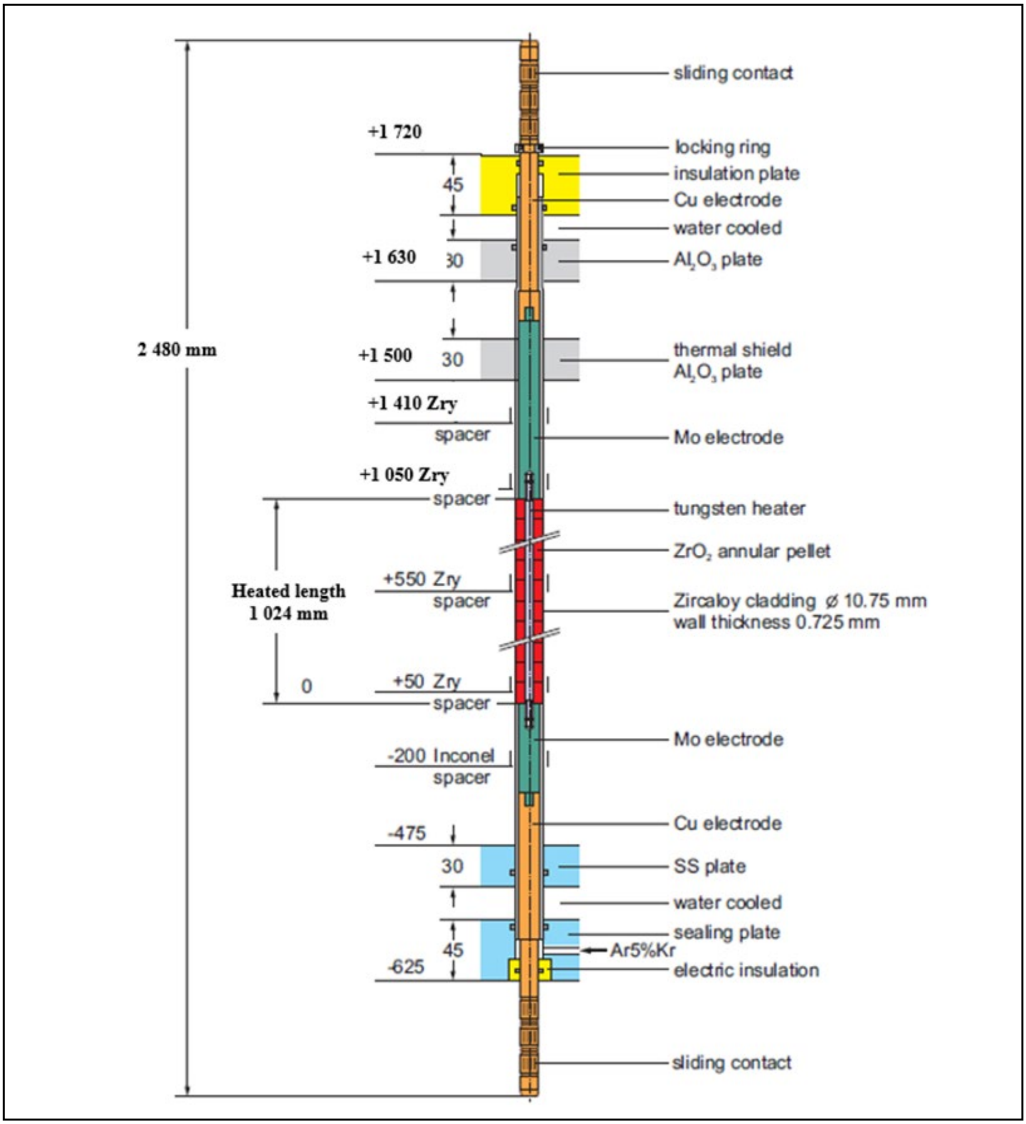

Fig. 21. Heated Fuel Rod Simulator [63]

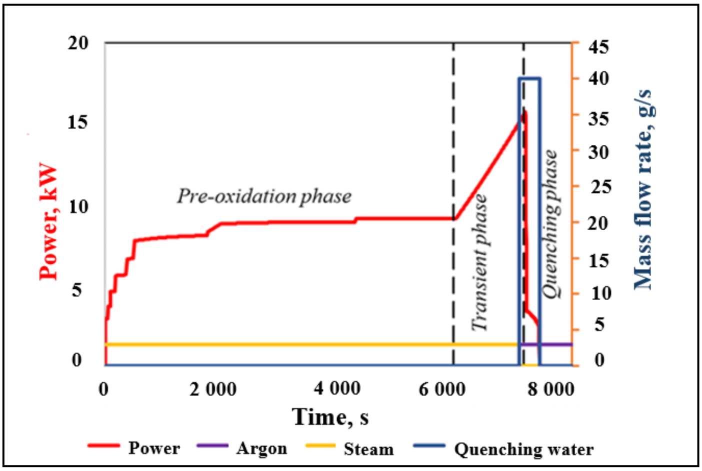

Fig. 22. QUENCH-06 Test. Power and Mass Flow Rate of Argon, Steam, and Quenching Water [77]

Model Development

The QUENCH-06 test facility was modelled using the RELAP/SCDAPSIM code, with the RELAP part dedicated to capturing the boundary conditions and fluid dynamics. In the RELAP model, boundary conditions were represented by time-dependent volumes and junctions, ensuring accurate simulation of the test conditions. Specifically, time-dependent volumes 001, 003, and 005 were used to model the injection of Argon, Steam, and quenching water, respectively. These volumes were connected to the branch component 007 via time-dependent junctions 002, 004, and 006 (as shown in Fig. 23). The central rod, corner rods, inner ring, and outer ring of the test bundle were represented by a pipe component 010, which integrated these key elements into a cohesive model. The head of the bundle, responsible for removal processes, was modelled as a time-dependent volume 008. Surrounding the bundle was an annular cooling jacket, modelled using two pipe components, 013 and 018, which were connected to sinks and sources represented by time-dependent volumes 011, 016, 015, and 020. The flow of water and argon within this setup was precisely controlled by the time-dependent junctions, allowing for accurate simulation of the cooling and gas flow processes during the test.

For the SCDAP part of the model, the QUENCH-06 test bundle was divided into five components, as depicted in Fig. 24. Component 1 represented the central rod, which was modelled using the SCDAP Fuel component. Component 2 corresponded to the inner ring, consisting of eight fuel rod simulators, and was modelled using the SCDAP Cora component. Component 3 represented the outer ring, featuring twelve fuel rod simulators, which were also modelled as an SCDAP Cora component.

Component 4 included the four corner rods, which were modelled as an SCDAP Fuel component. Finally, Component 5 represented the shroud, modelled using the SCDAP

Shroud component. This detailed modelling approach ensured that all critical aspects of the QUENCH-06 test were accurately represented, allowing for a comprehensive analysis of the physical phenomena, including heat transfer, cladding oxidation, and hydrogen generation, under severe accident conditions.

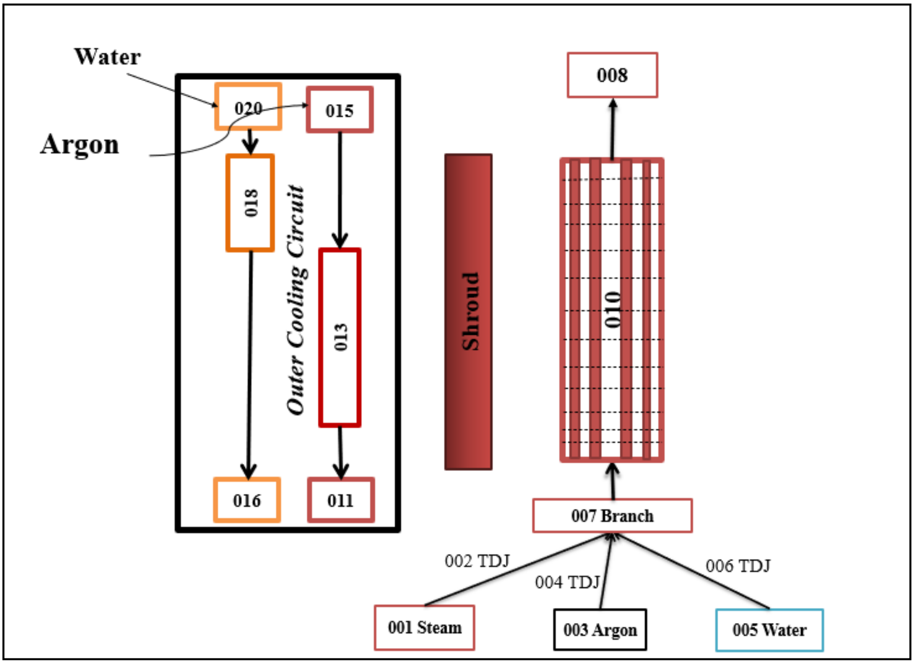

Fig. 23. QUENCH-06 Test Nodalization Scheme RELAP Part

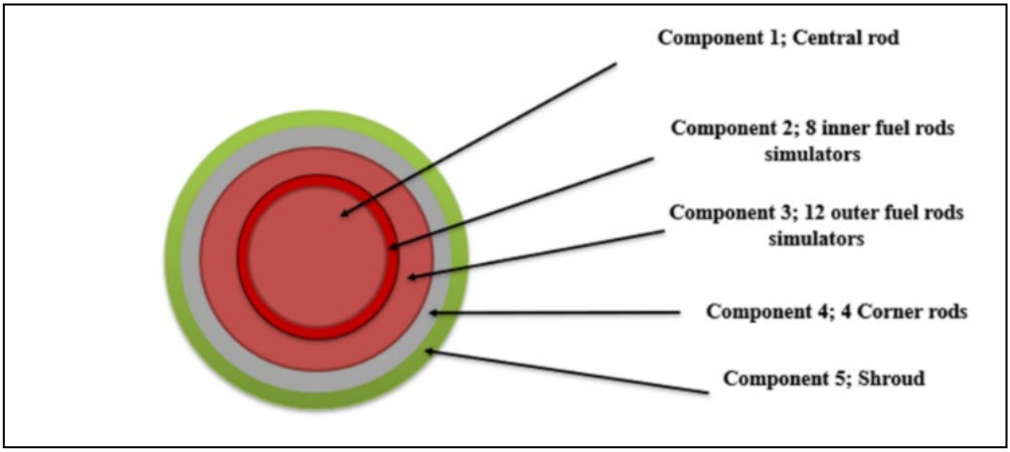

Fig. 24. QUENCH-06 Scheme SCDAP Part

2.4.3 Selection of the BE Method and Tool for the Application of BEPU Approach to Calculation Results

For the application of the BEPU approach to calculation results (to quantify calculation uncertainties), it is necessary to select the BE method that will be applied and to choose the statistical tool for easier application of this method. BE methods and tools were presented in the Section 1.5 and in the Table 3, the advantages and disadvantages of different BE methods were introduced. From this table, the GRS method [44] is selected for this work based on the comparison between the BE methods, which are presented in Table 3. The GRS method is more appropriate for severe accident analysis due to its systematic and comprehensive approach, which focuses on uncertainty and sensitivity analysis. The GRS method was extensively validated using different severe accident codes, such as ATHLET-CD, to ensure its reliability in modelling complex reactor core behaviour under accident conditions. The strength of the GRS method lies in its capability to manage and quantify uncertainties. The GRS method uses the Wilks formula [31], which helps calculate the minimum number of simulations required to estimate output variables with a 95% probability and confidence levels.

The statistical tools for the easier application of the selected BE method were discussed in the Section 1.5. The comparison between these tools is presented in Table 4, according to which the SUSA tool [49], [50] was selected for this work. The SUSA tool, developed by GRS, is considered an advanced tool for performing uncertainty and sensitivity analysis. The SUSA tool employs statistical methods, such as Monte Carlo simulations, to evaluate the influence of uncertain input parameters on severe accident simulation results. Monte Carlo methods are based on extensive random sampling of input uncertain parameters to create a probabilistic understanding of the model’s behaviour. The coupling between RELAP/SCDAPSIM severe accident code and the SUSA tool enables a comprehensive analysis of uncertainty and sensitivity, identifying which input uncertain parameters have the highest influence on selected FOMs. In addition, the SUSA tool includes a user-friendly graphical interface that provides better visualisation and interpretation of the results.

The schematic view of the application of the best estimate approach and the evaluation of uncertainties and sensitivities in the calculation results is presented in Fig. 25. The starting point is the selection of uncertain parameters based on the selected FOMs. In this work, uncertain parameters are initial parameters, boundary conditions and modelling parameters. The statistical tool SUSA generates sets of uncertain parameters for the calculations of the RELAP/SCDAPSIM code in order to evaluate calculation uncertainties. The number of the calculation runs depends on the probability and confidence level, which is calculated according to the Wilks formula [78]. For the uncertainty analysis, a 95% confidence level was selected.

According to Wilks' formula, it is necessary to perform 93 calculation runs with the RELAP/SCDAPSIM code. SUSA analyses the calculation results and gives lower and upper uncertainty limits of the calculation results.

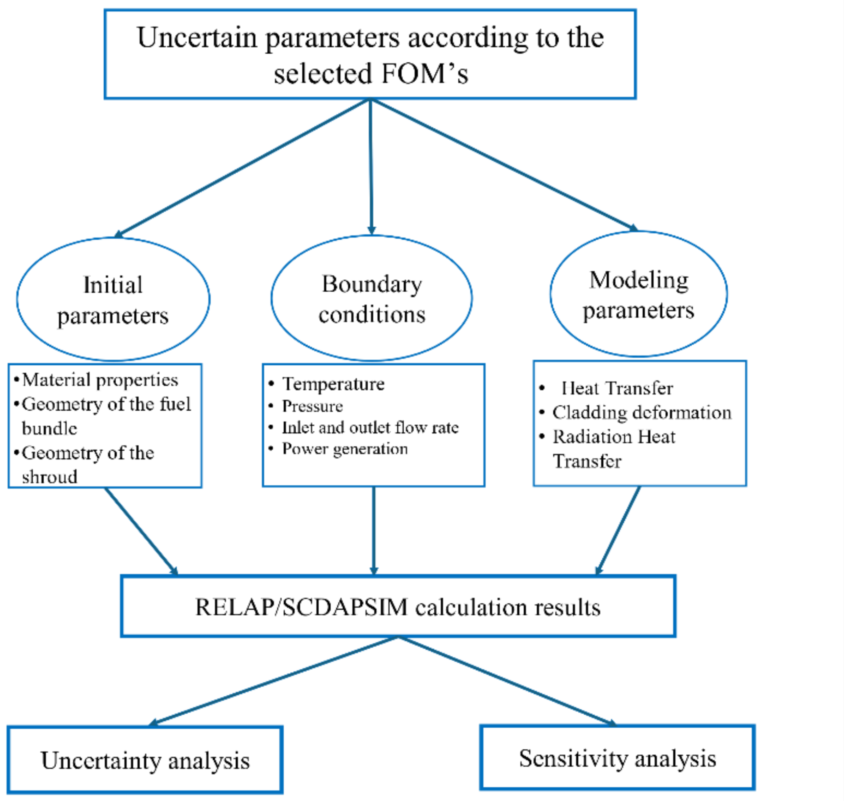

Fig. 25. Application of the Best Estimate Approach Plus Uncertainty

The next step is to perform a sensitivity analysis of the calculation results. For the sensitivity analysis, various correlations are used to evaluate the influence of initial uncertain parameters on the results. For sensitivity analysis in the nuclear field, Pearson's correlation, Spearman's rank correlation, and Kendall's rank correlation are commonly used.

- **Pearson Correlation:** The Pearson correlation coefficient is widely used to measure the linear relationship between input parameters and output results. It provides a quantitative assessment of how strongly two variables are linearly related, making it a valuable tool for identifying direct proportionality between uncertain inputs and their effects on the system's behaviour [79].

- **Spearman Rank Correlation:** The Spearman rank correlation is a non-parametric measure that evaluates the monotonic relationship between two variables. Unlike Pearson, which assumes a linear relationship, Spearman is useful for capturing both linear and non-linear relationships, particularly when the data does not meet the assumptions of normality. This makes it highly effective in scenarios where the relationship between variables is complex or non-linear [80], [81].
- **Kendall Rank Correlation:** Kendall's tau coefficient is another non-parametric statistic used to assess the ordinal association between two variables. It is especially useful in situations where the data may contain ties or when the sample size is small. Kendall's correlation is often preferred when the goal is to understand the concordance between the ranks of the variables, providing a robust measure of association in cases where other correlations might be less effective [80], [82].

Each of these correlation methods offers distinct advantages, and the choice of which to use depends on the specific nature of the data and the analysis goals. Analysing these correlations, analysts in the nuclear field can gain a deeper understanding of how initial uncertainties propagate through the system, ultimately influencing the safety and performance outcomes of nuclear reactors. Here is a detailed exploitation for each correlation:

- **The Pearson correlation coefficient (r):**

It quantifies the linear correlation that exists between two variables. It applies to the parametric approach. The range of the Pearson correlation coefficient is between -1 and +1. As the coefficient approaches values of +1 or -1, the strength of the linear correlation (be it negative or positive) between the variables increases [79]. Pearson correlation coefficient (r) is given in Equations 2-3, 2-4, and 2-5.

$$r(a,b) = \frac{\sum_{i=1}^{n}(x_i+\bar{X})(y_i-\bar{Y})}{\left(\sum_{i=1}^{n}(x_i-\bar{X})^2\sum_{i=1}^{n}(y_i-\bar{Y})^2\right)^{0.5}} \quad \text{(Equation 2-3)}$$

$$\bar{X} = \frac{1}{n}\sum_{i=1}^{n} x_i \quad \text{(Equation 2-4)}$$

$$\bar{Y} = \frac{1}{n}\sum_{i=1}^{n} y_i \quad \text{(Equation 2-5)}$$

where $\bar{X}$ and $\bar{Y}$ the means of variables X, Y, and *n* is the size of the sample.

- **The Spearman rank correlation coefficient (r_S):**

It applies to the non-parametric approach. The Pearson correlation coefficient has been viewed as an application to the rank R [80], [81]. Its range is equivalent to the Pearson rank correlation coefficient. The Spearman rank correlation coefficient (r_S) is given by Equation 2-6.

$$r_s(a,b) = \frac{\sum_{n=1}^{n}\left(R(x_i)-\frac{1}{2}(n+1)\right)(R(y_i)-\frac{1}{2}(n+1))}{\sum_{n=1}^{n}\left(Rx_i-\frac{1}{2}(n+1)\right)^2\left[\sum_{n=1}^{n}(R(y_i)-\frac{1}{2}(n+1))^2\right]^{0.5}} \qquad \text{(Equation 2-6)}$$

where *R* means the rank of variables X, and Y.

- **The Kendall rank correlation coefficient (τ):**

This approach is applicable to non-parametric methods. Similar in range to the Pearson and Spearman rank correlation coefficients, it extends a range of -1 to +1 [80], [82]. The Kendall rank correlation coefficient (τ) is given by Equation 2-7.

$$\tau = \frac{c-d}{\frac{1}{2}n(n-1)} \qquad \text{(Equation 2-7)}$$

where *c* means concordant, *d* means discordant, and *n* is the number of observations.

- Concordant (c): means that the ranks agree for any pair of observations; $X_i > X_j$ and $Y_i > Y_j$, or $X_i < X_j$ and $Y_i < Y_j$,
- Discordant (d): means that the ranks disagree for any pair of observations; $X_i > X_j$ and $Y_i < Y_j$ or $X_i < X_j$ and $Y_i > Y_j$.
- Tied pairs: when the variables have the same ranks. Kendall's rank coefficient (τ_b) for tied pairs is given in Equation 2-8:

$$\tau_b = \frac{c-d}{\sqrt{0.5n(n-1)}-t\sqrt{0.5n(n-1)\grave{u}}} \qquad \text{(Equation 2-8)}$$

Where t indicates tied pairs in X when $X_i = X_j$, and $\grave{u}$ indicates tied pairs in Y when $Y_i=Y_j$. A strong positive or negative correlation between variables is indicated by the Kendall's rank correlation coefficient when its value is approximately equal to or less than +1 or -1. A correlation between variables is absent when their values are equal to or near zero.

- **The Determination coefficient (R^2):**

This R^2 coefficient is determined as the square of the population correlation coefficient, which measures the connection between the code result Y and the variable X obtained from linear regression Y using the parameters $X_1, X_2, \ldots\ldots, X_{npar}$. The data provided illustrates the percentage of the overall variance in code results Y that can be accounted for by the uncertain parameters $X_1, X_2, \ldots, X_{npar}$, as represented by the linear regression of Y on the parameters [83], [84]. The Determination coefficient (R^2) is given by Equation 2-9:

$$R^2 = \frac{var\ (\hat{y})}{var\ (y)} \qquad \text{(Equation 2-9)}$$

The R^2 value is employed to evaluate the quality of the correlation coefficient. R^2 values vary from 0 to +1. The regression coefficient of the sensitivity parameters may be erroneous if R^2 is less than 0.6; this is due to an excessive number of incomprehensible parameter variations. In such situations, it is important to employ different methodologies when assessing the sensitivity of calculation results to parameter variations, such as:

1. The Sobol' method is a variance-based global sensitivity analysis technique, which handles non-linearity and non-monotonicity. The Sobol' method can manage complex models that exhibit non-linear and non-monotonic behaviour. It provides quantitative sensitivity indices, which are more informative than qualitative results from screening methods. It can account for interactions between parameters, providing a comprehensive understanding of how parameters jointly influence the model output [85], [86].
2. Support Vector Machines (SVM), which is known as a powerful supervised learning algorithm used for classification and regression. It is particularly effective in high-dimensional spaces and when dealing with small datasets [87].
3. Kriging (Gaussian process models) is widely used in spatial statistics, engineering, and machine learning for predicting unknown values based on spatial correlations [88].

2.5 Asymmetric Geometry Experiments

Some advanced or experimental nuclear facilities may use asymmetrical core geometries to optimise neutron flux and cooling efficiency. Additionally, spent fuel pools and waste storage facilities usually have asymmetrical configurations, which is due to non-uniform loading from past operations or safety considerations for cooling and criticality control.

The QUENCH-20 test is considered a test from the QUENCH program which was conducted in KIT [89]. The QUENCH-20 test is an out-of-pile test equipped with a fuel rod simulator. The QUENCH-20 test is the first QUENCH test equipped with a BWR fuel bundle. The test bundle consists of a ¼ SEVA-96 OPTIMMA-2 BWR bundle with two plates of absorber blades. The test bundle contains 24 fuel rod simulators, which are arranged as seen in Fig. 26.

Description from previous works is used to describe the asymmetric geometry experiments[2]. The fuel rod simulators are electrically heated using tungsten heaters installed in the centre of each fuel rod simulator. The length of the heated part is 1024 mm. The fuel rod simulator pellet material is ZrO_2. The cladding material of the fuel rod simulators is identical to that of BWR fuel rod cladding, specifically Zircaloy-2 alloy. The fuel rod simulators were filled with krypton gas to an inner pressure of 5.5 bar. To maintain the fuel rod simulators in their position and reduce oscillation, five Inconel grid spacers are used, distributed along the test section. The fuel channel box separates the flow around the fuel rod simulators and the bypass flow between the fuel channel box and the shroud and is located around the fuel rod simulators. The fuel channel box and water channel box are made from ZIRLO alloy. A corner rod is located inside the water channel box and is made from Zircaloy-4. It could be removed during the test to measure the thickness of the oxide layer [89]. Two plates of absorber blades are located on either side, made from stainless steel and filled with B_4C pins. The Zircaloy-4 shroud is placed at the outer part of the fuel bundle and is surrounded by porous ZrO_2 thermal insulation. Out of insulation material, two Inconel cooling jackets are placed around. The inner and outer cooling jacket rings have argon flow between them.

The QUENCH-20 test has three test operational phases, which are pre-oxidation (0-14 400 s), transient (14 400 to 15 890 s), and quenching (15 890 to 17 760 s) (see Fig. 27). The Argon is injected at a constant mass flow rate of 3 g/s until the end of the test. Steam is injected with a constant mass flow rate of 3 g/s until the beginning of the quench phase. The water is injected at a rate of 50 g/s from the beginning of the quench phase until the end of the test. The total amount of hydrogen generated during the test is 57.5 g (47.5 g from Zr oxidation and 10 g from B_4C oxidation). The pre-oxidation phase is necessary to generate an oxide layer, similar to the one that forms in the reactor core over its operational lifetime. The transient phase simulates the accident scenario, specifically the fuel drying out. The quenching phase replicates the

[2] Elsalamouny N., Kaliatka T., Kaliatka A. "QUENCH-20 test analysis using RELAP/SCDAPSIM severe accident code". Nuclear Engineering and Design. Elsevier, 2024, Vol. 419, 112995, p. 1-12. ISSN 0029-5493. https://doi.org/10.1016/j.nucengdes.2024.112995.

application of safety measures, such as injecting water into the hot core, to restore the reactor's coolability [72].

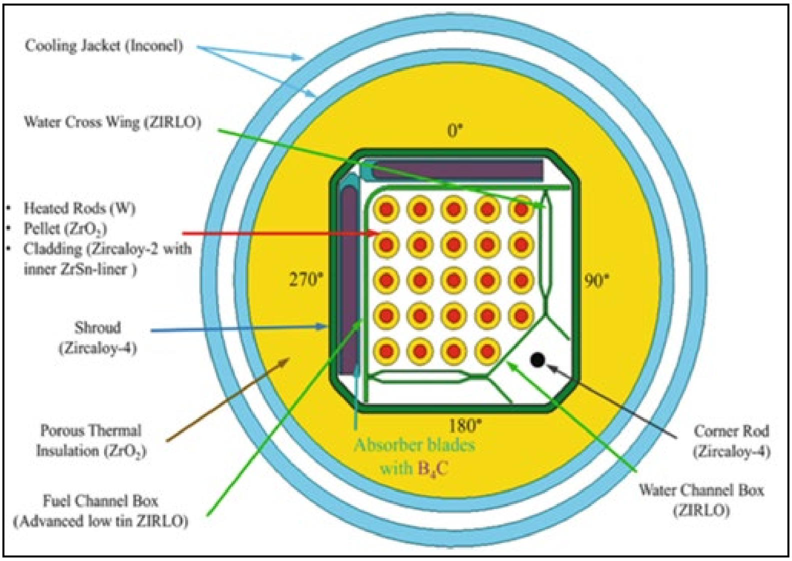

Fig. 26. QUENCH-20 Test Bundle [89]

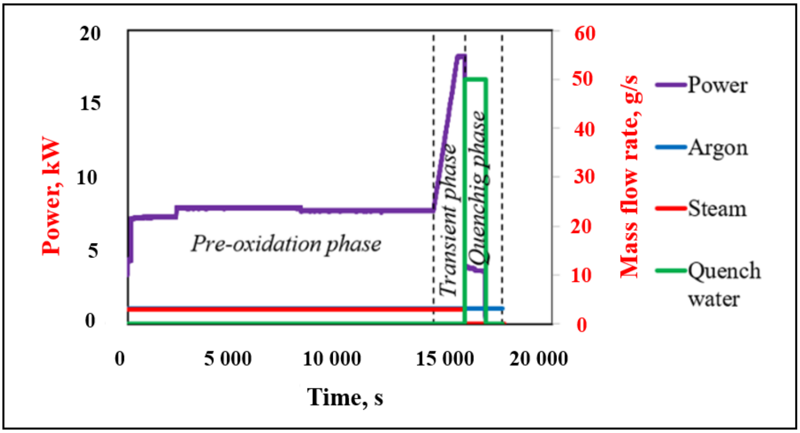

Fig. 27. QUENCH-20 Test, Power and Mass Flow Rate of Argon, Steam, and Quench Water

2.5.1 Model Development of QUENCH-20 Test

The QUENCH-20 test bundle features a square configuration, as illustrated in Fig. 26. The test assembly comprises two plates of absorber blades, filled with B_4C pins, positioned at the corners corresponding to 0° and 270°. In the corners at 90° and

180°, a water wing and corner rod are located. This arrangement results in a non-uniform temperature distribution in the radial direction during the test, primarily due to the varying coolability of the fuel rod simulators. These bundle characteristics present challenges for simulating thermal-hydraulic processes, as most thermal-hydraulic codes are designed to have cylindrical coordinates. Additionally, the oxidation of absorber blades containing B_4C is challenging to be evaluated, particularly for severe accident codes to evaluate the generated hydrogen, CO, CO_2, and CH_4. As previously mentioned, the RELAP/SCDAPSIM code includes two main components: RELAP for thermal-hydraulic processes and SCDAP for analysing processes within the bundle. To more accurately simulate the processes in the QUENCH-20 test, different modelling approaches were developed for the RELAP/SCDAPSIM severe accident code. Each approach has its advantages and disadvantages. More details could be found in the author's related work[3].

2.5.2 Pseudo-Symmetrical Model

Based on the experience gained from modelling symmetric experiments (PHEBUS FPT-1 and QUENCH-06) and the application of the best-estimate approach to symmetric geometry, this pseudo-symmetrical model was developed. At the beginning of the modelling process of QUENCH-20 test, it was observed that there are similarities in the boundary conditions and test operational phases between QUENCH-20 [72], [89] and QUENCH-06 [17], [63] tests. However, there are differences between the two tests (bundle structure, bundle type). QUENCH-20 test has a BWR fuel bundle, and QUENCH-06 test has a PWR fuel bundle. Fig. 28 (a & b) shows the similarities and differences in the boundary conditions between the two tests.

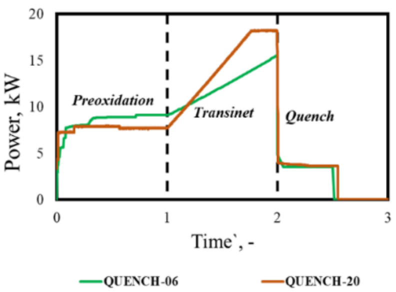

a) Power Values of QUENCH-20 and QUENCH-06 Test During Test Phases

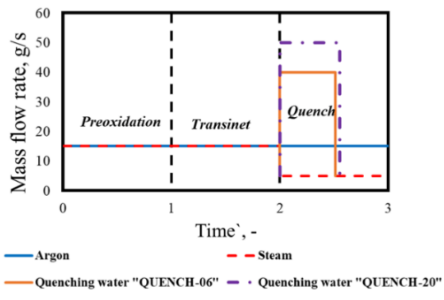

b) Argon, Steam and Quench Water Values During Test Phases

Fig. 28. Similarities and Differences Between QUENCH-20 and QUENCH-06 Tests

As previously mentioned, QUENCH-06 and QUENCH-20 share similar boundary conditions, power distribution, and operational test phases. Therefore, it was

[3] Elsalamouny N., Kaliatka T., Kaliatka A. "QUENCH-20 test analysis using RELAP/SCDAPSIM severe accident code". Nuclear Engineering and Design. Elsevier, 2024, Vol. 419, 112995, p. 1-12. ISSN 0029-5493. https://doi.org/10.1016/j.nucengdes.2024.112995.

decided to initially use the model developed for QUENCH-06, with necessary adaptations for the QUENCH-20 test bundle to a pseudo-symmetrical model. The RELAP nodalisation part of the model required minimal modifications; only component 010 was adjusted to align with the specific geometry of the QUENCH-20 test bundle (see Fig. 29). Regarding the SCDAP part of the model, the structure was maintained as it was for QUENCH-06, with updates made to the geometrical data to reflect the specific characteristics of the QUENCH-20 bundle. Five SCDAP components (Fig. 30) were used: where the central rod is modelled as a Cora component, the inner ring 8 fuel rod simulators is modelled as a Cora component, the outer ring 15 fuel rod simulators is modelled as a Cora component. The water channel box, fuel channel box, water wings, absorber blades and shroud are modelled as a Shroud component. Fig. 31 shows the heat transfer modelling for the pseudo-symmetrical model, where the heat generated from the fuel rod simulators is transferred directly to the shroud.

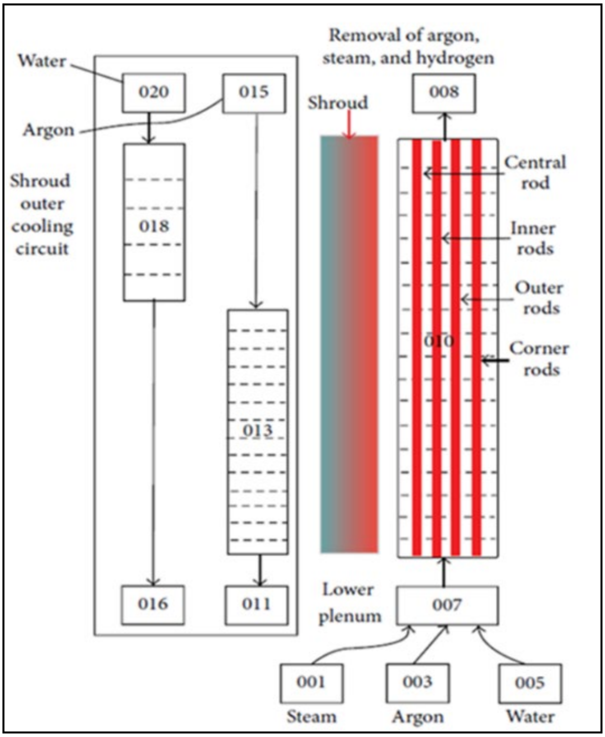

Fig. 29. Nodalisation Scheme RELAP for the Pseudo-Symmetrical Model [64]

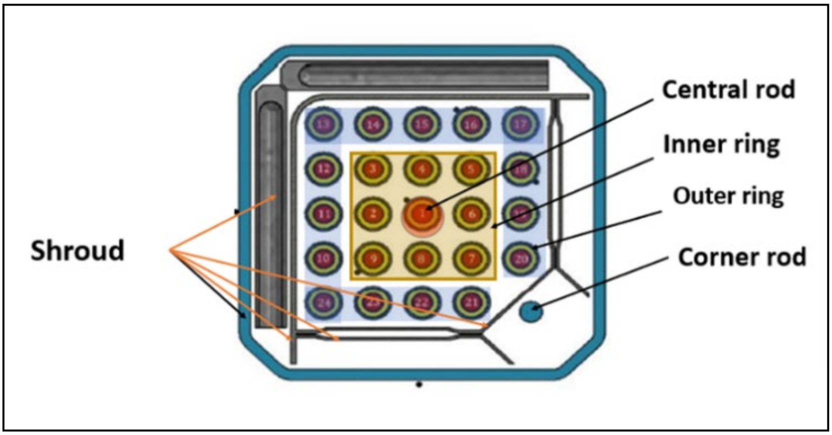

Fig. 30. The Nodalisation Scheme SCDAP for the Pseudo-Symmetrical Model [4]

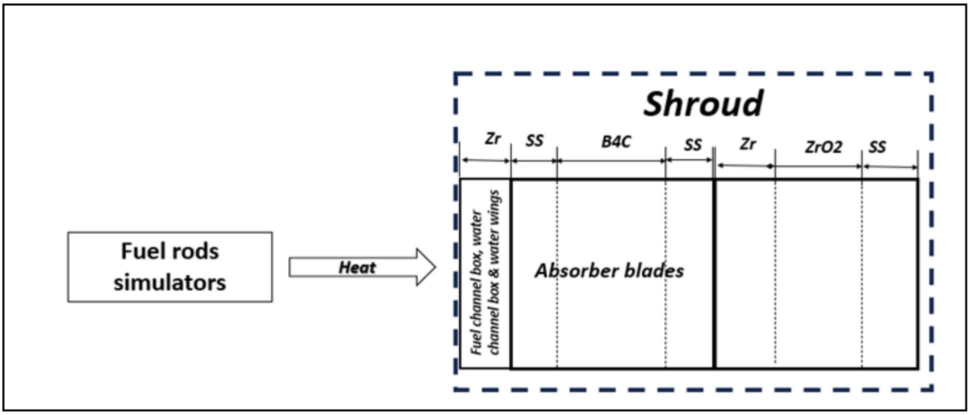

Fig. 31. Heat Transfer Modelling in the Pseudo-Symmetrical Model [4]

2.5.3 Component-Level Modelling

Most of the discussions in this section come from the author's related work [4]. To achieve a more realistic and accurate simulation of the QUENCH-20 test, component-level modelling is employed. Three different modelling approaches were developed to model the QUENCH-20 test components. All modelling approaches utilise the same RELAP nodalisation scheme, with identical initial parameters and boundary conditions. Fig. 32 and Fig. 33 illustrate the RELAP nodalisation scheme. The boundary conditions for the QUENCH-20 test bundle model are defined by time-dependent volumes 001, 003, 005, and 008. Volumes 001, 003, and 005 correspond to the parameters for steam, argon, and quench water, respectively. Time-dependent volume 008 serves as a sink. Time-dependent junctions 002, 004, and 006 manage the

[4] Elsalamouny N., Kaliatka T., Kaliatka A. "QUENCH-20 test analysis using RELAP/SCDAPSIM severe accident code". Nuclear Engineering and Design. Elsevier, 2024, Vol. 419, 112995, p. 1-12. ISSN 0029-5493. https://doi.org/10.1016/j.nucengdes.2024.112995.

injection of steam, argon, and quench water into the bundle. The lower part of the bundle is represented by branch component 007, while the bundle itself is described by two pipe components, 010 and 100, connected to branch component 007 below and branch component 090 above, which represents the top part of the bundle. Component 010 covers the hydraulic area (0.0046 m^2) within the fuel channel box, including the water wings and water channel box. Component 100 represents the hydraulic area around the absorber blades, having a total value of 0.000114 m^2. Branch 090 is connected to the time-dependent volume 008 via a single junction 023.

The shroud of the QUENCH-20 test facility is cooled by an outer cooling circuit. The RELAP module was used to model this circuit, incorporating time-dependent volumes and pipe components connected by time-dependent and single junctions. Time-dependent volumes 015 and 020 serve as sources (boundary conditions) for argon and water coolants, while volumes 011 and 016 act as sinks. These volumes are connected to pipe components 013 and 018 via time-dependent junctions 014 and 019, which provide cooling flow rates of 16 g/s for argon and 100 g/s for water, respectively. These flow rates feed into the cooling circuit through single junctions 012 and 017.

According to the experiment, the bundle length is approximately 2 500 mm, with a heated length of 1 024 mm. The absorber blades and fuel channel box have a length of 1 560 mm. The elevation measurements begin at 0 mm, located at the bottom of the heated assembly part. In the developed model, the bundle is simulated from an elevation of -475 mm to +1 600 mm. The bottom 175 mm of the bundle is covered by the branch component 007. The section from 300 mm to +1 260 mm is represented by the two pipe components 010 and 100, corresponding to the absorber blades and fuel channel box lengths as observed in the experiment. The top of the bundle, from +1260 mm to +1 600 mm, is modelled using the branch component 090. Pipe components 010 and 100 are divided into 15 internal nodes, with the first 12 nodes having a length of 100 mm each. Node 13 has a height of 124 mm, and the final two nodes have heights of 118 mm each. The heated section extends from node 3 to node 13, resulting in a total heated length of 1 024 mm, consistent with the experiment. In the model, the outer cooling circuit length corresponds to the length of the bundle. Cooling with argon is achieved using pipe component 013, which extends from -300 mm to +1 024 mm in elevation. Cooling with water is achieved through pipe component 018, which covers an elevation range from +1024 mm to +1600 mm. The internal nodalisation of pipe components 013 and 018 mirrors that of pipe components 010 and 100.

The fuel rod simulators, absorber blades, corner rod, and shroud were modelled using SCDAP components, as illustrated in Fig. 34. The 24 electrically heated fuel rod simulators were represented by three distinct SCDAP Cora components. The first Cora component models the central rod. The second component represents the inner ring, which comprises eight fuel rods surrounding the central rod. The third component models the outer ring, consisting of 15 fuel rod simulators. The corner rod, which is unheated, was modelled as a Fuel component using the SCDAP components.

For the shroud, including its thermal insulation, the Shroud component of SCDAP was employed. These SCDAP components form the core of all modelling approaches used for the QUENCH-20 test. However, the modelling of absorber blades, the fuel channel box, the water channel box, and the water wings varies between different approaches, reflecting the specific requirements and characteristics of each modelling scenario.

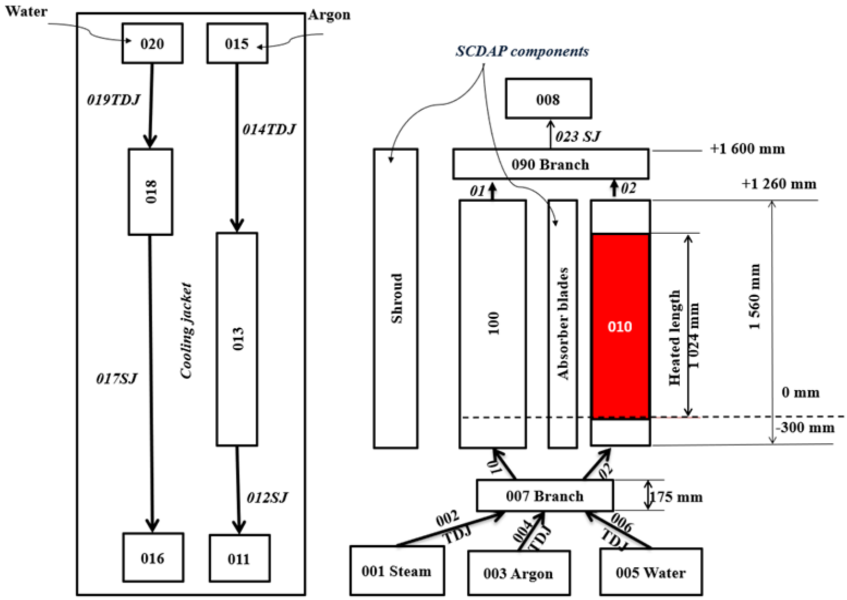

Fig. 32. QUENCH-020 Test Nodalization for the RELAP Part of the Model [5]

[5] Elsalamouny N., Kaliatka T., Kaliatka A. "QUENCH-20 test analysis using RELAP/SCDAPSIM severe accident code". Nuclear Engineering and Design. Elsevier, 2024, Vol. 419, 112995, p. 1-12. ISSN 0029-5493. https://doi.org/10.1016/j.nucengdes.2024.112995.

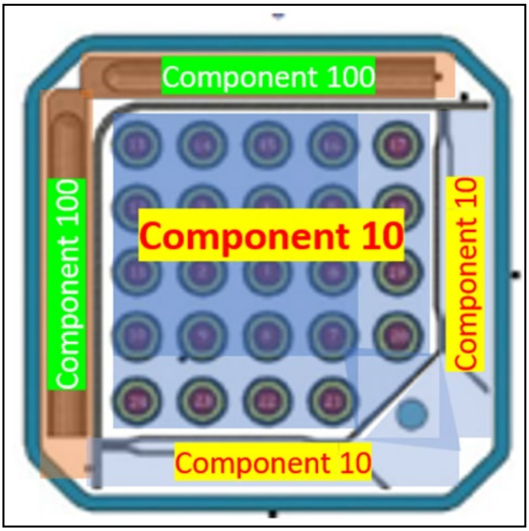

Fig. 33. Components of QUENCH-20 Test for the RELAP Part of the Model [6]

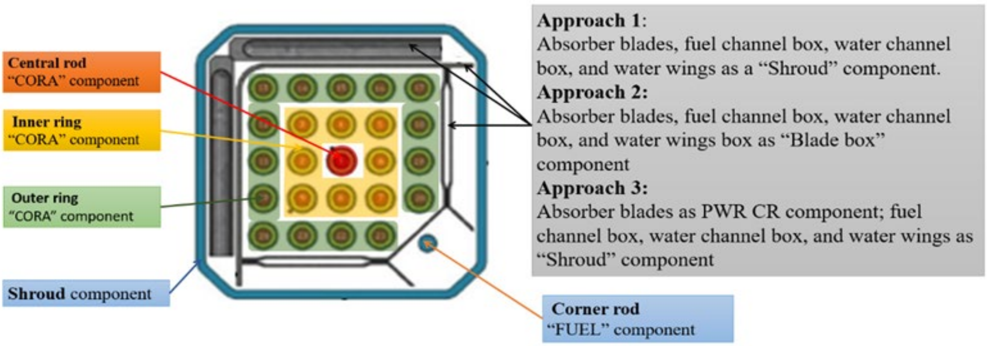

Fig. 34. QUENCH-20; SCDAP Part Scheme [9]

Table 7 presents the physical phenomena that are modelled for each component-level modelling approach and how they are modelled using different SCDAP components.

[6] Elsalamouny N., Kaliatka T., Kaliatka A. "QUENCH-20 test analysis using RELAP/SCDAPSIM severe accident code". Nuclear Engineering and Design. Elsevier, 2024, Vol. 419, 112995, p. 1-12. ISSN 0029-5493. https://doi.org/10.1016/j.nucengdes.2024.112995.

Table 7. The Phenomena Modelled Using Different Component-Level Approaches

Components	Phenomena	Pseudo-symmetrical model	Approach 1	Approach 2	Approach 3
Fuel rod simulators	Cladding oxidation, hydrogen generation, degradation	Cora component used in all components and all phenomena are covered in this component.			
Fuel channel box	Heat transfer between fuel rods and absorber blades. Zr oxidation. Degradation	Shroud component	Shroud component	Blade box component	Shroud component
		All phenomena are covered.	All phenomena are covered.	Limited heat transfer.	All phenomena are covered.
Water wings	Heat transfer between fuel rods and coolant inside the fuel channel box. Zr oxidation. Degradation	Shroud component	Shroud component	Blade box component	Shroud component
		All phenomena are covered.	All phenomena are covered.	Limited heat transfer.	All phenomena are covered.
Water channel box	Heat transfer between fuel rods and coolant inside the fuel channel box. Zr oxidation. Degradation	Shroud component	Shroud component	Blade-box component	Shroud component
		All phenomena are covered.	All phenomena are covered.	Limited heat transfer.	All phenomena are covered.
Absorber blades	Heat transfer between fuel rods and the shroud through absorber blades. SS, Zr and B_4C oxidation. Degradation	Shroud component	Shroud component	Blade-box component	PWR control rod component
		All phenomena are covered.	All phenomena are covered.	Limited heat transfer.	All phenomena are covered.
Corner rod	Heat transfer between fuel rods and the corner rod	Fuel component	Fuel component	Fuel component	Fuel component
		All phenomena are covered in this component.			

Components	Phenomena	Pseudo-symmetrical model	Approach 1	Approach 2	Approach 3
	through the water channel box. Zr oxidation. Degradation				
Shroud and insulation	Heat transfer between the fuel rod simulators and the shroud through internal structures. Zr oxidation	Shroud component	Shroud component	Shroud component	Shroud component
		Impossible to describe	All phenomena covered		

- **The first component level modelling approach, Approach 1**

The absorber blades, fuel channel box, water channel box, and water wings were modelled using the SCDAP Shroud component, as illustrated in Fig. 34. This component can be defined as either a single-layer or multi-layer structure, composed of various materials. In this particular modelling approach, the SCDAP Shroud component was divided into four layers: 1) zirconium (Zr), 2) stainless steel (SS), 3) boron carbide (B_4C), and 4) another layer of stainless steel, as shown in Fig. 35. The Zr layer represents the fuel channel box, water channel box, and water wings. The absorber blades are modelled as two stainless-steel blades that encase B_4C pins. The stainless-steel layers correspond to the SS blades that surround the B_4C pins, while the B_4C layer represents the pins themselves. The geometrical dimensions of these layers were determined based on the material masses used in the QUENCH-20 test. The SCDAP Shroud component is positioned between the outer ring of fuel rod simulators and the Shroud component, which, in this context, represents the actual shroud of the test bundle. Heat generated in the fuel rod simulators is transferred radially to this component, which then conducts the heat to the test bundle's shroud.

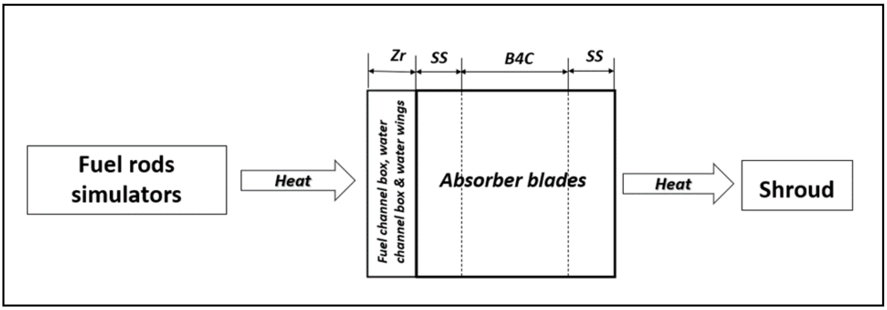

Fig. 35. Approach 1: Heat Transfer Modelling in a Radial Direction [7]

- **The second component level modelling approach, Approach 2**

In the QUENCH-20 test, the absorber blades, fuel channel box, water channel box, and water wings were modelled using the SCDAP Blade box component. This component within the SCDAP models is specifically designed to model Boiling Water Reactor (BWR) control blades and channel boxes [90], [91]. The Blade box component effectively captures the complex geometry and material composition of the BWR control blades and channel box. The internal modelling of these elements is accomplished through a set of local dimensions, which accurately represent the cross-sectional portion of the channel box and half of the control blade, as illustrated in Fig. 36. This approach ensures that the intricate interactions between the materials, such as heat transfer and structural integrity, are realistically simulated [90]. By using the Blade box component, the model faithfully replicates the behaviour of the absorber blades and channel box under test conditions, providing valuable insights into the thermal and mechanical responses during the QUENCH-20 experiment.

The dimensions on Fig. 36 are as described in the list below.

(1) The inner diameter of the stainless-steel absorber tube.
(2) The thickness of the stainless-steel absorber tube wall.
(3) The thickness of the gap between the absorber tube and the control blade sheath.
(4) The thickness of the stainless-steel control blade sheath.
(5) The distance between the control blade and the channel box.
(6) The thickness of the zircaloy channel box wall.
(7) The distance between the channel box and the fuel rods.
(8) The length (wetted perimeter) of the control blade and channel box SEGMENT NO. 1.
(9) The length (wetted perimeter) of channel box SEGMENT NO. 2.

[7] Elsalamouny N., Kaliatka T., Kaliatka A. "QUENCH-20 test analysis using RELAP/SCDAPSIM severe accident code". Nuclear Engineering and Design. Elsevier, 2024, Vol. 419, 112995, p. 1-12. ISSN 0029-5493. https://doi.org/10.1016/j.nucengdes.2024.112995.

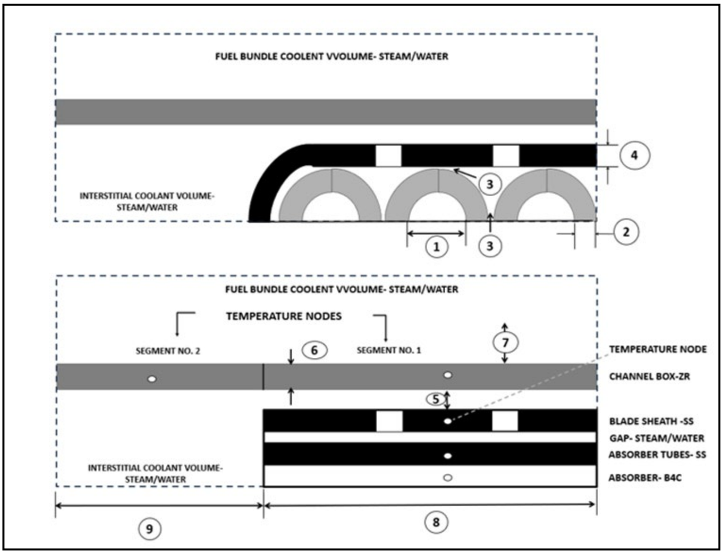

Fig. 36. Control Blade/Channel Box Dimensions Specified by the User [90]

The BWR control blade and channel box in the model are represented using two segments (more details are presented in the author's related article [8]). Segment 1 simulates the portion where the blade is located, including the B_4C (boron carbide), absorber tube, blade sheath, and part of the channel box itself [90]. This segment is divided into three radial nodes for the blade and one for the channel box, allowing for detailed modelling of the heat transfer and material behaviour within these regions. Segment 2 focuses solely on a portion of the channel box, utilising one radial node, and includes the region representing the interstitial coolant volume. The model explicitly computes axial conduction, relocation/solidification, oxidation, and radiation heat transfer using data from the previous timestep, incorporating these effects as constant terms in the energy equations. When considering material interactions such as B_4C/stainless steel and stainless steel/zircaloy, the melting temperatures of the combined materials are reduced due to Hofmann's reaction kinetics. In scenarios where material interaction occurs within a node, the model uses a eutectic liquefaction temperature for melting calculations, rather than the pure material's melting temperature. The liquefaction temperatures are approximately 1 505 K for B_4C/stainless steel mixtures and around 1 523 K for stainless steel/zircaloy mixtures [90], [91].

However, there are notable differences between the QUENCH-20 test and the Blade box component model that must be evaluated. The QUENCH-20 test features asymmetric geometry, resulting in a non-uniform temperature distribution. Additionally, the absorber blades in QUENCH-20 represent only half of the absorber blade cross-section, with B_4C pins horizontally located inside the stainless-steel

[8] Elsalamouny N., Kaliatka T., Kaliatka A. "QUENCH-20 test analysis using RELAP/SCDAPSIM severe accident code". Nuclear Engineering and Design. Elsevier, 2024, Vol. 419, 112995, p. 1-12. ISSN 0029-5493. https://doi.org/10.1016/j.nucengdes.2024.112995.

blades. These blades are also surrounded by a shroud, which differs from the standard Blade box component configuration. To accurately model the QUENCH-20 test using the Blade box component, it was necessary to adjust and recalculate the parameter values. The geometrical parameters required by the SCDAP Blade box component were recalculated based on the masses and volumes of materials used in the QUENCH-20 test, including the absorber blades, fuel channel box, water channel box, and water wings. The volume of B_4C was increased to match the B_4C density assumed by the Blade box component, which considers B_4C in powder form. In the QUENCH-20 test, there is only one channel box, and the side length of the absorber blade is nearly equal to the wall side length of the channel box. As a result, the heat generated in the fuel rod simulators is transferred radially to the channel box, which then transfers heat to the absorber blades, with no heat transfer to another channel box. Moreover, the Blade box component model does not account for heat transfer from the control blades. Consequently, when the Blade box component was used to model the absorber blades, fuel channel box, water channel box, and water wings of the QUENCH-20 test, no heat transfer was observed between this component and the shroud in the radial direction (see Fig. 37).

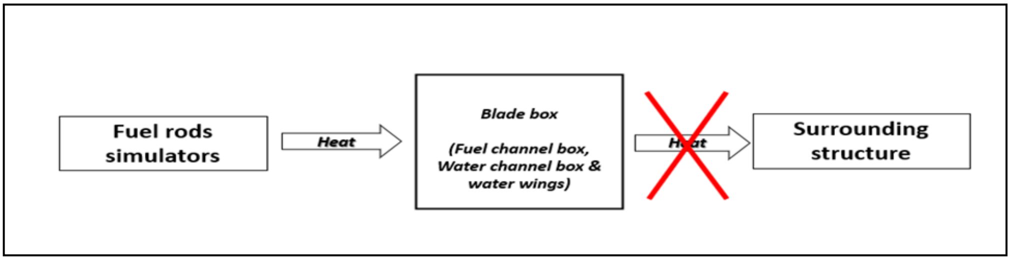

Fig. 37. Approach 2: Heat Transfer Modelling in Radial Direction [9]

- **The third component level modelling approach, Approach 3**

In this approach, two SCDAP components were utilised: the PWR control rod component to model the absorber blades, and the Shroud component to model the fuel channel box, water channel box, and water wings of the QUENCH-20 test (see Fig. 34). The PWR control rod component is specifically designed to simulate the behaviour of PWR control rods.

It calculates the control rod temperatures using the same heat conduction model as that used for fuel rods. These computational models account for 2D heat conduction, the oxidation of stainless steel (SS), zirconium (Zr), and boron carbide (B_4C), as well as the interactions between SS/B_4C and SS/Zr. Additionally, they simulate the melting and relocation of SS, Zr, and B_4C, and the generation of hydrogen from the oxidation reactions of these materials. The models also incorporate convective and radiative heat transfer from the shroud of the fuel rod simulators and the surrounding coolant [30]. PWR control rods consist of a set of absorber pins that are inserted inside a guide

[9] Elsalamouny N., Kaliatka T., Kaliatka A. "QUENCH-20 test analysis using RELAP/SCDAPSIM severe accident code". Nuclear Engineering and Design. Elsevier, 2024, Vol. 419, 112995, p. 1-12. ISSN 0029-5493. https://doi.org/10.1016/j.nucengdes.2024.112995.

tube. These control rods are strategically positioned within the fuel bundle to manage the nuclear reactions and power distribution (see Fig. 38). For the SCDAP PWR control rod component model, it is essential to specify the number of control rods and the pitch between them to reflect the physical arrangement and interactions within the system accurately.

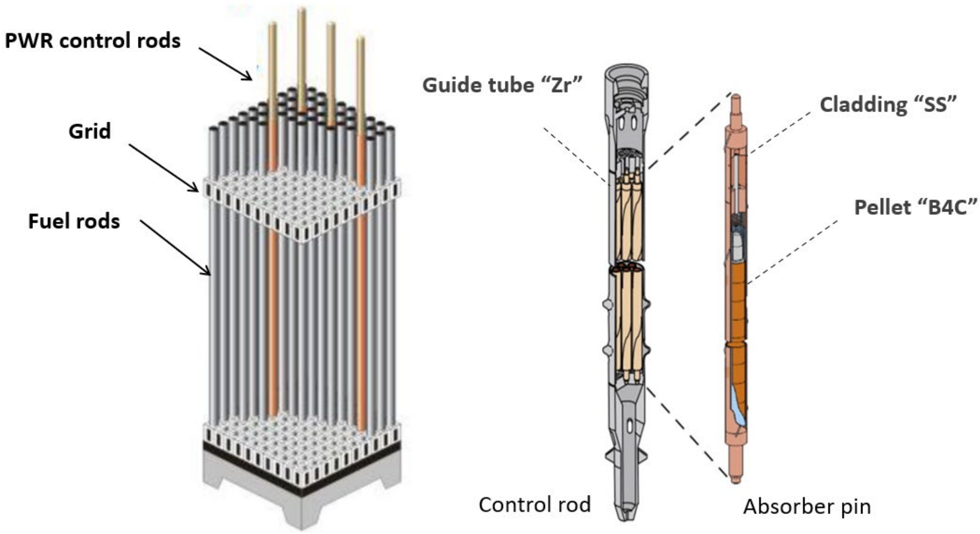

Fig. 38. PWR Fuel Rod [91]

In this third approach, the absorber blades are modelled based on the material masses and volumes of stainless steel (SS), zirconium (Zr), and boron carbide (B_4C) used in the QUENCH-20 test. To represent these characteristics, six PWR control rods were selected. The pitch between the PWR control rods was set to match the pitch between the fuel rod simulators [30], [31]. Additionally, in this approach, the SCDAP Shroud component was modelled as a single layer of Zr, allowing for the accurate determination of the geometrical dimensions of the fuel channel box, water channel box, and water wings in the QUENCH-20 test.

Fig. 39 introduces a schematic view of the radial heat transfer between the SCDAP components in this third modelling approach.

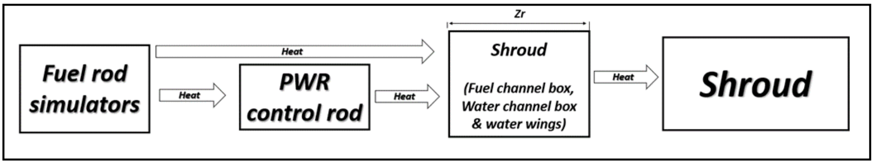

Fig. 39. Apsproach 3: Heat Transfer in Radial Direction [10]

3 RESULTS AND DISCUSSION

In this chapter, the results of the model developments of symmetric (PHEBUS FPT-1 and QUENCH-06) and asymmetric (QUENCH-20) geometry experiments are presented.

3.1 Results of Reference Calculations of Experiments Having Symmetric Geometry

3.1.1 PHEBUS FPT-1 Test

The selected FOMs for the investigation are total hydrogen generation, cladding temperature at 700 mm elevation (at the hottest elevation), and Cs/I release fraction. The reference calculation result of total hydrogen generation is presented in Fig. 40. The reference calculation yielded higher values compared to the experimental data for the pre-oxidation, oxidation, power plateau, and heat-up phases by 10, 6, 9, and 5 grams, respectively. However, the reference calculation and the experimental data have the same amount of hydrogen produced by the end of the test, ~96 g. This result shows that RELAP/SCDAPSIM calculated more intensive oxidation in the pre-oxidation, oxidation, and power plateau phases, and slower oxidation in the heat-up phase. More intensive oxidation could be explained by higher calculated cladding temperatures in these phases (Fig. 41). Slower oxidation in the heat-up phase could be explained by the ZrO2 layer formed during previous phases, which protects the Zr cladding from intensive oxidation. As it is shown in Fig. 41, the reference calculation of the cladding temperature has lower values compared with the experimental data during all test phases, except at the start of the oxidation phase, where the experimental data have a higher peak. However, at the heat-up phase and the end of the test, the reference calculation shows good agreement with the experimental data. The experimental data also showed disturbances at the heat-up phase due to the failure of the thermocouple.

The reference calculation of the Cs/I fission fraction release is presented in Fig. 42, which shows significantly lower values in all phases compared to the experimental data for Cs and I. At the end of the test, the reference calculation fission release fraction is ~0.65, and the experimental data are 0.87 and 0.85 for Cs and I. This result indicates that the proposed CORSOR-M model is suitable for evaluating the Cs/I

[10] Elsalamouny N., Kaliatka T., Kaliatka A. "QUENCH-20 test analysis using RELAP/SCDAPSIM severe accident code". Nuclear Engineering and Design. Elsevier, 2024, Vol. 419, 112995, p. 1-12. ISSN 0029-5493. https://doi.org/10.1016/j.nucengdes.2024.112995.

release fraction in early degradation phases; however, the latter phases require revising the coefficients used in this model or employing other modelling methods that consider not only temperature-based propagation of fission product release.

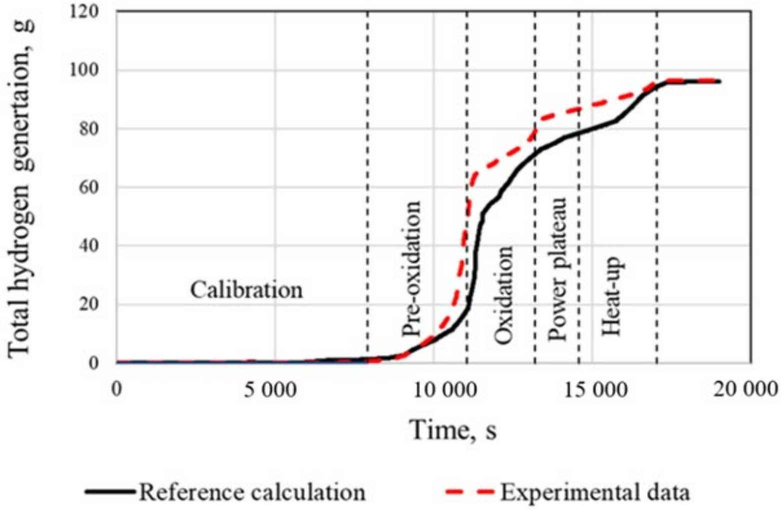

Fig. 40. The Reference Calculation of Total Hydrogen Generation

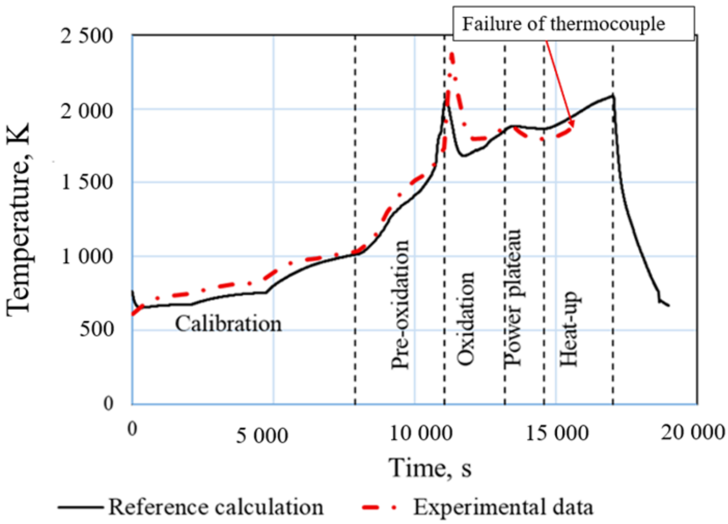

Fig. 41. The Reference Calculation Results of the Cladding Temperature

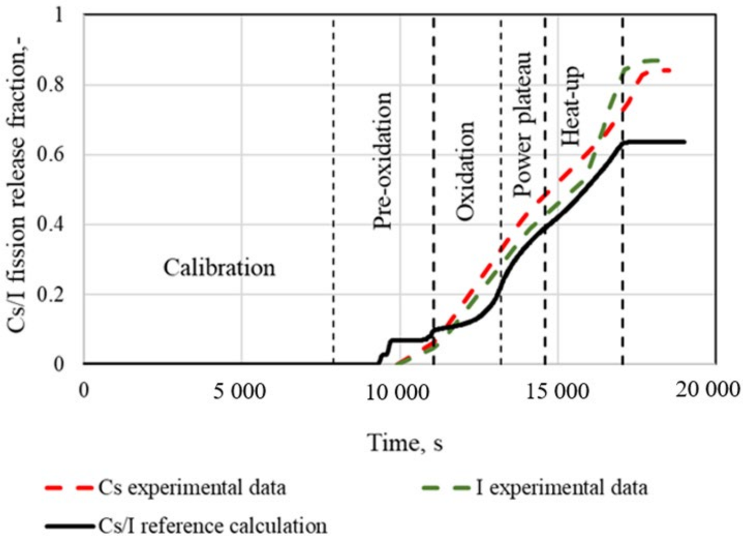

Fig. 42. The Reference Calculation Results of CS/I Fission Release Fraction

3.1.2 QUENCH-06 Test

The selected FOMs for the QUENCH-06 test investigation are total hydrogen generation, cladding temperature at 950 mm elevation (the hottest elevation), and oxide layer thickness before and after quenching. The reference calculation result of total hydrogen generation is presented in Fig. 43. The reference calculation showed good agreement with the experimental data in the pre-oxidation phase. In the transient phase, the reference case has higher values compared with the experimental data by 5%. At the end of the test, the reference case values are 15% lower than the experimental data. The reference calculation of the cladding temperature at 950 elevation is presented in Fig. 44, which has a good agreement with the experimental data during all test phases. The reference calculation of oxide layer thickness before and after quenching is presented in Fig. 45 and Fig. 46. The reference calculation of oxide layer thickness before quenching showed higher values compared with the experimental data at lower elevations; however, at higher elevations, it showed good agreement with the experimental data. The reference calculation of the oxide layer after quenching showed significantly lower values compared with the experimental data, especially at high elevations.

This result indicates that the oxidation model implemented in the RELAP/SCDAPSIM code did not accurately evaluate oxidation during the quenching phase. This issue was presented to the code developers, and model updates are planned for the code version. Despite these discrepancies, the code gives quantitative agreement with experimental data.

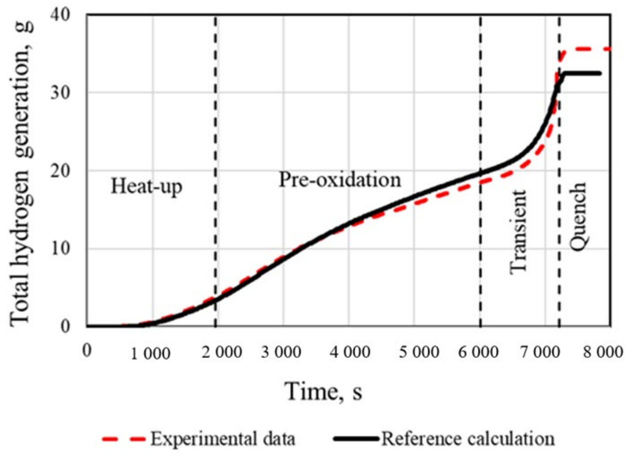

Fig. 43. The Reference Calculation of Total Hydrogen Generation

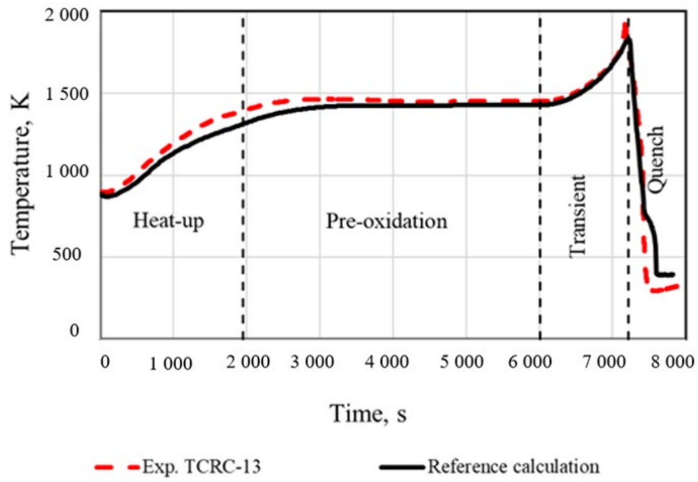

Fig. 44. The Reference Calculation of the Cladding Temperature at 950 MM Elevation

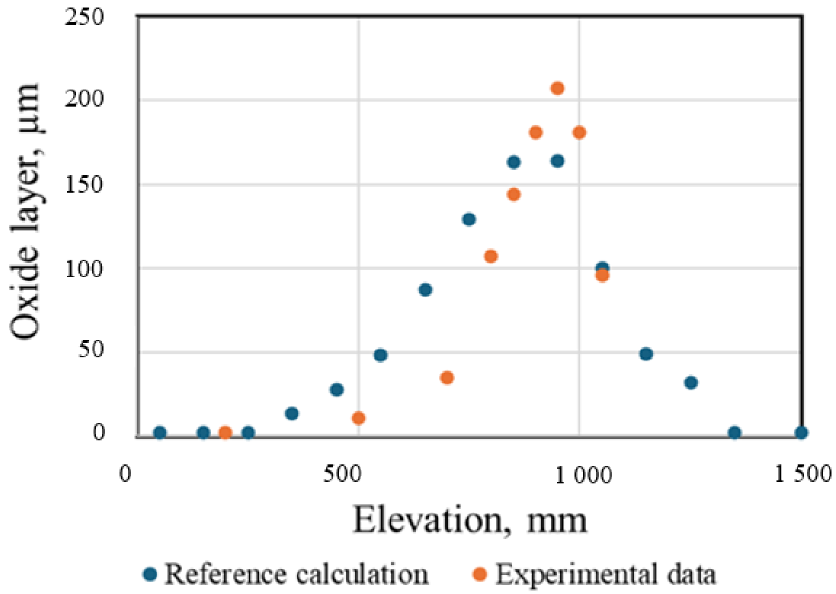

Fig. 45. Reference Calculation for the Oxide Layer Thickness Pre-Quenching

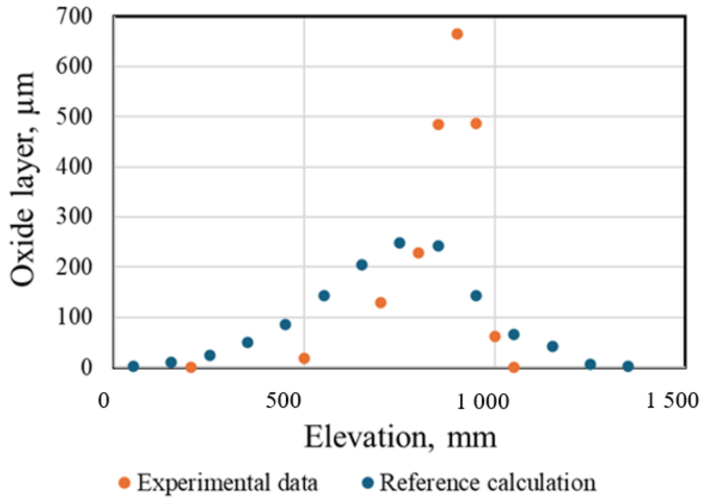

Fig. 46. Reference Calculation for the Oxide Layer Thickness Pre-Quenching

3.2 Application of the BE Approach

According to the research methodology presented in Fig. 15, the BE approach, incorporating uncertainty, was applied to the reference calculation of the symmetric geometry experiments. To quantify the uncertainties of the selected FOMs, a number of input uncertain parameters were selected in addition to their ranges and PDFs. The uncertainty tool SUSA (Section 2.4.3) was used for performing uncertainty and sensitivity analysis.

3.2.1 PHEBUS FPT-1 Test

The specification of uncertainty parameters (reference values, their ranges, and probability distribution function) is compiled in the first step of the GRS method application. Evaluation of uncertain parameters and their corresponding uncertainty parameters (uncertainty range and probability distribution function (PDF)) was determined. The determination of the uncertainty analysis ranges, and PDF was based on engineering judgment and experience [92], [93], [94]. Certain SCDAP parameters have uncertainty ranges that increase by 50% from their initial values. This is because the extent to which these uncertainties will impact the calculation results in the event of a severe catastrophe is unknown. Normal PDF is applied to parameters whose characteristics are evident. A uniform PDF is typically employed in situations where the allocation of these parameters lacks clarity. Uncertain input parameters, their range and PDF are presented in Table 8.

Table 8. Uncertain Parameters Evaluated in PHEBUS FPT-1 Test Numerical Investigation

Parameters of material thermal properties			
Material thermal properties		**PDF**	**Reference value and Uncertainty range**
Specific heat, J/kg.K	Zircaloy-4, Gap (between fuel pellet and the cladding), ThO_2, ZrO_2, Gap for the shroud cooling, Inconel-625.	Normal	Reference values of the material properties (value vs time) were selected according to ISP-46 [74]
Density, kg/m^3	Zircaloy-4, Gap (between fuel pellet and the cladding), ThO_2, ZrO_2, Gap for the shroud cooling, Inconel-625.		

Thermal conductivity, W/mK	Zircaloy-4, Gap (between fuel pellet and the cladding), ThO_2, ZrO_2, Gap for the shroud cooling, Inconel-625.		

SCDAP modelling parameters

SCDAP parameters	**PDF**	**Reference value and uncertainty range**
Temperature for the failure of the oxide shell on the outer surface of the fuel and cladding (K)	Uniform	2500+-10%
Fraction of the oxidation of the fuel rod cladding for a stable oxide shell	Uniform	0.6+-50%
The Hoop strain threshold for the double-sided Oxidation	Uniform	0.07+-50%
Pressure drops caused by ballooning	Discrete: 0-0.5 probability 1-0.5 probability	Modelled 0= modelled 1= not modelled
The surface area fraction covered with drops that result in blockage, which stops the local oxidation	Uniform	0.2+- 50%
The velocity of drops of cladding material slumping down outside the fuel rod surface (m/s)	Uniform	0.5+-50%
Gamma heat fraction	Uniform	0.026 +-50%
Mass of grid spacer, kg	Normal	0.0037+-20%
Height of grid spacer, m	Normal	0.043 +- 20%
Plate thickness of grid spacer, m	Normal	0.004 +-20%
Core slumping model definition	Discrete 50% probability	Latest possible. 0 = latest possible, 1 = earliest possible.

The minimum flow area per fuel rod in cohesive debris in the core region, m^2	Normal	4.4 x 10e-5 +-50%
Cladding rupture, transition, limit strains	Normal	Reference value +-20%

Much of the discussion here and onwards in this section is adapted from the author's related work [11]. The calculation results for total hydrogen generation, cladding temperature, and Cs/I fission fraction release from 100 calculations are presented in Figs. 47, 48, and 49. All 100 RELAP/SCDAPSIM calculations reached the heat-up phase and bundle cool-down conditions and were conducted to analyse uncertainty and sensitivity. From the analysis of the calculation results, different behaviours were observed in the four calculations (samples of parameters). For these four calculations, earlier oxidation was observed during the pre-oxidation phase. These results were determined due to the presence of a sample of parameters that caused the earlier oxidation. For calculations 62, 68, and 95, it was observed that the parameters related to the temperature for failure of the oxide shell on the outer surface of the fuel and cladding, as well as the fraction of oxidation of the fuel rod cladding for a stable oxide shell, had maximum values. However, the hoop strain threshold for double-sided oxidation had its minimum values, as per the reference values. In this case, a combination of these parameters, which are related to the oxidation process, caused earlier oxidation processes even at a relatively low power region. Another calculation, 85, had also undergone earlier oxidation processes due to the ZrO_2 thermal conductivity and gamma heat fraction parameter values. For this calculation, the values of ZrO_2 thermal conductivity were close to its minimum range, and gamma heat fraction values were close to its maximum range. The thermal conductivity of ZrO2 affects the heat transfer from the bundle; lower values of ZrO2 thermal conductivity result in more heat being transferred to the bundle. The gamma heat fraction refers to the fraction of power used to heat the coolant directly through gamma heating. These parameter combinations caused earlier oxidation, compared to the reference case and other calculations.

[11] Elsalamouny N., Kaliatka T. "Uncertainty Quantification of the PHEBUS FPT-1 Test Modelling Results". Energies. Basel: MDPI, 2021, Vol. 14, 7320, p. 1-17. ISSN 1996-1073. https://doi.org/10.3390/en14217320.

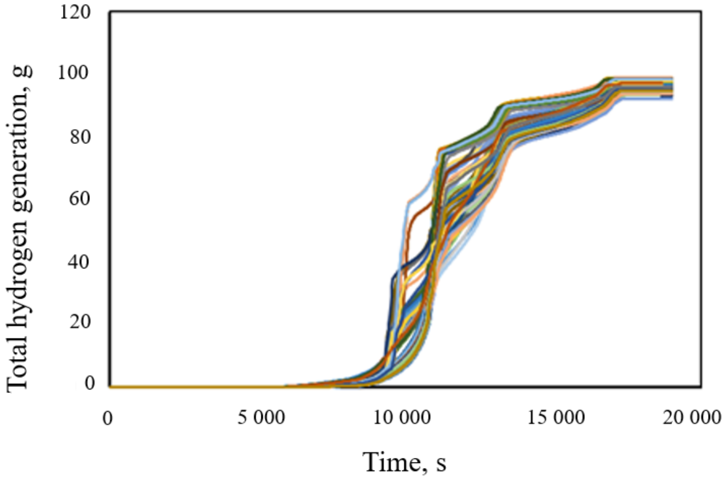

Fig. 47. The 100 Calculations of Total Hydrogen Generation[12]

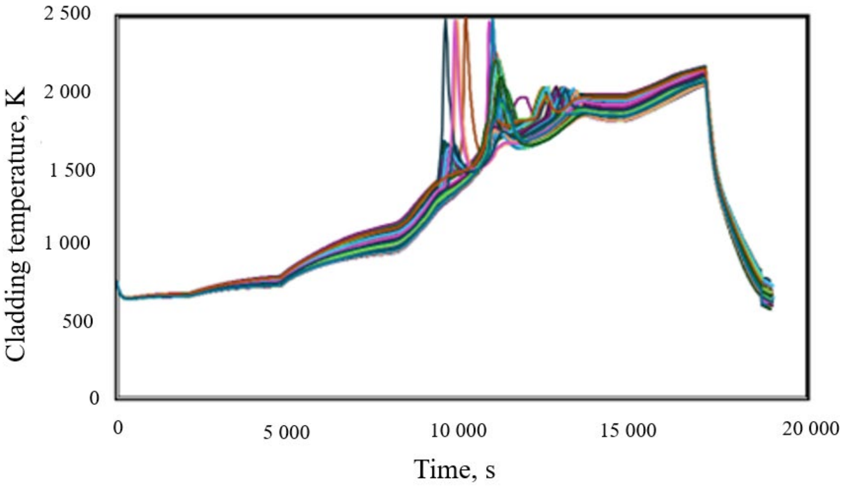

Fig. 48. The 100 Calculations of Cladding Temperature[12]

[12] Elsalamouny N., Kaliatka T. “Uncertainty Quantification of the PHEBUS FPT-1 Test Modelling Results”. Energies. Basel: MDPI, 2021, Vol. 14, 7320, p. 1-17. ISSN 1996-1073. https://doi.org/10.3390/en14217320.

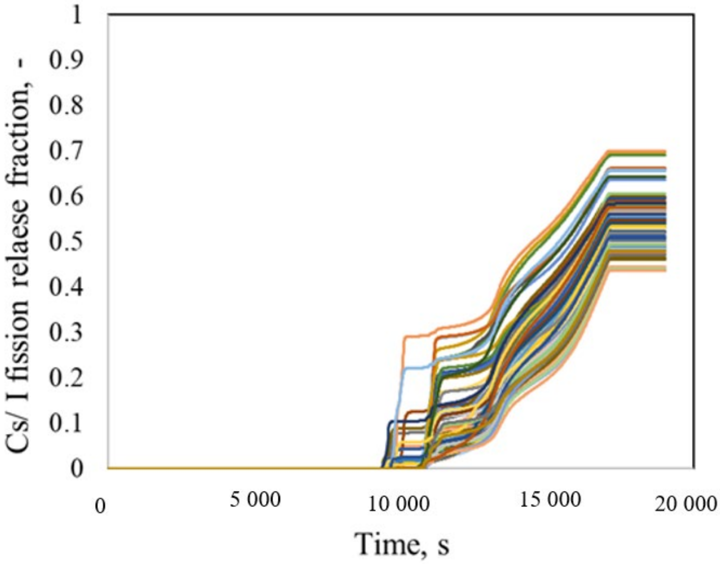

Fig. 49. The 100 Calculations of Cs/I Fission Release Fraction[13]

The experimental uncertainty associated with the raw signal of the sensor for total hydrogen generation is approximately 5%. This uncertainty corresponds to a variation of roughly 14% in the estimated value of the total mass of hydrogen generated.

Fig. 50 presents the upper and lower uncertainty limits of total hydrogen generation. The upper and lower uncertainty limits of total hydrogen generation bound the experimental data for approximately the entire time interval. There is an indication of overestimation during the oxidation phase. Comparing the final values of hydrogen generated as a result of the calculation, however, experimental uncertainties exceed the upper and lower uncertainty limits. Fig. 51 presents the uncertainty limits of cladding temperature. The upper and lower uncertainty limits bound the experimental data. The experimental data have higher values during the oxidation phase compared with the uncertainty limits. However, at the end of the heat-up phase, the experimental data showed significantly lower values due to the failure of the thermocouple. Fig. 52 presents the upper and lower uncertainty limits for the Cs/I release fraction at a 95% confidence level and a 95% probability. The upper and lower uncertainty limits bound the experimental data until the middle of the heat-up phase. However, the calculated upper uncertainty limit is 20% lower than the experimental data at the end of the test. This result indicates that, even considering the given uncertainties, the CORSOR-M model in the latter fuel rod degradation phase (when the fuel rod temperature is high) does not correspond to the experimental data. It is needed to revise the coefficients

[13] Elsalamouny N., Kaliatka T. "Uncertainty Quantification of the PHEBUS FPT-1 Test Modelling Results". Energies. Basel: MDPI, 2021, Vol. 14, 7320, p. 1-17. ISSN 1996-1073. https://doi.org/10.3390/en14217320.

used in this model or use other modelling methods that consider not only the temperature-based propagation of fission product release.

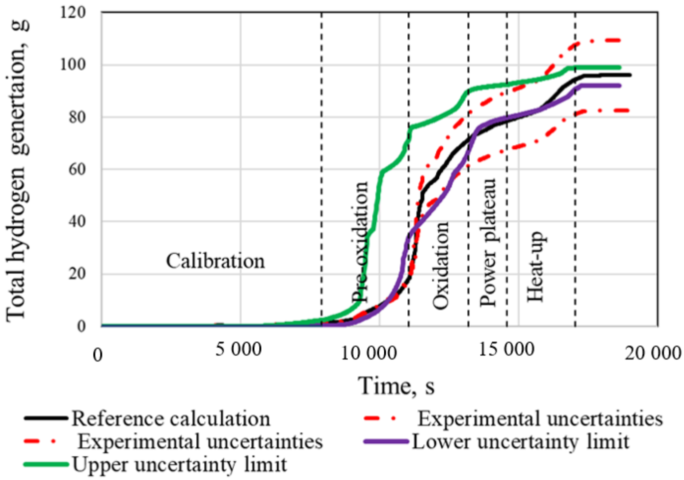

Fig. 50. Uncertainty Limits for Total Hydrogen Generation

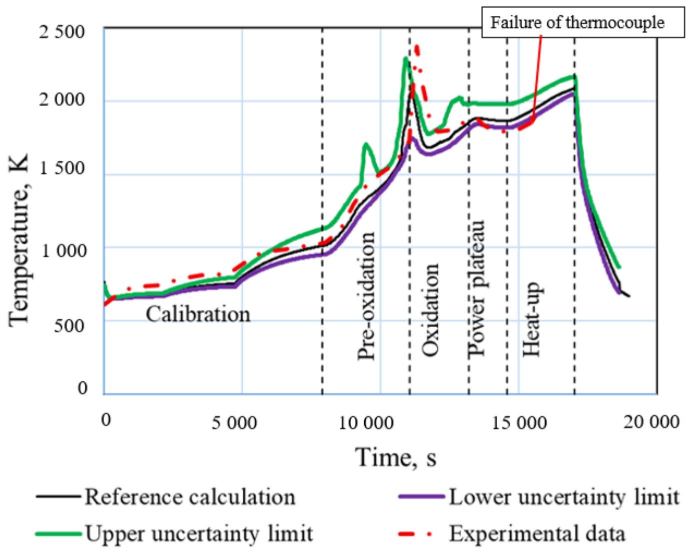

Fig. 51. Uncertainty Limits of Cladding Temperature

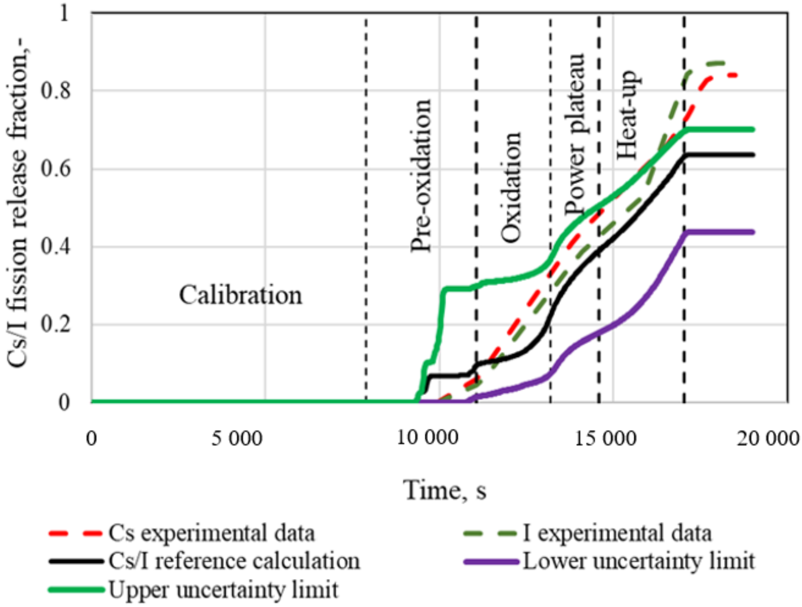

Fig. 52. Uncertainty Limits of Cs/I Fission Release Fraction

Fig. 53 presents the R^2 of total hydrogen generation, where the Spearman correlation coefficient shows that the values of R^2 are higher than 0.6 for all the periods of calculation results. The values of R^2 are lower than 0.6 in a small period at the end of the pre-oxidation and beginning of the oxidation phases. Fig. 54 presents the R^2 of cladding temperature. R^2 follows the same explanation as in the case of total hydrogen generation. Fig. 55 presents the R^2 of the Cs/I fission release fraction. It shows that R^2 values are equal to 0 during the calibration phase. After the midpoint of the calibration phase, the Spearman correlation coefficient indicates that R^2 values are consistently higher than 0.6 during the calculation period. Summarising this result, it is possible to conclude that the linearity between uncertain parameters and calculation results is high, and the sensitivity analysis could be provided. At times, the R^2 coefficient decreases due to the calculation switching between different models.

In the sensitivity analysis: Fig. 56, Fig. 57 and Fig. 58 show the influence of uncertain parameters on the calculation results of total hydrogen generation, cladding temperature, and Cs/I fission release fraction, respectively. Table 9 shows the uncertain parameters with the highest influence on the calculation results of total hydrogen generation, cladding temperature, and Cs/I release fraction during different test phases at the selected time moment. It was observed that the thermal conductivity of ZrO_2 and the boundary conditions that describe the heat transfer from the fuel bundle to the surrounding structures have the highest influence on all calculation results throughout all test phases.

Table 9. Sensitivity Analysis of the PHEBUS FPT-1 Test

Calculation Results	Phases				
	Calibration (6000 s)	**Pre-oxidation (9000 s)**	**Oxidation (12500 s)**	**Power plateau (14000 s)**	**Heat-up (16000 s)**
Total Hydrogen generation	ZrO_2 thermal conductivity (influence -0.98), Gamma heat fraction (influence -0.4).	ZrO_2 thermal conductivity (influence -0.98), Gamma heat fraction (influence –0.4).	Temperature for failure of oxide shell on outer surface of fuel and cladding (influence -0.37), ZrO_2 thermal conductivity (influence 0.26), Hoop strain threshold for double-sided oxidation (influence -0.35).	ZrO_2 thermal conductivity (influence -0.4), Height of grid spacer (influence -0.36), Mass of grid spacer (influence 0.41).	ZrO_2 thermal conductivity (influence -0.6), Mass of grid spacer (influence 0.4), Height of grid spacer (influence -0.3).
Cladding temperature	ZrO_2 thermal conductivity (influence 0.98).	ZrO_2 thermal conductivity (influence 0.85), Gap (inner and outer) thermal conductivity (influence 0.25).	ZrO_2 thermal conductivity (influence 0.83), ThO_2 density (influence -0.32), Spray coating thermal conductivity (influence 0.21).	ZrO_2 thermal conductivity (influence 0.88), ThO_2 thermal conductivity (influence -0.25).	ZrO_2 thermal conductivity (influence 0.98), ZrO_2 specific heat (influence -0.6), ThO_2 thermal conductivity (-influence 0.22).

Calculation Results	Phases				
	Calibration (6000 s)	Pre-oxidation (9000 s)	Oxidation (12500 s)	Power plateau (14000 s)	Heat-up (16000 s)
Cs/I fission release fraction	ZrO_2 thermal conductivity (influence -0.98), Gamma heat fraction (influence -0.36).	ZrO_2 thermal conductivity (influence -0.98), Gamma heat fraction (influence -0.33).	Temperature for failure of oxide shell on outer surface of fuel and cladding (influence -0.37), ZrO_2 thermal conductivity (influence 0.26), Hoop strain threshold for double-sided oxidation (influence -0.35).	ZrO_2 thermal conductivity (influence -0.7), Height of grid spacer (influence -0.37), Mass of grid spacer (influence 0.37).	ZrO_2 thermal conductivity (influence -0.8), Mass of grid spacer (influence 0.33), Height of grid spacer (influence -0.32).

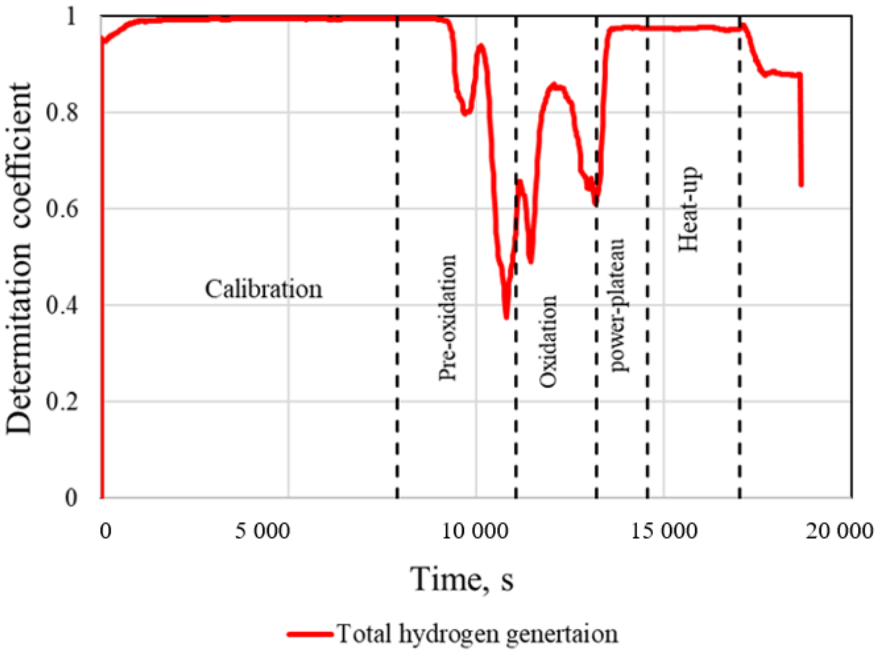

Fig. 53. Determination Coefficient for Total Hydrogen Generation

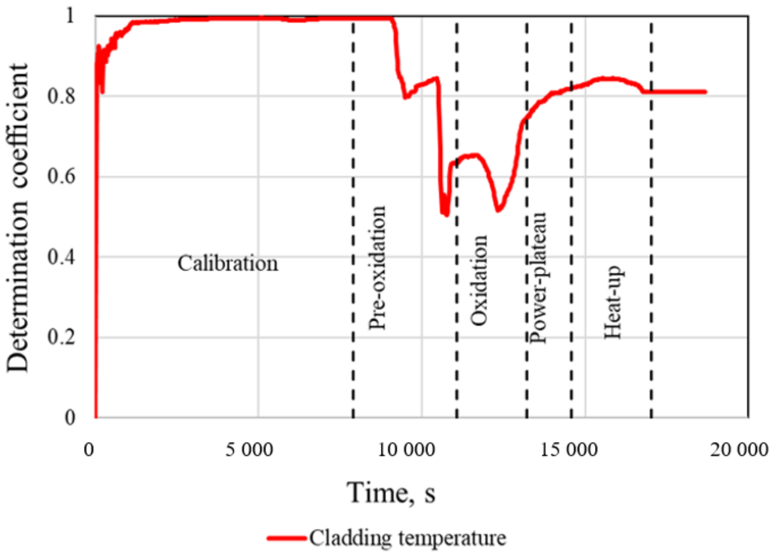

Fig. 54. Determination Coefficient of Cladding Temperature

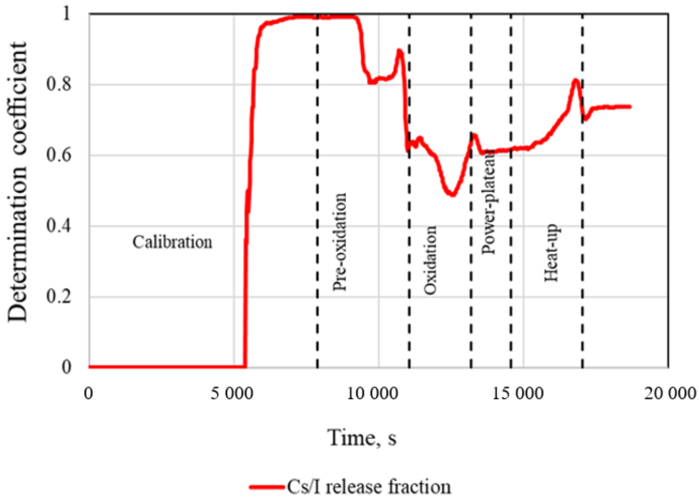

Fig. 55. Determination Coefficient of Cs/I Fission Release Fraction

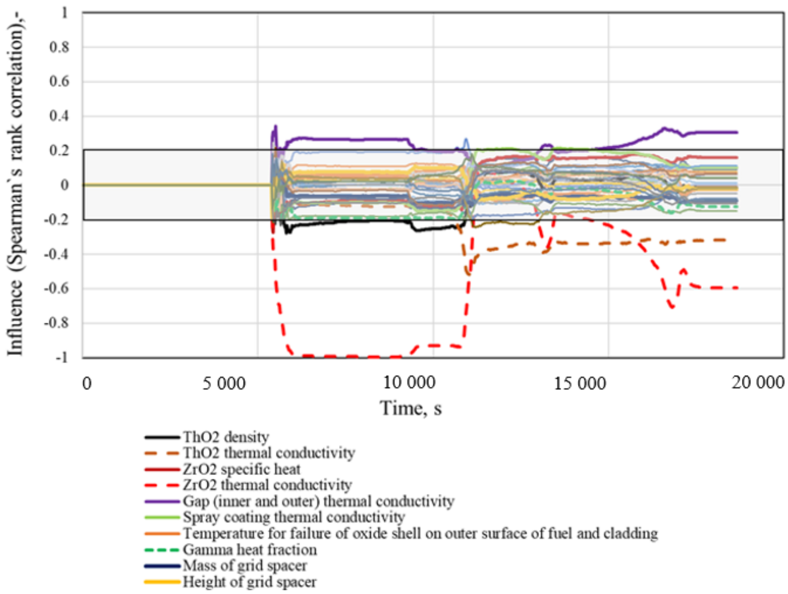

Fig. 56. The Uncertain Parameters Influence the Hydrogen Generation Calculation Results

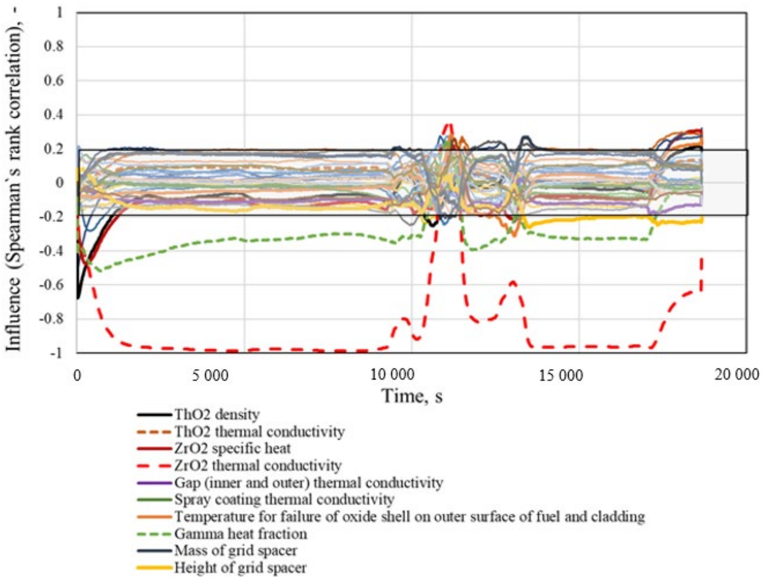

Fig. 57. The Uncertain Parameter Influences the Cladding Temperature Calculation Results

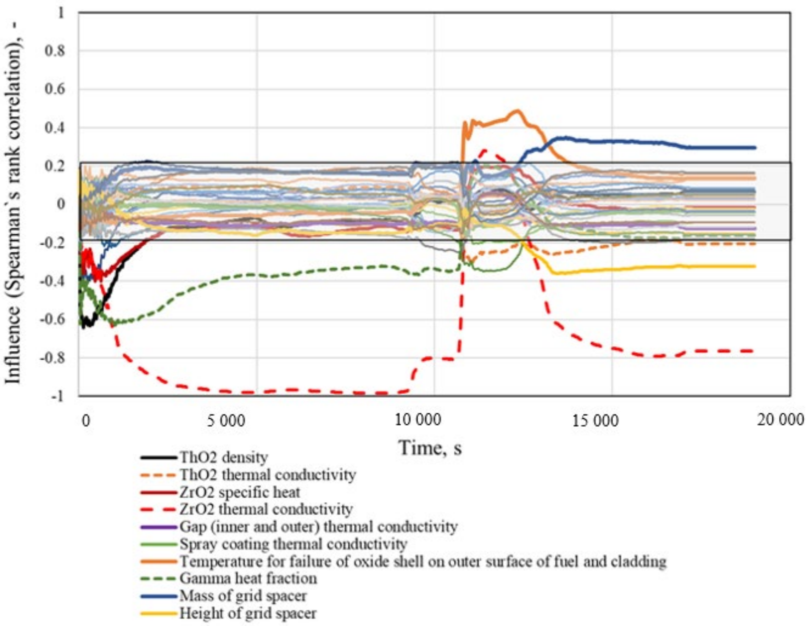

Fig. 58. The Uncertain Parameter Influence on Cs/I Fission Release Fraction Calculation Results

3.2.2 QUENCH-06 Test

The same uncertainty quantification steps as for PHEBUS FPT-1 were provided with the QUENCH-06 calculation results. It was decided to consider hydrogen generation, temperature evolution during the test, and oxide thickness before and after the quench phase. This solution was developed because it yields important results reflecting bundle degradation during severe accident conditions, and these results were supported by a comprehensive experimental database provided by KIT.

According to the selected FOM's, the table (see Table 10) of uncertain parameters with their ranges and probability distribution functions (PDF) was developed. All parameter uncertainties were discussed and agreed upon with KIT and the QUENCH experiment team. In total, 19 uncertain parameters with their uncertainties were selected for the analysis. More detail information available in the author's article [14].

Table 10. Uncertain Parameters and Their Ranges and PDF [14]

Uncertainty parameters	Parameter	Reference value with uncertainty range	PDF
Related to geometry	Rod pitch (mm)	14.3 ± 1%	Uniform
	Fuel pellet simulator (ZrO_2) external diameter (mm)	9.15 ± 0.2%	
	Cladding thickness (mm)	0.725 ± 1%	
	Internal diameter shroud (mm)	80 ± 1%	
	The thickness of the shroud (mm)	2.38 ± 1%	
	The thickness of the insulator (mm)	37.0 ± 1%	
Related to boundary conditions	Quench water injection it to experiment section (s)	7215 ± 0.5%	Uniform
	Quench water mass flow rate at the bundle inlet (kg/s)	Ref. value [63] ± 2%	Normal
	Argon mass flow rate at the bundle inlet (kg/s)	Ref. value [63] ± 2%	
	Steam mass flow rate at the bundle inlet (kg/s)	Ref. value [63] ± 2%	
	Pressure at the bundle outlet (10^5 Pa)	2.0± 2%	
	Electrical power (W)	Ref. value [63] ± 2%	
	Quenching water temperature (K)	Ref. value [63] ± 2%	
	Fuel/Clad internal pressure (10^5 Pa)	2.2± 2%	
	Fraction of oxidation of fuel rod cladding for stable oxide shell	0.6 ± 10%	Uniform

[14] IAEA, Advancing the State of the Practice in Uncertainty and Sensitivity Methodologies for Severe Accident Analysis in Water Cooled Reactors in the QUENCH-06 Experiment. IAEA-TECDOC-2045, 2024.

Uncertainty parameters	Parameter	Reference value with uncertainty range	PDF
Related to the integrity of cladding	Failure temperature of the ZrO_2 layer (K)	2374 ± 5%	
To convective heat transfer modelling	Fraction of surface area covered with drops that result in a blockage that stops local oxidation.	0.2 ± 5%	Uniform
	Surface temperature for freezing of drops of liquefied/slumping fuel rod cladding (K)	1750 ± 5%	
	The velocity of drops of cladding material slumping down the outside surface of the fuel rod (m/s)	0.5 ± 5%	

Fig. 59 and Fig. 60 present the dispersion plot of 100 RELAP/SCDAPSIM calculation results for the total hydrogen generation. Fig. 61 illustrates the upper and lower uncertainty bounds in comparison with experimental data and the reference calculation of hydrogen generation. At the end of the QUENCH test, the difference between the lowest and highest calculation results amounts to 14.2%. However, the uncertainty of upper and lower limits bounds experimental data in the all-time region of the QUENCH-06 experiment. A different situation is for the calculation results of the temperature of the central rod at 950 mm elevation. The temperature variation between the coolest and hottest points in the pre-oxidation phase is only approximately 50 K (roughly 2.5% of the highest temperature computed). But by comparing upper and lower uncertainty limits to the experimental data, good agreement was achieved, see Fig. 62.

Scalar uncertainty analysis was provided for the results of the oxide layer thickness, which are presented in Fig. 63 and Fig. 64. During the QUENCH-06 experiment, one of the corner rods was removed at 6 620 s to investigate the thickness of the oxide layer before the quenching phase. The measurements of the oxide layer thickness before quenching are compared with the upper and lower limits of RELAP/SCDAPSIM calculation results. Comparison results show that the calculated values slightly overestimate the test measurements. The best agreement is at 950 mm elevation. In Fig. 64, the oxide layer thickness was measured after the QUENCH-06 test ended, and it was compared with the upper and lower limits of the calculation results at the end of the test. Calculated values are overestimated in the lower elevation region (up to 850 mm), but experimental data have significantly higher values in the elevation range from 850 mm to 1 000 mm. This result shows that during the experiment (quench phase) in the region 850 mm to 1 000 mm, zircaloy cladding oxidation was much more intensive compared to the results given by RELAP/SCDAPSIM code. This result indicates the limitation of the oxidation model in the RELAP/SCDAPSIM code.

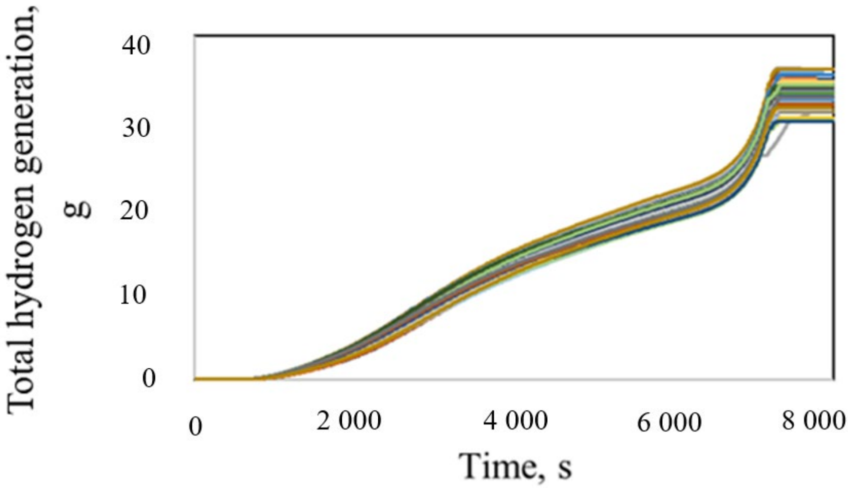

Fig. 59. The 100 Calculations of Total Hydrogen Generation [15]

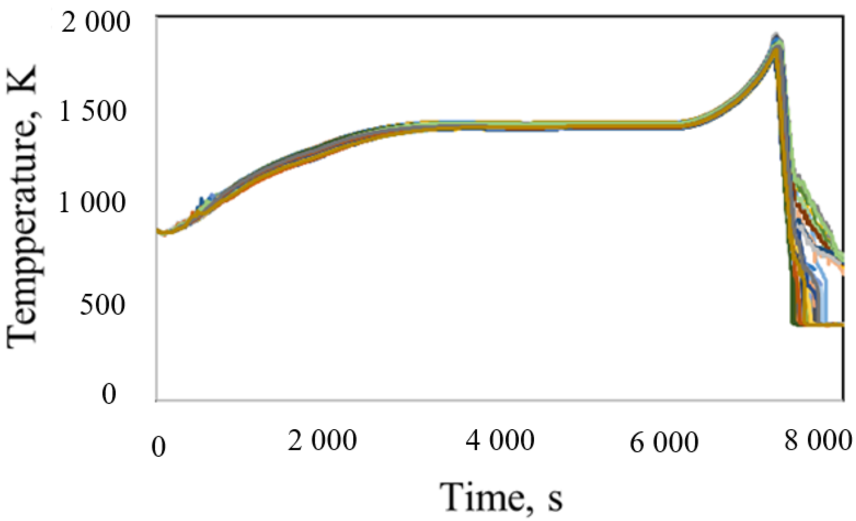

Fig. 60. The 100 Calculations of Cladding Temperature at 950 MM Elevation [15]

[15] IAEA, Advancing the State of the Practice in Uncertainty and Sensitivity Methodologies for Severe Accident Analysis in Water Cooled Reactors in the QUENCH-06 Experiment No. IAEA-TECDOC-2045, 2024. [Online]. Available: IAEA-TECDOC-2045

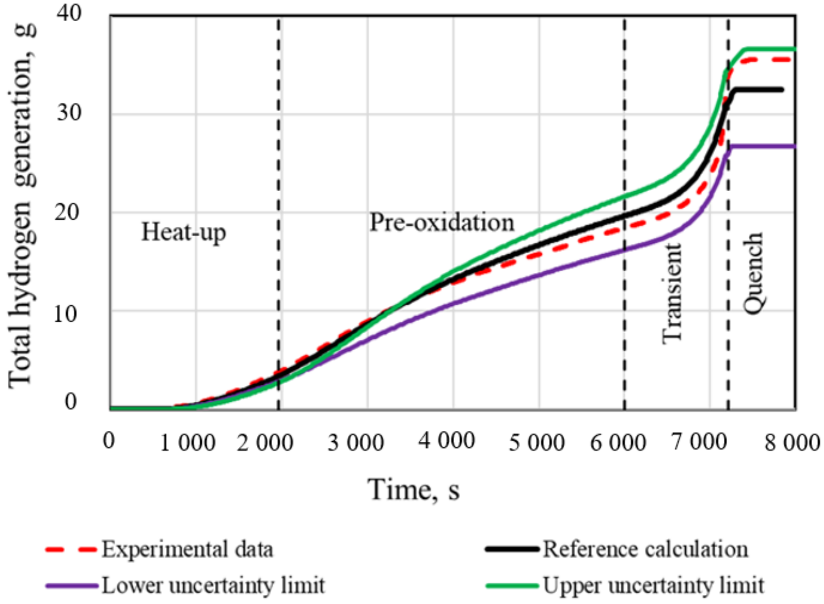

Fig. 61. Uncertainty Limits of Total Hydrogen Generation [16]

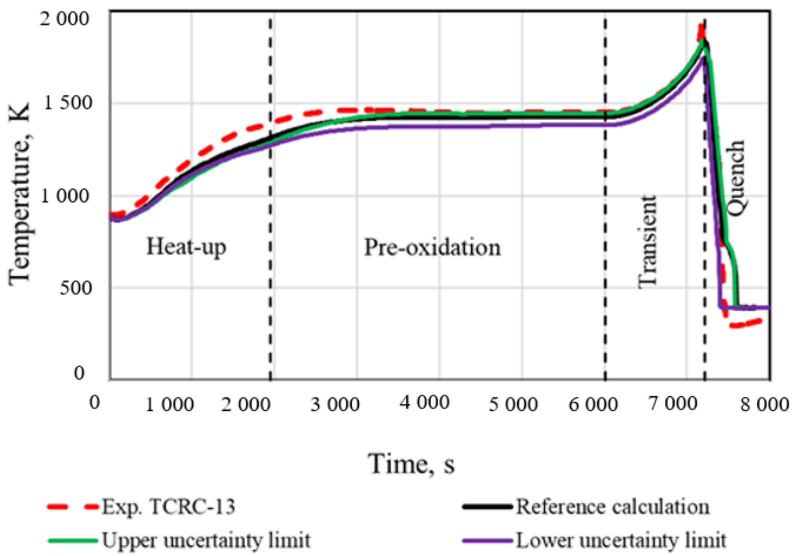

Fig. 62. Uncertainty Limits of Cladding Temperature at 950 mm Elevation [16]

[16] IAEA, Advancing the State of the Practice in Uncertainty and Sensitivity Methodologies for Severe Accident Analysis in Water Cooled Reactors in the QUENCH-06 Experiment No. IAEA-TECDOC-2045, 2024. [Online]. Available: IAEA-TECDOC-2045

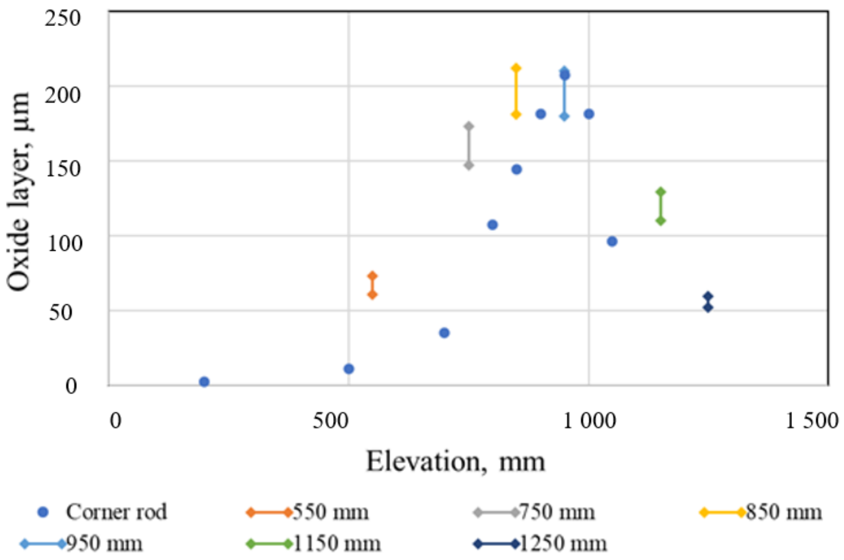

Fig. 63. Scalar Uncertainty Analysis of Oxide Layer Thickness Before Quenching [17]

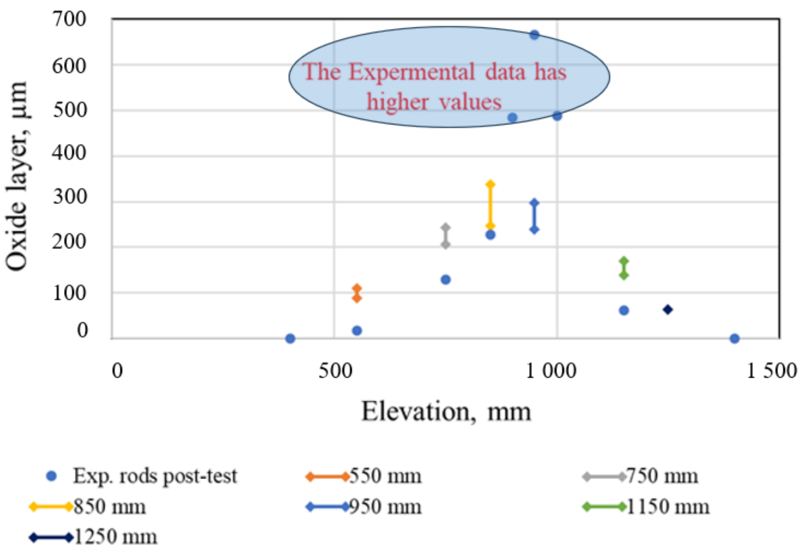

Fig. 64. Scalar Uncertainty Analysis of Oxide Layer After Quenching [17]

[17] IAEA, Advancing the State of the Practice in Uncertainty and Sensitivity Methodologies for Severe Accident Analysis in Water Cooled Reactors in the QUENCH-06 Experiment No. IAEA-TECDOC-2045, 2024. [Online]. Available: IAEA-TECDOC-2045

In Fig. 65, the determination coefficient R^2 of total hydrogen generation and central rod`s cladding temperature at 950 mm elevation is presented. For both FOMs, the determination coefficient has a high value exceeding 0.9, throughout the entire experiment time, except for the beginning of the heat-up phase, during which a calibration was performed for relatively low temperatures. Thus, it is possible to conclude that the linearity between uncertain parameters and simulation results is high, and the sensitivity analysis could be provided.

The sensitivity analysis was provided for all test time periods. According to Spearman's rank correlation coefficient, the uncertain parameters slightly change over time. Fig. 66 and Fig. 67 present the uncertain parameters influence the calculation results of total hydrogen generation and the cladding temperature at 950 mm elevation. The uncertain parameters` influence of total hydrogen generation and temperature of the central tube at 950 mm elevation at specific time points at different phases of the experiment is presented in Table 11. For the total hydrogen generation, at the heat up phase, the thickness of the cladding is the most influenced parameter. However, at all test phases, electrical power is the most influenced uncertain parameter. The steam mass flow rate at the bundle inlet also shows significant influence on all phases of the experiment. Results of the sensitivity analysis for the temperature of the central rod at 950 mm showed that the most influenced parameter is electrical power for the heat-up, pre-oxidation, and transient phases. As for the quench phase, the most influenced parameter is the quenched water injection time to the test section, see Table 11.

Table 11. The Influence of Uncertain Input Parameters on Calculated Results

Influence of uncertain parameters	**Phase**			
	Heat up (the 1500s)	**Pre-oxidation (5000s)**	**Transient (6500s)**	**Quench (7350s)**
Total hydrogen generation	Cladding thickness (influence +0.85), Electrical power (influence +0.55), Thickness of the Insulator (influence -0.27).	Electrical power (influence +0.82), Cladding thickness (influence +0.43), Steam mass flow rate at the bundle inlet (influence -0.35).	Electrical power (influence +0.85), Steam mass flow rate at the bundle inlet (influence -0.36), Cladding thickness (influence +0.32).	Electrical power (influence +0.81), Steam mass flow rate at the bundle inlet (influence -0.35), Thickness of the Insulator (influence -0.29).
Temperature of the central rod at 950 mm	Cladding thickness (influence +0.8), Electrical power	Electrical power (influence +0.78), Steam mass flow rate at the	Electrical power (influence +0.81), Steam mass flow rate at the bundle inlet (influence -0.39).	Quench water injection to the experiment section (influence +0.97).

	(influence +0.58).	bundle inlet (influence -0.43).		
Oxide layer thickness			Electrical power (influence +0.8), Steam mass flow rate at the bundle inlet (influence -0.4), Cladding thickness (influence +0.35).	Electrical power (influence +0.8), Steam mass flow rate at the bundle inlet (influence -0.4).

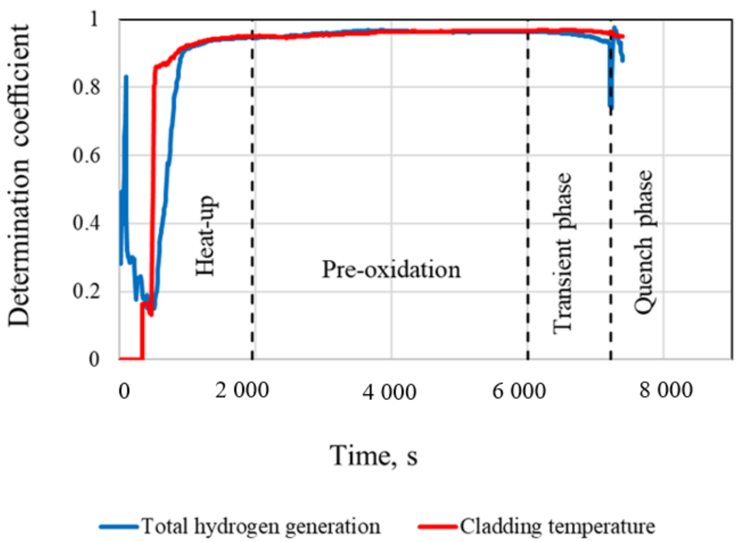

Fig. 65. Determination Coefficient of Total Hydrogen Generation and Cladding Temperature at 950 mm Elevation

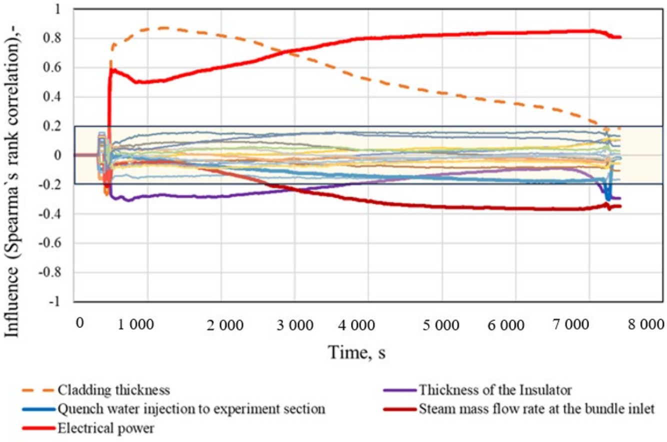

Fig. 66. The Influence of Uncertain Parameters on the Calculation Results of Total Hydrogen Generation

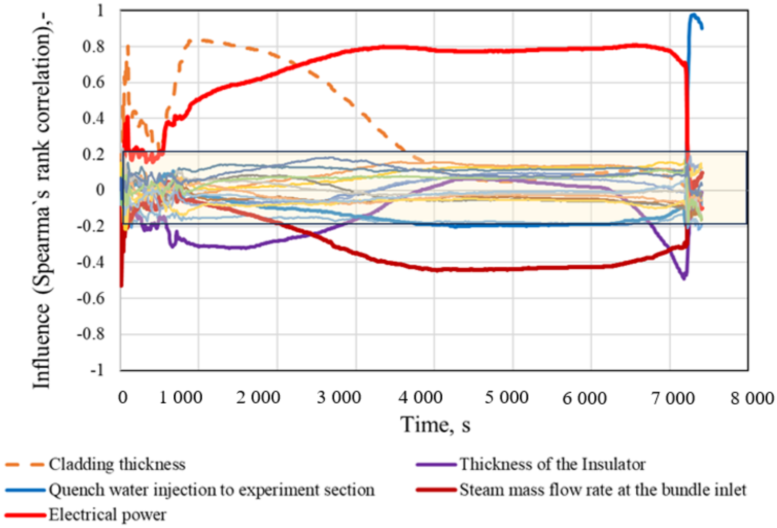

Fig. 67. The Influence of Uncertain Parameters on the Calculation Results of Cladding Temperature at 950 mm Elevation

3.3 Results of Calculations of the Experiment Having Asymmetric Geometry

The comparison of the total hydrogen generation calculated using the pseudo-symmetrical, 1st, 2nd, and 3rd modelling approaches and the experimental data is presented in Fig. 68. More details could be found in the author's related work [18]. The hydrogen generation calculated using the pseudo-symmetrical approach begins approximately 3 000 seconds later than observed in the experimental data, due to the delayed initiation of the Zr oxidation process. Throughout the test, the hydrogen generation remained about 30% lower than the experimental data until 1 400 seconds. By the end of the test, the total calculated hydrogen generation was 30 g, which is approximately 50% less than the experimental result. In the 1st modelling approach, hydrogen generation started approximately 1 500 seconds later than in the experimental data, also due to a delayed onset of Zr oxidation. Initially, the calculated hydrogen generation was lower than the experimental values until 8 000 seconds. However, the rate of increase in hydrogen generation was higher in calculations, leading to results that were up to 20% higher than the experimental data by the end of the pre-oxidation phase.

This discrepancy appears throughout the transient phase, and at the end of the quench phase, the total calculated hydrogen generation was 47 g, about 18% lower than the experimental data. The 2nd modelling approach produced a hydrogen generation curve that closely followed the experimental trend during the pre-oxidation and transient phases, with calculated values only 3% lower than the experimental data. However, this model did not capture the peak in hydrogen generation observed during the quench phase. Consequently, the total hydrogen generation at the end of the quench phase was approximately 27 g, which is around 50% lower than the experimental data. In the 3rd modelling approach, hydrogen generation began about 3 000 seconds later than in the experimental data, similar to the first approach, due to the late start of Zr oxidation. The calculated values were lower than the experimental data until 8 000 seconds, after which they exceeded the experimental values by 2% during the pre-oxidation and transient phases. This approach predicted the highest hydrogen generation during the quench phase compared to all other approaches, with a total hydrogen generation of 52 g, though this was still 10% lower than the experimental data.

[18] Elsalamouny N., Kaliatka T., Kaliatka A. "QUENCH-20 test analysis using RELAP/SCDAPSIM severe accident code". Nuclear Engineering and Design. Elsevier, 2024, Vol. 419, 112995, p. 1-12. ISSN 0029-5493. https://doi.org/10.1016/j.nucengdes.2024.112995.

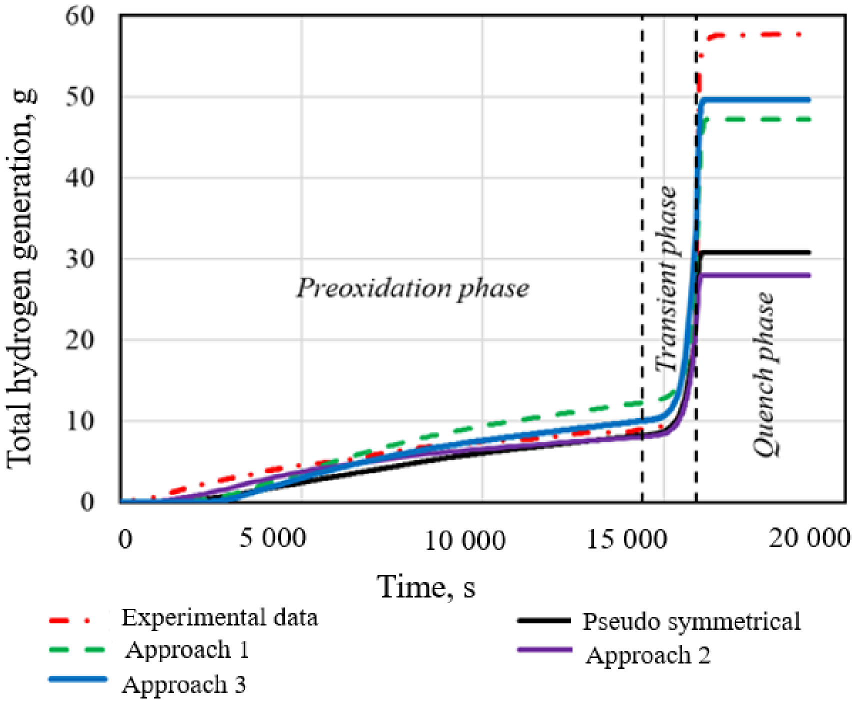

Fig. 68. Total Hydrogen Generation [19]

Fig. 69 shows a comparison of the calculated cladding temperature with the registered data of the thermocouples. In the QUENCH-20 test, the claddings of the fuel rod imitators have attached thermocouples for the registration of the temperature variance during the experiment. At an elevation of 950 mm from the bottom of the heated length, there are three thermocouples: TFS 1/13, TFS 9/13, and TFS 16/13. In the coding of thermocouples, TFS represents the thermocouple attached to the outer surface of the rod cladding. Two digits separated by a slash represent the number of fuel imitators and elevation. In this case, thermocouples were attached to the fuel rod simulator located in the centre, corner of the inner ring and the upper corner of the outer ring of the bundle. The temperature scattering distribution around ~150 K is observed in the readings of these thermocouples. This is due to the asymmetry and nonuniform temperature distribution during the QUENCH-20 test. The calculated cladding temperature results using the pseudo-symmetrical model show lower values compared with the experimental data, TSF 16/13, by 5% until ~12 000 s. Then the calculated results are identical to the experimental data TSF 16/13. The calculated results using the 1st modelling approach are located between the TSF 9/13 and TFS

[19] Elsalamouny N., Kaliatka T., Kaliatka A. "QUENCH-20 test analysis using RELAP/SCDAPSIM severe accident code". Nuclear Engineering and Design. Elsevier, 2024, Vol. 419, 112995, p. 1-12. ISSN 0029-5493. https://doi.org/10.1016/j.nucengdes.2024.112995.

16/13 thermocouple readings during the pre-oxidation and transient phases. During the quench phase, this modelling approach has the highest peak compared with all other modelling approaches. This peak is lower by 6% (150 K) than the TSF 1/13 thermocouple readings. As in the results of the 1st modelling approach, using the 2nd approach, the cladding temperature at 950 mm elevation is between the TSF 9/13 and TFS 16/13 thermocouple readings during the pre-oxidation and transient phases. During the quench phase, this modelling approach showed the lowest temperature peak compared with other modelling approaches. Compared to the TFS 1/13, the thermocouple reading is 15% lower (315 K). The calculation results using the 3rd approach give 6% (95 K) lower values compared with all thermocouple readings during the pre-oxidation and transient phases. During the quench phase, the peak calculated cladding temperature at 950 mm elevation is 12% lower (by 250 K) compared to the experimental data.

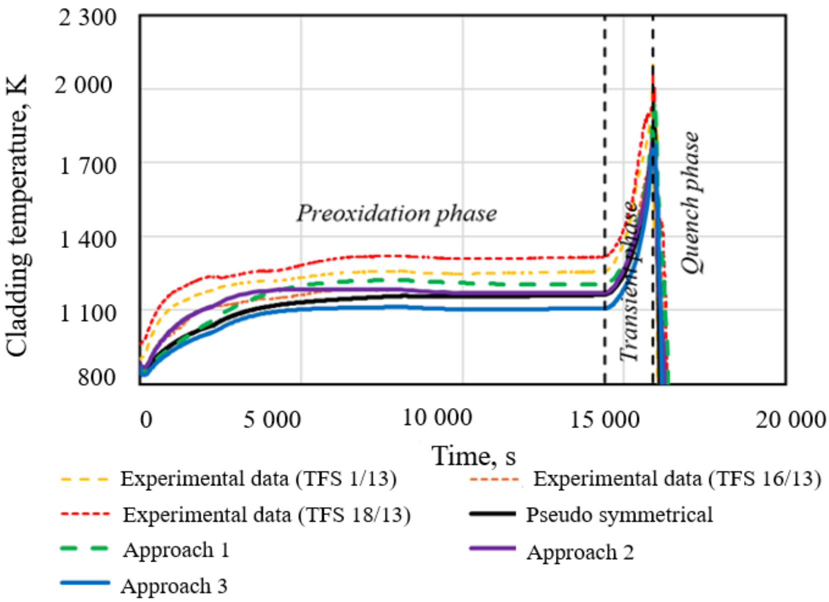

Fig. 69. Cladding Temperature at 950 mm Elevation [20]

Fig. 70 presents the comparison between the calculated shroud temperature at 950 mm elevation using the pseudo-symmetrical, 1st, 2nd, and 3rd modelling approaches and the readings of the thermocouples [20]. There are two thermocouples located at this elevation: TSH 13/180 and TSH 13/270. These thermocouples (TSH) are attached to the outer surface of the shroud. The thermocouples are coded using two digits separated by a slash. First, indicate elevation (in this case, at 950 mm), and the second shows the thermocouple's position angle in the test. During the

[20] Elsalamouny N., Kaliatka T., Kaliatka A. "QUENCH-20 test analysis using RELAP/SCDAPSIM severe accident code". Nuclear Engineering and Design. Elsevier, 2024, Vol. 419, 112995, p. 1-12. ISSN 0029-5493. https://doi.org/10.1016/j.nucengdes.2024.112995.

experimental setup, the legs of these thermocouples are relatively strongly bent to conduct them not along the shroud, but outside the thermal insulation. During the experiment, these thermocouples are subjected to mechanical loads, and internal damage could be expected in the legs of the double-sheathed thermocouples. This could affect the readings of thermocouples. After discussion with test organisers (KIT), it was agreed that TSH 13/270 readings should be treated with some caution, because this thermocouple registered higher temperatures from the beginning of the test. Thus, calculation results were compared with data registered by thermocouple TSH 13/180. The calculated shroud temperature using the pseudo-symmetrical model is in good agreement with the experimental data, TSH 13/180, they are almost identical. The calculated shroud temperature using the 1st modelling approach is higher by up to 3 % (35 K) compared with the experimental data during the pre-oxidation phase. However, the calculated results are 10% lower (130 K) compared to the experimental data during the transient phase.

In the quench phase, the peak of the calculated shroud temperature at 950 mm elevation is 8% (130 K) higher than TSH 13/180 thermocouple readings. The 2nd modelling approach calculation results are 40% (450 K) lower than the thermocouple readings during the pre-oxidation and transient phases. Additionally, during the quench phase, the peak shroud temperature, calculated at a 950 mm elevation, is 50% (800 K) lower than the TSH 13/180 thermocouple readings. Using the 3rd modelling approach, the calculated shroud temperature at 950 mm elevation is lower than the experimental data up to 6% (65 K) during the pre-oxidation and transient phases. In the quench phase, the peak of the calculated shroud temperature is 5% (90 K) higher compared with the TSH 13/180 thermocouple readings.

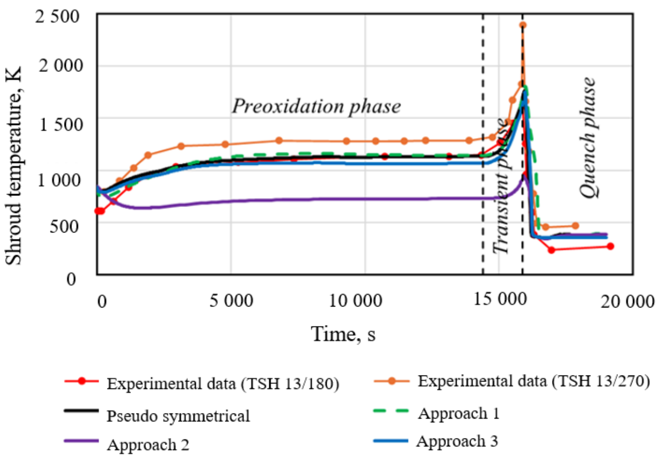

Fig. 70. Shroud Temperature at 950 mm Elevation [21]

[21] Elsalamouny N., Kaliatka T., Kaliatka A. "QUENCH-20 test analysis using RELAP/SCDAPSIM severe accident code". Nuclear Engineering and Design. Elsevier, 2024, Vol. 419, 112995, p. 1-12. ISSN 0029-5493. https://doi.org/10.1016/j.nucengdes.2024.112995.

The 3rd modelling approach was able to evaluate the B_4C oxidation process and triggered the production of CO, CO_2, CH_4, and H_2 see Fig. 71, but the calculated values of CO, CO_2, CH_4, and H_2 are lower than experimental data. This is because of the different starting points of the oxidation reactions in the experiment and the model calculation. The difference between the starting time of the model and the experiment is ~500 s. Also in the experiment, the oxidation of B_4C with steam started at a temperature of ~ 1 600 K. However, the model started at ~1 719 K.

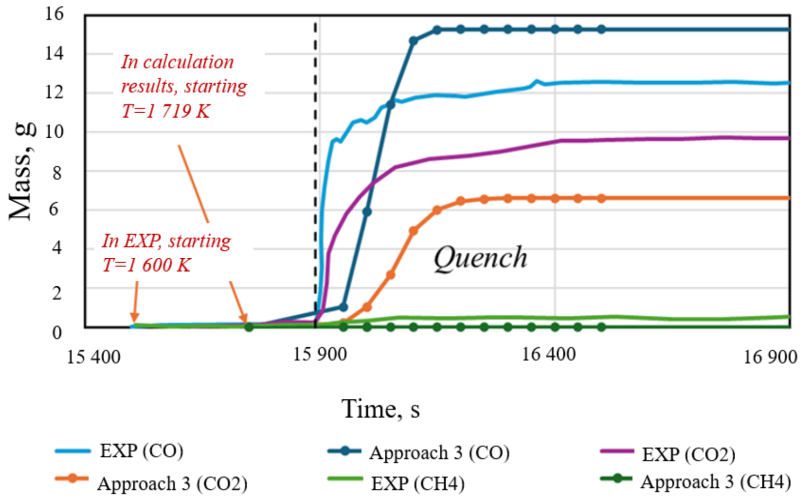

Fig. 71. The Gas Release from the B_4C Oxidation Processes [22]

[22] Elsalamouny N., Kaliatka T., Kaliatka A. "QUENCH-20 test analysis using RELAP/SCDAPSIM severe accident code". Nuclear Engineering and Design. Elsevier, 2024, Vol. 419, 112995, p. 1-12. ISSN 0029-5493. https://doi.org/10.1016/j.nucengdes.2024.112995.

CONCLUSIONS AND RECOMMENDATIONS

To develop a methodology for investigating physical processes in nuclear facilities with both symmetric and asymmetric geometries, numerical investigations of severe accident experiments that resulted in partial core melting were conducted. The investigations, performed applying the BEPU approach and severe accident code RELAP/SCDAPSIM together with the SUSA statistical tool, allowed us to summarise the following conclusions:

1. The CORSOR-M model effectively estimates Cs/I release in early degradation phases. However, later phases require models that account for more than just temperature-driven release of fission products.
2. The BEPU-based uncertainty analysis confirms the reliability of simulation results for the facilities with symmetric geometry; in most analysed cases, the calculated ranges bound experimental data. Sensitivity analysis highlights:
   - Material properties and boundary conditions strongly affect results (Spearman rank correlation coefficient >0.78).
   - SCDAP parameters related to cladding rupture and oxidation significantly influence late-phase degradation (Spearman rank correlation coefficient >0.4).
3. Building on insights from symmetric geometry experiments (PHEBUS-FPT1, QUENCH-06), a methodology for the asymmetric geometry was developed and applied. Pseudo-symmetrical and three-component-level modelling approaches were developed and evaluated using the asymmetrical QUENCH-20 experiment:
   - <u>Pseudo-symmetrical:</u> this approach allows obtaining accurate pre-quenching results but underestimates hydrogen generation during quenching by ~30%.
   - <u>SCDAP Shroud component:</u> using this approach, the obtained results match temperature data well; underestimates hydrogen (~18% or 10g) due to missing B_4C oxidation modelling.
   - <u>SCDAP Blade box component:</u> this approach allows obtaining a good temperature match for cladding; it lacks heat transfer modelling, causing underestimation of oxidation and hydrogen (~50% lower).
   - <u>SCDAP PWR control rod + Shroud components:</u> this approach allows the best match with experimental data, calculated hydrogen generation (~12% less); includes B_4C oxidation effects.

4 SANTRAUKA

ĮVADAS

Branduolinė energetika gali reikšmingai prisidėti sprendžiant dabartinius energetikos klausimus Europos Sąjungoje ir Lietuvoje[1], taip padidinant energijos tiekimo saugumą, užtikrinant kainų stabilumą, taip pat mažinant anglies dvideginio emisiją [2], [3], [4]. Deja, tragiški įvykiai Trijų Mylių salos [5], [6], Černobylio [6] ir Fukušimos [7] branduolinėse elektrinėse išryškino sunkias branduolinių avarijų pasekmes. Šios katastrofos parodė, kaip svarbu tobulinti saugos priemones, gerinti avarijų valdymo strategijas ir kurti skaitines priemones, kad būtų galima tiksliai numatyti avarijų scenarijus ir sumažinti avarijų pasekmes [8]. Tokie atvejai parodo esamų ir naujų branduolinių elektrinių saugos klausimų tyrimo aktualumą. Sunkiųjų avarijų, ypač sukeliančių dalinį aktyviosios zonos išsilydymą, metu vyksta sudėtingi fizikiniai reiškiniai, tokie kaip šiluminių elementų irimas, vandenilio susidarymas ir skilimo produktų išsiskyrimas. Šiuos reiškinius lėmė daugybė veiksnių: termohidrauliniai procesai, medžiagų elgsena aukštoje temperatūroje ir cheminės reakcijos [9]. Reaktoriaus saugumui padidinti ir sunkiųjų avarijų grėsmei sumažinti reikia suprasti šiuos fizikinius reiškinius ir tiksliai juos modeliuoti.

Šioje disertacijoje nagrinėjami sunkiųjų avarijų reiškiniai, grįsti eksperimentiniais tyrimais, daugiausiai dėmesio skiriant PHEBUS [10] ir QUENCH eksperimentinėms programoms [11]. Šie eksperimentai suteikia vertingos informacijos apie šiluminių elementų elgseną, vandenilio susidarymą ir skilimo produktų išsiskyrimą sunkiųjų avarijų metu. Šiluminių elementų irimas, vandenilio susidarymas ir skilimo produktų išsiskyrimas išsamiai nagrinėjamas PHEBUS eksperimentinėje programoje, kurioje naudojamas apšvitintas kuras [10]. QUENCH eksperimentinė programa orientuota į kuro rinklės perkaitimo ir užpylimo vandeniu procesus [11], o vietoj tikro branduolinio kuro naudojami imitatoriai. Šiais eksperimentais detaliai tiriamas šiluminių elementų apvalkalų irimas ir vandenilio susidarymas, kuomet įkaitusi aktyvioji zona užpilama vandeniu, taip imituojant aušinimo sistemų darbo atkūrimą.

Minėtiems sudėtingiems reiškiniams modeliuoti naudojami skaitiniai įrankiai paremti geriausio įverčio (BE) metodu [12], [13]. Šie skaitiniai įrankiai nuolat tobulinami ir validuojami pagal eksperimentinių tyrimų rezultatus. Deja, sunkiųjų avarijų skaitiniai tyrimai turi daug neapibrėžčių, dėl kurių skaitinės prognozės gali būti netikslios. Siekiant tiksliau sumodeliuoti fizikinius reiškinius reikia įvertinti rezultatų neapibrėžtis. Projektinių avarijų analizei sukurtą geriausio įverčio ir neapibrėžčių metodą (angl. Best Estimate + Uncertainty, BEPU) taip pat galima taikyti ir sunkiųjų avarijų modeliavime [14], [15]. HORIZON 2020 MUSA [16] projektas ir Tarptautinės atominės energijos agentūros (TATENA) koordinuojamas tyrimų projektas [17],Vandeniu aušinamų reaktorių sunkiųjų avarijų analizei skirtų neapibrėžties ir jautrumo metodikų pritaikymo tobulinimas (angl. Advancing the State-of-Practice in Uncertainty and Sensitivity Methodologies for Severe Accident

Analysis in Water-Cooled Reactors) buvo vienas iš pirmųjų tokių bandymų tarptautiniu mastu. Šioje disertacijoje toliau tiriamas BEPU metodo taikymas sunkiųjų avarijų modeliavimui. Kitas skaitinėje analizėje iškylantis sunkumas yra sunkiųjų avarijų modeliavimas branduolinės energetikos objektuose, turinčiuose asimetrinę geometrinę struktūrą. Dauguma esamų skaitinių modeliavimo įrankių paremti simetriniais modeliais. Šiame darbe nagrinėjamas tokių modeliavimo priemonių taikymo ribotumas ir pateikiama fizikinių procesų ne simetrinės struktūros objektuose įvertinimo metodika.

Darbo aktualumas

Katastrofos Trijų Mylių salos, Černobylio ir Fukušimos branduolinėse elektrinėse paskatino daugiau tyrinėti fizikinius reiškinius, vykstančius sunkiųjų avarijų metu, ir peržiūrėti branduolinių reaktorių saugos gaires. Šiems reiškiniams tirti įgyvendintos PHEBUS, QUENCH, CORA ir kitos eksperimentinių tyrimų programos, kartu atliekant skaitinį modeliavimą pasitelkus tokius sunkiųjų avarijų skaitinio modeliavimo įrankius kaip ASTEC, AC2, MELCOR, RELAP/SCDAPSIM ir kitus. Iš pradžių vertinant branduolinių reaktorių saugą modeliavimui buvo naudojami konservatyvūs metodai. Tačiau tokie metodai galėjo pateikti per daug konservatyvų įvertinimą ir (arba) užmaskuoti kai kuriuos svarbius saugos klausimus. Šiuolaikinėse skaitinėse analizėse tikslumui pagerinti naudojami geriausiu įverčiu (BE) grįsti įrankiai, kurie validuojami atsižvelgiant į atliktus eksperimentus. Deja, modeliuojant sunkiąsias avarijas, vis dar susiduriama su reikšmingomis neapibrėžtimis, kurias būtina įvertinti. Projektinėms avarijoms analizuoti sukurtas geriausio įverčio ir neapibrėžties metodas (BEPU) pradėtas taikyti ir sunkiųjų avarijų skaitiniams tyrimams. BEPU metodas naudotas HORIZON 2020 MUSA ir TATENA koordinuojamuose tyrimų projektuose, tačiau šio metodo taikymui reikalingi išsamesni tyrimai. Asimetrinės geometrinės struktūros branduolinių įrenginių modeliavimas yra kitas skaitinių tyrimų iššūkis, kadangi dauguma skaitinių tyrimo įrankių sukurti simetrišką struktūrą turintiems įrenginiams. Labai svarbu apibrėžti tokių modelių ribotumą ir ieškoti alternatyvių būdų asimetrinės konfigūracijos įrenginiams analizuoti.

Darbo objektas

Šioje disertacijoje nagrinėjamos sunkiosios avarijos, sukeliančios dalinį aktyviosios zonos išsilydymą lengvojo vandens reaktoriuose, taikant RELAP/SCDAPSIM programų paketą kartu su BEPU metodu.

Darbo tikslai

Fizikinių reiškinių simetrinės ir asimetrinės struktūros branduoliniuose įrenginiuose skaitiniams tyrimams pasiūlyti eksperimentiniais duomenimis paremto tyrimo metodologiją, kurios pagrindas yra BEPU metodas.

Darbo uždaviniai

1. Sukurti eksperimentinių įrenginių skaitinius modelius, imituojančius dalinį aktyviosios zonos išsilydymą sunkiųjų avarijų metu, ir įterpti CORSOR-M skaitinį modelį į RELAP/SCDAPSIM programų paketą, taip sprendžiant programų paketo ribotumą apskaičiuojant skilimo produktų išsiskyrimą.

2. Taikant BEPU metodą apskaičiuoti rezultatų neapibrėžtis, atsižvelgiant į pradinių parametrų, kraštinių sąlygų bei modelio parametrų neapibrėžtumus. Taip pat nustatyti šių neapibrėžtų parametrų įtaką modeliavimo rezultatams.

3. Išanalizuoti sunkiųjų avarijų metu asimetrinės struktūros įrenginiuose vykstančius fizikinius procesus.

Darbo naujumas

BEPU metodo taikymas analizuojant dalinį aktyviosios zonos išsilydymą sukeliančias sunkiąsias avarijas simetrinės ir asimetrinės struktūros eksperimentiniuose įrenginiuose yra nauja metodika, kuri išplečia sunkiųjų avarijų analizės įrankių panaudojimą ir įvertina modeliavimo neapibrėžtis.

Praktinė vertė

Sukurta metodika, pagrįsta BEPU metodu, leido analizuoti sunkias avarijas įrenginiuose su simetrine ir asimetrine struktūra. Parengtos rekomendacijos skaitiniams tyrimams.

Ginamieji teiginiai

1. RELAP/SCDAPSIM programų paketas su į jį įtrauktu CORSOR-M skaičiavimo modeliu gali būti naudojamas Cs ir I išsiskyrimo frakcijai ankstyvos degradacijos fazėje įvertinti.

2. Skaitmeninio modeliavimo neapibrėžtumų įvertinimas, taikant BEPU metodą, padeda geriau suprasti sunkių avarijų skaitinį modeliavimą ir modeliavimo rezultatų patikimumo lygį.

3. Naudojant pseudosimetrinį modelį (sukurtą remiantis PHEBUS ir QUENCH eksperimentų modeliavimo patirtimi) asimetrinei struktūrai, galima įvertinti procesus kuro rinklėje tik prieš oksidacijos ir pereinamojoje fazėse. Norint geriau skaitmeniniu būdu įvertinti intensyvius oksidacijos procesus remiantis asimetrinės struktūros

įrenginių eksperimentiniais duomenimis, reikalingas detalus atskirų komponentų modeliavimas.

4.1 Mokslinių tyrimų apžvalga

Branduolinėje elektrinėje sunkioji avarija įvyksta tuomet, kai nesuveikia kelios saugos sistemos, dėl to gali būti pažeista reaktoriaus aktyvioji zona ir į aplinką išsiskirti radioaktyvių medžiagų. Nors tokios avarijos retos, jos gali turėti sunkių pasekmių aplinkai ir žmonių sveikatai. Sunkiosios avarijos priskiriamos neprojektinėms avarijoms, tarp kurių žymiausi istoriniai pavyzdžiai yra avarija Trijų Mylių salos elektrinėje (1979 m.) [5], Černobylio elektrinėje (1986 m.) [6] ir Fukušimos elektrinėje (2011 m.) [7]. Visos šios avarijos sukėlė reaktoriaus aktyviosios zonos išsilydimą. Yra daug scenarijų ar įvykių, kurie gali sukelti sunkias avarijas lengvosiose vandens sistemose, pvz., LOCA, SBO ir kt [9], [13].

Šiluminiai elementai lengvojo vandens reaktoriuose gali būti pažeisti ir dėl reaktoriaus galios padidėjimo (padidėjęs reaktyvumas) arba nepakankamo aušinimo, pavyzdžiui, aušinančio srauto sumažėjimo arba šilumnešio praradimo (LOCA). Lengvojo vandens reaktoriuose padidėjusį reaktyvumą galima kontroliuoti ribojant reaktyvumo greitį ir neigiamo reaktyvumo grįžtamojo ryšio mechanizmais, skirtingai nei didelės galios kanaliniuose reaktoriuose (rus. Реактор Большой Мощности Канальный, RBMK), tokiuose kaip Černobylio elektrinėje. Vis dėlto, išanalizavus daugelį sunkiųjų avarijų, matome, kad branduolinio kuro šiluminių elementų pažeidimus dažniausiai sukelia nepakankamas jų aušinimas, kaip Trijų Mylių salos [9] ar Fukušimos [7] elektrinių avarijų atveju.

4.1.1 Sunkiųjų avarijų lengvojo vandens reaktoriuje etapai

1. Pradžia. Įvyksta priežastinis įvykis, o dėl saugos sistemų gedimų aušinimas yra nepakankamas. Reaktorius sustabdomas (įvedami valdymo strypai), tačiau dalis radioaktyviųjų medžiagų skyla toliau ir išskiriama šiluma.

2. Aktyvioji zona nusausėja ir kaista. Sumažėjus šilumnešio kiekiui nusausėja aktyvioji zona ir dėl to staigiai pakyla branduolinio kuro temperatūra [9].

3. Cirkonio reakcija su garu, vandenilio susidarymas. Perkaitintas cirkonio apvalkalas reaguoja su garais, sudarydamas cirkonio oksido sluoksnį, išskirdamas vandenilį ir papildomą šilumos kiekį, kuris dar padidina šilumos kiekį reaktoriuje [18], [19], [20].

$$Zr + 2H_2O \rightarrow ZrO_2 + 2H_2 \qquad \text{(4-1 lygtis)}$$

4. B_4C oksidacija – taip pat svarbus veiksnys, kai reaktoriaus aktyvioji zona užpilama vandeniu. Tai skatina vandenilio ir kitų degiųjų dujų susidarymą [20], [21], [22], [23].
   $B_4C + 7H_2O \rightarrow 2B_2O_3 + CO + 7H_2 + Heat$ (4-2 lygtis)
   $B_4C + 8H_2O \rightarrow 2B_2O_3 + CO_2 + 8H_2 + Heat$ (4-3 lygtis)
   $B_4C + 6H_2O \rightarrow 2B_2O_3 + CH_4 + 4H_2 + Heat$ (4-4 lygtis)
5. Branduolinio kuro lydimasis ir branduolinio kuro lydalo susidarymas. Išsilydę cirkonio kuro elementų apvalkalai maišosi su urano oksidu, susidaro branduolinio kuro lydalas (U-Zr-O) [9].
6. Skilimo produkto išsiskyrimas. Iš besilydančio branduolinio kuro išsiskiria skilimo produktai, kurie gali išsiskirti iš reaktoriaus slėginio indo.
7. Aktyviosios zonos nutekėjimas į reaktoriaus apačią ir garų sprogimas. Išsilydęs branduolinis kuras nuteka į slėginio indo apačią, kur yra susikaupusio vandens. Karštas lydalas, reaguodamas su vandeniu, sukelia staigų garavimą, didėja slėgis reaktoriaus kiaute, o tai silpnina reaktoriaus konstrukcijas ir skatina likusio branduolinio kuro lydymąsi.
8. Betono erozija ir galimas prasiskverbimas į žemę. Branduolinio kuro lydalas ardo betoninį pagrindą (išskirdamas CO_2 ir kitas dujas) ir gali pro jį prasiskverbti. Jei tai įvyktų, radioaktyvios medžiagos patektų į aplinką.

Sunkiųjų avarijų skaitinio modeliavimo įrankių apžvalga

Sunkiųjų avarijų eksperimentuose modeliuojami pirmiau aprašyti konkretūs sunkiosios avarijos vyksmo reiškiniai. Sukurta keletas skaitinio modeliavimo įrankių, kurie remiasi arba (ir) yra validuoti atsižvelgiant į eksperimentinius duomenis. Norint ištirti ir imituoti pasirinktų reiškinių sąveiką ir įvertinti reaktoriaus saugą, būtina naudoti integralinius sunkiųjų avarijų modeliavimo įrankius (ASTEC, RELAP/SCDAPSIM, MELCOR ir kt.), kurie modeliuoja sunkiųjų avarijų eigą ir gali įvertinti vandenilio susidarymą, branduolinio kuro irimą, skilimo produktų išsiskyrimą ir kitus analizuoti pasirinktus reiškinius. 12 lentelėje palyginami keli sunkiųjų avarijų modeliavimo įrankiai, skirti modeliuoti pasirinktus sunkiosios avarijos reiškinius.

12 lentelė. Sunkiųjų avarijų modeliavimo įrankių palyginimas

Reiškinys	**ASTEC** [24], [34]	**MAAP** [34]	**MELCOR** [32]	**ICARE /CATHARE** [29]	**RELAP5 /SCDAPSIM** [31]
Termo-hidraulinių procesų modeliavimo dalis	Supaprastinta	Supaprastinta	Supaprastinta	Detali	Detali
Sunkiųjų avarijų modeliavo dalis	Detali	Supaprastinta	Detali	Detali	Detali

Reiškinys	ASTEC [24], [34]	MAAP [34]	MELCOR [32]	ICARE /CATHARE [29]	RELAP5 /SCDAPSIM [31]
Šiluminio elemento apvalkalo išsipūtimas	✓	✓	-	✓	✓
Zr, SS, B_4C oksidacija	✓	✓	✓	✓ -	✓
Apvalkalo suirimas	✓	✓	✓	✓	✓
Šiluminių elementų rietinės deformacija	✓	✓	✓	✓	✓
Vandenilio susidarymas	Išsamūs ir integruoti modeliai	Supaprastinti modeliai	Išsamūs modeliai	Išsamūs modeliai	Išsamūs modeliai
Neutronus sugeriančių menčių modeliai	Oksidacijos, apvalkalo suirimo ir skilimo produktų išsiskyrimo modeliai	Oksidacijos modeliai	Oksidacijos, apvalkalo suirimo ir skilimo produktų išsiskyrimo modeliai	Oksidacijos ir mechaninio suirimo modeliai	Oksidacijos ir mechaninio suirimo modeliai
Skilimo produktų išsiskyrimas	Išsamūs ir integruoti skilimo produktų išsiskyrimo, pernašos ir nusėdimo modeliai.	Supaprastinti skilimo produktų išsiskyrimo modeliai.	Detalūs skilimo produktų išsiskyrimo, pernašos ir cheminės sąveikos modeliai.	Pažangūs skilimo produktų išsiskyrimo ir pernašos modeliai.	Tik iš tarpo ištekėjusių skilimo produktų tokių kaip (Xe+Kr+He) ir (CsI+CsOH) modeliai. Galima įdiegti papildomus modelius.

4.1.2 Eksperimentinių sunkiųjų avarijų tyrimo programų apžvalga

Po avarijos Trijų Mylių salos elektrinėje pradėtos kelios tarptautinės eksperimentinės programos, skirtos sunkiųjų avarijų reiškiniams lengvojo vandens reaktoriuose tirti. Šios programos pagal eksperimentų atlikimo sąlygas skirstomos į realias (naudojami tikri šiluminiai elementai) ir imitacines (naudojami elektra kaitinami imitaciniai šiluminiai elementai). Jose daugiausiai dėmesio skiriama aktyviosios zonos elgsenai sunkiųjų avarijų sąlygomis, vandenilio susidarymui, pradiniam aktyviosios zonos pažeidimui ir daliniam reaktoriaus zonos išsilydymui analizuoti. Žinomiausios eksperimentinių tyrimų programos yra CORA [35], QUENCH [11], CODEX [36], PHEBUS [10] ir kt. Šios tyrimų programos taip pat naudojamos kompiuterinio modeliavimo programoms validuoti.

4.1.3 Geriausio įverčio metodika ir įrankiai

Per pastaruosius dešimtmečius branduolinės energetikos įrenginių sauga buvo analizuojama taikant skirtingus metodus, kuriuose atsižvelgiama į medžiagų techninių duomenų pasiekiamumą, pradinių ir kraštinių sąlygų atspindėjimą kompiuterinėse programose. Skaitiniai tyrimai buvo atliekami remiantis skirtingais požiūriais [37]:

- Konservatyvusis požiūris. Pradžioje branduolinės saugos analizė rėmėsi konservatyviomis prielaidomis. Kadangi skaičiavimo galimybės buvo ribotos, o eksperimentinių duomenų nebuvo daug. Pradinės ir kraštinės sąlygos būdavo sąmoningai parenkamos taip, kad būtų galima pagrįsti itin konservatyvius įverčius. Galimos neapibrėžtys kompensuojamos konservatyviomis prielaidomis, o skaitiniams tyrimams atlikti naudojamos konservatyvios modeliavimo programos. Tokių tyrimų rezultatai gali būti per daug konservatyvūs ir neatskleisti kai kurių svarbių saugos klausimų.

- Geriausio įverčio ir neapibrėžčių metodas (BEPU) – tai metodika ir skaitiniai modeliavimo įrankiai, apjungiantys informaciją, surinktą iš istorinių duomenų, eksperimentų, skaitmeninio modeliavimo ir ekspertinio vertinimo. Tokia metodika leidžia gauti tikslesnius ir tikroviškesnius modeliavimo rezultatus. Šioje metodikoje yra naudojami geriausio įverčio skaitinio modeliavimo įrankiai ir realistiškesnės prielaidos. Geriausio įverčio modeliavimo įrankiai validuojami eksperimentinių tyrimų rezultatais. Tačiau, skaitinė sunkių avarijų analizė naudojant šį metodą susiduria su dideliais neapibrėžtumais, todėl reikia taikyti neapibrėžties kiekybinio įvertinimo metodus, kurie aptariami kitame skyriuje.

Geriausio įverčio metodai

Geriausio įverčio (BE) metodais siekiama tiksliau modeliuoti fizikinius procesus. Šiuose metoduose yra mažiau konservatyvių prielaidų, todėl galima geriau suprasti sudėtingus reiškinius ir tiksliau numatyti sunkiųjų avarijų eigą [13]. BE metodai skirstomi į dvi pagrindines kategorijas: deterministinius ir tikimybinius metodus. Deterministiniais metodais analizuojami jau sukurti scenarijai, neapibrėžčių skaičiavimuose įvedamos konservatyvios apribojimų ribos. Galimoms avarijoms saugos ribos nustatomos remiantis eksperimentiniais duomenimis ir inžineriniais sprendimais. Tikimybiniai metodai leidžia išsamiau analizuoti įvairių avarijų scenarijų tikimybę ir jų poveikį. Tikimybiniai metodai leidžia suprasti konkrečių įvykių pasireiškimo tikimybę. Taip pat jais galima įvertinti neapibrėžtis, o tai papildo scenarijų analize paremtus deterministinius metodus [38]. 13 lentelėje surašyti įvairių BE metodų privalumai ir trūkumai.

13 lentelė. Geriausio įverčio metodų palyginimas

Metodas	Privalumai	Trūkumai
GRS	▪ Validuotas naudojant įvairias sunkiųjų avarijų kompiuterinio modeliavimo programas, tokias kaip ATHLET-CD ir kt. ▪ Akcentuojamas neapibrėžties ir jautrumo analizių vertinimas. ▪ Gali būti naudojamas tiek su deterministiniais, tiek su tikimybiniais metodais. ▪ Identifikuoja daug parametrų. ▪ Pritaikomas įvairiems avarijų scenarijams.	▪ Kelių avarijų scenarijams apdoroti prireiks didesnių skaičiavimo pajėgumų. ▪ Ribotas pritaikymas tarptautiniu mastu lyginant su kitais metodais.
IPSN	▪ Išsamioje analizėje derinami deterministiniai ir tikimybiniai metodai. ▪ Patikimas validavimas eksperimentiniais tyrimais, ypač pagal PHEBUS programą.	▪ Labai priklauso nuo sudėtingų eksperimentų ir išsamaus validavimo, o tai gali riboti metodo pritaikomumą kai kuriems sunkiųjų avarijų scenarijams. ▪ Reikalinga prieiga prie išsamių eksperimentinių duomenų (kurių gali ir nebūti).
CSAU	▪ Naudojamas sisteminis metodas, leidžiantis, pritaikyti eksperimentuose gautus modeliavimo rezultatus modeliuojant avarijas branduolinėje elektrinėje. ▪ Išsamiai kiekybiškai įvertinama neapibrėžtis. ▪ Naudojamas JAV ir pripažintas tarptautiniu mastu	▪ Užima daug laiko dėl intensyvaus eksperimentų rezultatų pritaikymo branduolinėse elektrinėse ir neapibrėžties kiekybinio įvertinimo proceso. ▪ Konservatyvūs įverčiai apibrėžiami pasikliaunant ekspertiniu vertinimu.
ENUSA	▪ Daugiausia dėmesio skiriama išsamiam sunkiųjų avarijų modeliavimui Ispanijos branduolinėse elektrinėse. ▪ Didelė patirtis modeliuojant avarijas Europos branduolinėse elektrinėse.	▪ Ribotas taikymas už Ispanijos ribų. ▪ Palyginti siaura tarptautinių sunkiųjų avarijų lyginamosios analizės taikymo sritis

Metodas	Privalumai	Trūkumai
GSUAM	▪ Pateikiama sunkiųjų avarijų neapibrėžties analizės sistema. ▪ Gera galimybė nagrinėti sudėtingus fizikinius reiškinius sunkiųjų avarijų sąlygomis taikant tikimybinius metodus.	▪ Gali reikėti didelių skaičiavimo resursų. ▪ Norint gauti tikslius rezultatus, reikia įvesti daug duomenų.
BEAU	▪ Pateikia tikroviškas geriausio įverčio prognozes su neapibrėžties analize. ▪ Leidžia geriau suprasti avarijos eigą.	▪ Gana naujas palyginti su kitais BE metodais. ▪ Norint naudoti šį metodą, reikia jį validuoti remiantis eksperimentiniais duomenis (reikalauja daug laiko ir duomenų).

BEPU įrankiai

BEPU įrankiai skirti apskaičiuoti rezultatų neapibrėžtis. Taikant šiuos įrankius gaunamos tikroviškesnės modeliavimo rezultatų prognozės. Šiame skyriuje apžvelgiami sunkiųjų avarijų analizėje naudojami BEPU statistiniai įrankiai. BEPU įrankių palyginimas pateikiamas 14 lentelėje. Lentelėje nurodomas kiekvieno įrankio kūrėjas, naudojama BE metodologija ir vartotojo sąsaja.

14 lentelė. Geriausio įverčio įrankiai

Funkcija / Įrankis	**SUSA** [49]	**SUNSET** [55]	**DAKOTA** [56]	**RAVEN** [52], [53]
Programos kūrėjas	GRS (Gesellschaft für Anlagen- und Reaktorsicherheit)	IRSN (Institut de Radioprotection et de Sûreté Nucléaire)	Sandia National Laboratories	Idaho National Laboratory (INL)
Pagrindinis dėmesys	Branduolinės saugos neapibrėžties ir jautrumo analizė	Branduolinės saugos neapibrėžties ir jautrumo analizė	Projektavimo ir analizės priemonių rinkinys optimizavimui ir neapibrėžties kiekybiniam įvertinimui	Rizikos analizė ir poveikio aplinkai vizualizavimas
Taikymo sritis	Branduolinės saugos analizė	Branduolinės saugos analizė	Platus pritaikymas pramonėje, įskaitant orlaivių ir erdvėlaivių sektorių,	Branduolinė sauga, rizikos vertinimas ir poveikio aplinkai analizė

Funkcija / Įrankis	**SUSA** [49]	**SUNSET** [55]	**DAKOTA** [56]	**RAVEN** [52], [53]
			statybos sektorių ir branduolinę energetiką	
Metodikos	Statistinė atranka, koreliacinė analizė	Statistinė atranka, dispersinės analizės metodai	Optimizavimas, parametrų įvertinimas, neapibrėžties kiekybinis įvertinimas	Tikimybinė analizė, neapibrėžties kiekybinis įvertinimas, rizikos vertinimas
Integracija	Integruojamas su įvairiais branduolinės saugos skaitiniais įrankiais (pvz., RELAP, MELCOR).	Integruojama su įvairiais branduolinės saugos skaitiniais įrankiais (pvz., ASTEC, CATHARE).	Sąsajos su įvairiomis modeliavimo priemonėmis ir modeliais	Integruojamas su RELAP5-3D, MOOSE sistema ir kitais INL įrankiais
Rezultatų analizė	Išsami statistinė analizė, grafikai	Statistinė analizė, jautrumo indeksai	Išsamios ataskaitos, grafinis atvaizdavimas	Modernios vizualizavimo priemonės, išsamios rizikos analizės ataskaitos
Vartotojo sąsaja	Komandinės eilutės ir grafinė vartotojo sąsaja	Komandinės eilutės sąsaja	Komandinės eilutės ir grafinė vartotojo sąsaja	Grafinė vartotojo sąsaja

4.1.4 Autorės indėlis į nagrinėjamą temą

Literatūros šaltinių analizė parodė, kad daug dėmesio skiriama sunkiosioms avarijoms, ypač sukeliančioms dalinį aktyviosios zonos išsilydymą. Šių avarijų metu vyksta sudėtingi fizikiniai reiškiniai, tokie kaip šiluminių elementų irimas, vandenilio susidarymas ir skilimo produktų išsiskyrimas. Šie procesai nagrinėjami eksperimentiniuose tyrimuose naudojant skaitinio modeliavimo įrankius. Sunkiosioms avarijoms modeliuoti naudojami skaitinio modeliavimo įrankiai, kurie validuojami atsižvelgiant į eksperimentinių tyrimų rezultatus. Deja, skaičiavimo rezultatai turi neapibrėžčių. Neapibrėžčių įvertinimui galima naudoti BEPU metodą, tačiau dėl savo sudėtingumo jis nėra plačiai naudojamas sunkiųjų avarijų modeliavime.

Siekdama išspręsti šią problemą, autorė pasiūlė metodiką, skirtą fizikinių procesų skaitmeniniam tyrimui, kuri pagrįsta eksperimentiniais duomenimis ir BEPU metodo taikymu. PHEBUS FPT-1 ir QUENCH-06 eksperimentų skaitiniai modeliai buvo atnaujinti ir papildyti naujausiais duomenimis. Skaitmeniniai tyrimai buvo atlikti naudojant sunkiųjų avarijų programų paketą RELAP/SCDAPSIM, o gautų skaičiavimo rezultatų neapibrėžtumo kiekybiniam įvertinimui buvo taikomas BEPU metodas, pagrįstas GRS metodika ir naudojant SUSA statistinį įrankį.

Kita mokslinėje literatūroje pastebėta problema yra asimetrinės struktūros įrenginiuose vykstančių fizikinių procesų nagrinėjimas skaitinio modeliavimo priemonėmis. Dauguma sunkiųjų avarijų modeliavimo priemonių sukurtos simetriškos struktūros įrenginiams, o tai lemia galimus netikslumus taikant juos asimetrinės struktūros sistemoms (kai kuriems eksperimentiniams įrenginiams, panaudoto branduolinio kuro baseinams ir kt.).

Autorė, remdamasi ankstesnių simetrinės struktūros eksperimentų (PHEBUS-FPT1 ir QUENCH-06) modeliavimo patirtimi, sukūrė skaitinius modelius ir rekomendacijas RELAP/SCDAPSIM sunkiųjų avarijų programų paketui, siekdama ištirti fizikinius procesus QUENCH-20 eksperimente, pagrįstame asimetrine struktūra.

4.2 Tyrimo metodologija

Tiriamojo darbo metodologija grafiškai pavaizduota 72 pav. Pirmiausiai identifikuojami fizikiniai reiškiniai, sukeliantys dalinį aktyviosios zonos išsilydymą, įskaitant branduolinio kuro degradaciją, Zr oksidaciją, B_4C oksidaciją, vandenilio susidarymą, apvalkalo trūkį ir skilimo produktų išsiskyrimą. Tuomet pasirenkami eksperimentai šiems sunkiosios avarijos reiškiniams imituoti. Eksperimentai skirstomi į dvi kategorijas: simetrinės ir asimetrinės struktūros eksperimentus. Pasirenkamos skaitinio modeliavimo programos pasirinktiems eksperimentams modeliuoti ir ištirti eksperimentuose vykstančius fizikinius reiškinius. Analizė vykdyta dviem kryptimis: 1) Modelio kūrimas eksperimentams simetrinės struktūros objektuose. Atliekamas pasirinktų reiškinių etaloninis modeliavimas. Atliekama neapibrėžtumo ir jautrumo analizė modelio prognozėms patikslinti taikant geriausio įverčio metodą. Iš simetrinės struktūros objektų analizės gautos įžvalgos ir patirtis prisideda prie eksperimentų asimetrinės struktūros objektuose analizės. 2) Modelio kūrimas asimetrinės struktūros įrenginiuose ar eksperimentuose. Sukuriamas pseudosimetrinis modelis ir komponentų lygmens modeliai asimetrinės struktūros problemoms spręsti. Parengiamos rekomendacijos fizikiniams reiškiniams asimetrinės struktūros objektuose modeliuoti. Jos prisideda prie avarijų analizės metodologijų tobulinimo.

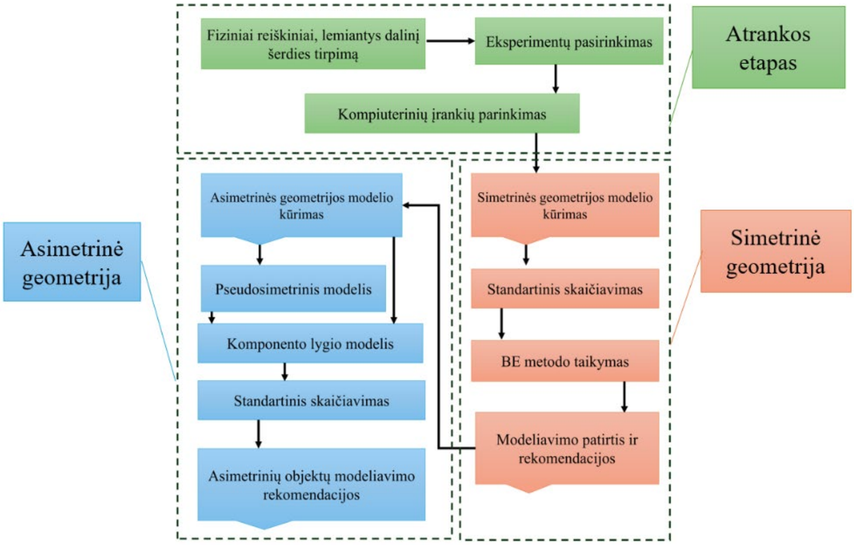

72 pav. Tyrimo metodologija

4.2.1 Fizikinių reiškinių, sukeliančių dalinį aktyviosios zonos išsilydymą, parinkimas

Detaliam tyrimui buvo atrinkti fizikiniai reiškiniai, kurie yra svarbūs analizuojant dalinį reaktoriaus aktyviosios zonos lydymąsi sunkios avarijos metu. Šie reiškiniai atspindi sunkiųjų avarijų eigą – aktyviosios zonos medžiagų, tokių kaip nerūdijantis plienas (SS), cirkonis (Zr) ir boro karbidas (B_4C) oksidacija ir šiluminių elementų irimas. Šiame tyrime nagrinėjamas skilimo produktų išsiskyrimas, ypač tų, kurie išsiskiria iš tarpo tarp kuro tablečių ir šiluminio elemento apvalkalo. Tai labai svarbu vertinant sunkiųjų avarijų radiologines pasekmes aplinkai ir žmonių sveikatai. Sunkiųjų avarijų analizėje svarbiu reiškiniu laikoma vandenilio susidarymas vykstant cirkonio apvalkalo ir garų reakcijai aukštoje temperatūroje. Vandenilis yra degios dujos, kurios padidina sprogimo tikimybę.

4.2.2 Skaitinio modeliavimo programų parinkimas

Po avarijos Trijų Mylių salos elektrinėje buvo sukurta daug skaitinio modeliavimo įrankių, skirtų modeliuoti sunkiųjų avarijų metu vykstančius fizikinius reiškinius. Šie modeliavimo įrankiai validuojami palyginus jais apskaičiuotus rezultatus su eksperimentiniais duomenimis. Palyginus 12 lentelėje apibendrintus sunkiųjų avarijų modeliavimo įrankius, šiame darbe analizei buvo pasirinktas

RELAP/SCDAPSIM programų paketas. RELAP/SCDAPSIM programų paketas išsamiai modeliuoja termohidraulinę elgseną ir dalinį aktyviosios zonos išsilydymą, atsižvelgiant į įvairius avarijų scenarijus. RELAP/SCDAPSIM programų pakete integruoti RELAP5 ir SCDAP modeliai leidžia detaliai imituoti reaktoriaus aušinimo sistemas, aktyviosios zonos pažeidimo eigą ir skilimo produktų išsiskyrimą. Su RELAP/SCDAPSIM programų paketu galima imituoti daugybę sunkiųjų avarijų, sukeliančių dalinį aktyviosios zonos išsilydymą, scenarijų taip pat ir asimetrinės struktūros objektuose.

4.2.3 Eksperimentų parinkimas

Šiame darbe analizuojami dviejų tipų eksperimentai, t. y., kurių geometrinė struktūra yra simetrinė ir kurių asimetrinė. Šie eksperimentai buvo pasirinkti siekiant įvertinti sunkiųjų avarijų, su daliniu aktyviosios zonos išsilydymu, eigą priklausomai nuo objekto geometrinės struktūros. Dėl skirtingos geometrinės struktūros gali atsirasti skirtingų fizikinių reiškinių (pvz., asimetrinis temperatūrinis pasiskirstymas), o tai sudaro papildomų sunkumų modeliuojant avariją. Simetrinės struktūros objektams buvo pasirinktos PHEBUS FPT-1 ir QUENCH-06 eksperimentinės programos. Eksperimentinių programų pasirinkimas simetrinės struktūros objektams grindžiamas tuo, kad šie eksperimentai imituoja skirtingus fizikinius reiškinius, kylančius sunkiosios avarijos metu, dėl kurių iš dalies išsilydo aktyvioji zona. Be to, šios eksperimentinės programos gerai žinomos ir turi išsamių eksperimentų duomenų. Pasirenkant analizuoti šiuos eksperimentus, taip pat buvo atsižvelgta ir į analizei reikalingų duomenų prieinamumą. Tirti procesus asimetrinės geometrinės struktūros objektuose buvo pasirinktas QUENCH-20 eksperimentas. QUENCH-06 ir QUENCH-20 eksperimentų kraštinės sąlygos panašios, tačiau skirtingos eksperimentuose naudojamos kuro rinklės (QUENCH-06 atitinka PWR, o QUENCH-20 atitinka BRW), todėl galima palyginti rezultatus ir pamatyti skirtingų rinklių bei simetrinių ir asimetrinių skirtumų įtaką. Eksperimentų detalės pateiktos 15 lentelėje.

15 lentelė. Eksperimentų, kuriais imituojamos sunkiosios avarijos, sukeliančios dalinį reaktoriaus aktyviosios zonos išsilydymą, atranka

Eksperimentai	Eksp. fazės	Eksp. fazės, palyginimas su reaktoriaus darbu	Analizuojami fizikiniai reiškiniai
PHEBUS FPT-1 *Suslėgtojo vandens reaktorių kurui. Bandymui naudoti apšvitinti šiluminiai elementai.*	Pirminė oksidacija, oksidacija, pastovi galia, kaitinimas, vėsinimas (garais)	Pirminės oksidacijos ir oksidacijos fazės reikalingos sukurti oksido sluoksnį, kuris susidaro reaktoriaus aktyviojoje zonoje	Šilumos perdavimas reaktoriaus aktyviojoje zonoje ir aplinkinėse konstrukcijose. Šiluminio elemento apvalkalo ir konstrukcinių

Eksperimentai	Eksp. fazės	Eksp. fazės, palyginimas su reaktoriaus darbu	Analizuojami fizikiniai reiškiniai
		per jo eksploatavimo laiką. Pastovios galios ir įkaitinimo fazės imituoja avarijos situaciją – branduolinio kuro nusausėjimą. Vėsinimo etapas naudojamas tik eksperimente	medžiagų oksidacija. Oksidacija yra egzoterminė reakcija, kuriai vykstant išskiriama papildoma šiluma ir susidaro vandenilis. Šiluminių elementų apvalkalų ir aplinkinių konstrukcijų deformacija. Skilimo produkto išleidimas Skilimo produktų pernaša
QUENCH-06 *Suslėgtojo vandens reaktorių kurui. Bandyme buvo naudojami šiluminių elementų imitatoriai* **QUENCH-20** *Verdančio vandens reaktorių kurui. Bandyme buvo naudojami šiluminių elementų imitatoriai*	Pirminė oksidacija, pereinamoji fazė, užpylimas vandeniu	Pirminės oksidacijos fazė reikalinga sukurti oksido sluoksnį, kuris susidaro reaktoriaus aktyviojoje zonoje per jo eksploatavimo laiką. Pereinamoji fazė imituoja avarijos situaciją – branduolinio kuro nusausėjimą. Užpylimo vandeniu fazės imituoja saugos priemonių taikymą (imituojamas reaktoriaus aušinimo sistemos veikimo atkūrimas) – įkaitusi aktyvioji zona užpilama vandeniu.	Šilumos perdavimas reaktoriaus aktyviojoje zonoje ir aplinkinėse konstrukcijose. Šiluminių elementų apvalkalo ir konstrukcinių medžiagų bei neutronus sugeriančių menčių oksidacija (QUENCH-20 bandyme). Oksidacija yra egzoterminė reakcija, kuriai vykstant išskiriama papildoma šiluma ir susidaro vandenilis. Šiluminių elementų apvalkalo ir aplinkinių konstrukcijų bei neutronus sugeriančių menčių deformacija (QUENCH-20 atveju). Dalinis šiluminių elementų imitatorių ir neutronus sugeriančių menčių išsilydymas (QUENCH-20 bandyme).

4.3 Eksperimentai, turintys simetrinę struktūrą

4.3.1 PHEBUS FPT-1 eksperimento skaitinio modelio kūrimas

Kaip buvo minėta 4.2.2 skyriuje, eksperimentų modeliavimui pasirinktas RELAP/SCDAPSIM programų paketas, kurio RELAP dalis atsakinga už termohidraulinius skaičiavimus, o SCDAP dalis modeliuoja procesus kuro rinklėje.

RELAP programų paketo daliai sudaryta nodalizacinė schema pavaizduota 73 (a) pav. (detalus modelio aprašymas pateiktas autorės straipsnyje [23]). Garui ir vandeniui tiekti eksperimento kraštinės sąlygos apibrėžtos naudojant nuo laiko priklausomus 80 ir 180 tūrius. Garas per nuo laiko priklausomą 85 jungtį įleidžiamas per 90 atšakos komponentą, o jo srautas į 102 vamzdžio komponentą valdomas 91 vožtuvu. Kita 92 jungtis jungia atšaką su 100 vamzdžiu. Abu šie komponentai žymi aktyviąją zoną. Aktyviosios zonos skersinis srautas imituojamas naudojant 11 atskirų jungčių (nuo 31 iki 41), jungiančių 100 ir 102 vamzdžio komponentus. Garo generatorius modeliuojamas 130, 140 ir 141 vamzdžiais, sujungtais 131, 132 ir 133 jungtimis ir prijungtais prie 142 atšakos. Papildomi 143 ir 144 vamzdžiai per 136 jungtį sujungti su nuo laiko priklausomu 150 tūriu. Apvalkalo aušinimas buvo modeliuojamas naudojant 200 vamzdį, į kurį per 185 jungtį iš 180 komponento įleidžiamas vanduo, o per 186 jungtį surenkamas į 230 tūrį.

SCDAP programų paketo dalis detaliai modeliuojama PHEBUS FPT-1 eksperimente naudojamą rinklę penkiais komponentais (73 (b) pav.): 1) Centrinis strypas 2) aštuonių apšvitintų šiluminių elementų vidinis žiedas; 3) dešimties apšvitintų šiluminių elementų išorinis žiedas; 4) du neapšvitinti šiluminiai elementai; 5) kuro rinklės apvalkalas.

[23] Elsalamouny N., Kaliatka T. “Uncertainty Quantification of the PHEBUS FPT-1 Test Modelling Results”. Energies. Basel: MDPI, 2021, Vol. 14, 7320, p. 1-17. ISSN 1996-1073. https://doi.org/10.3390/en14217320.

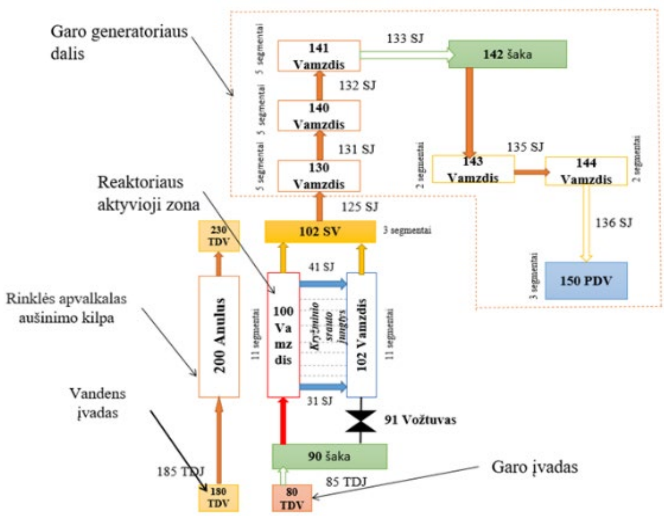

(a)

(b)

73 pav. PHEBUS FPT-1 eksperimento nodalizacinės schemos: **a)** RELAP dalis; **b)** SCDAP dalis

Šiame darbe naudojama RELAP/SCDAPSIM sunkiųjų avarijų tyrimo programų paketo versija turi apribojimų – nėra galimybės įvertinti skilimo produktų išsiskyrimo, jų pernašos ir procesų apsauginiame reaktoriaus kiaute. Todėl buvo naudojamas CORSOR−M modelis, kuris paprastas ir naudojamas tik skilimo produktų išsiskyrimui iš tarpelio įvertinti. Branduoliniame kure išsiskiriantys skilimo produktai apskaičiuojami atsižvelgiant į šiluminio elemento apvalkalo temperatūrą. CORSOR−M modelyje skilimo produktų dalinio išsiskyrimo greičio koeficientas apskaičiuojamas pagal Arėnijaus lygtį [4-5 lygtis].

$$k = k_0 \, exp\,(-\frac{Q}{RT}); \qquad \text{(4-5 lygtis)}$$

kur k – išsiskyrimo greičio koeficientas, k_0 ir Q – nuo skilimo produktų rūšies priklausančios konstantos (min^{-1} ir kcal/mol), T – absoliučioji temperatūra (K), o R – dujų konstanta 1,987 $\times 10^{-3}$ in (kcal/mol-K). k_0 *ir* Q turi daug skirtingų reikšmių, priklausomai nuo skilimo produktų rūšies ir CORSOR−M modelio modifikacijų. Cs ir I išsiskyrimui, naudojant CORSOR−M modelį, įvertinti buvo naudojamos šios konstantos: $k_0 = 2 \times 10^5$ min^{-1}; Q = 63,8 kcal/mol.

Iš branduolinio kuro išsiskyrusių skilimo produktų masė apskaičiuota pagal [4-6 lygtį]:

$$FP_r = FP(1 - exp(-k\Delta t)); \qquad \text{(4-6 lygtis)}$$

kur FP – skilimo produktų rūšies masė pirmajame laiko žingsnyje, o Δt – skirtumai tarp laiko žingsnių. CORSOR−M modelis naudojamas įvertinti išsiskiriančių skilimo produktų kiekį ir kitose sunkiųjų avarijų programų paketuose, pavyzdžiui MELCOR, ATHLET-CD.

4.3.2 QUENCH-06 eksperimento skaitinio modelio kūrimas

RELAP programų paketo daliai sudaryta nodalizacinė schema pavaizduota 74 (a) pav. (detalus modelio aprašymas pateiktas autorės straipsnyje [24]) Argonui, garui ir aušinimo vandeniui įvesti buvo naudojami nuo laiko priklausantys 001, 003 ir 005 tūriai, sujungti su 007 atšaka per nuo laiko priklausančias jungtis. Kuro rinklė, įskaitant centrinį strypą, kampinius strypus, vidinį ir išorinį šiluminių elementų imitatorių žiedus, modeliuojama kaip 010 vamzdžio komponentas, o rinklės viršuje nuo laiko priklausomas 008 tūris. Išorinis kuro rinklės aušinimas modeliuojamas naudojant 013 ir 018 vamzdžių komponentus, kuriais tiekiamas vanduo ir argonas, naudojant nuo laiko priklausančias jungtis, imituojant aušinančio vandens ir argono dujų srautus, kaip parodyta 74 (a) pav.

SCDAP programų paketo dalis modeliuoja QUENCH-06 eksperimento kuro rinklę, kuri buvo suskirstyta į penkis komponentus (74 (b) pav.). Centrinis strypas

[24] IAEA, Advancing the State of the Practice in Uncertainty and Sensitivity Methodologies for Severe Accident Analysis in Water Cooled Reactors in the QUENCH-06 Experiment No. IAEA-TECDOC-2045, 2024. [Online]. Available: https:// IAEA-TECDOC-2045

modeliuojamas kaip SCDAP Fuel komponentas. Vidinis žiedas, sudarytas iš aštuonių šiluminių elementų imitatorių, modeliuojamas naudojant SCDAP Cora komponentą. Išorinis žiedas su dvylika šiluminių elementų imitatorių, kuris taip pat modeliuojamas naudojant SCDAP Cora komponentą. Keturi kampiniai strypai modeliuojami kaip SCDAP FUEAL komponentai. Galiausiai, kuro rinklės apvalkalas, modeliuotas naudojant SCDAP Shroud komponentą.

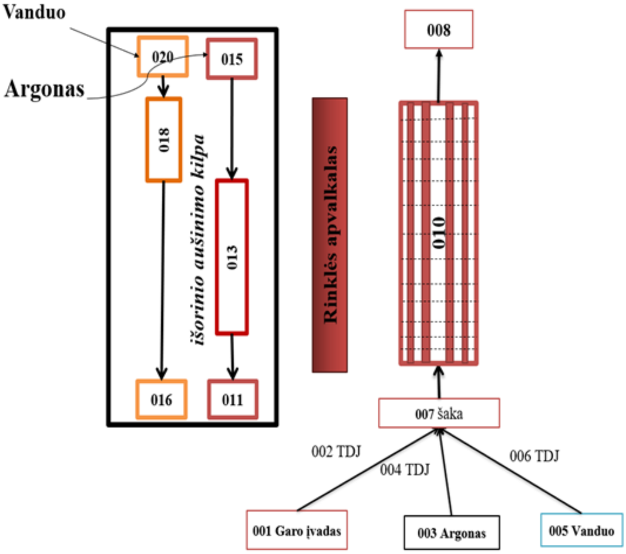

(a)

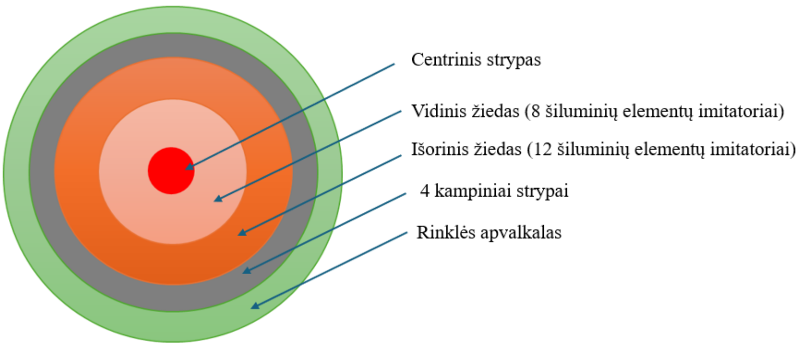

(b)

74 pav. QUENCH-06 eksperimento nodalizacinės schemos: **a)** RELAP dalis, **b)** SCDAP dalis

BE metodo ir jo taikymui skirtų statistinių priemonių pasirinkimas

Norint taikyti BEPU metodiką skaičiavimo rezultatams (siekiant įvertinti skaičiavimų neapibrėžtis), būtina pasirinkti BE metodą bei statistinį įrankį, kuris palengvintų šio metodo taikymą skaičiavimams. Šiame darbe pasirinktas GRS metodas [12]. GRS metodas tinkamas sunkiųjų avarijų analizėms, pasižymi sistemingu ir išsamiu požiūriu, orientuotu į neapibrėžčių ir jautrumo analizę. Didelis GRS metodo privalumas – kiekybiškai vertinti rezultatų neapibrėžtis. Šis metodas remiasi Wilks formule [44], [78], kuri padeda apskaičiuoti minimalų reikalingų skaičiavimų kiekį skaičiavimo neapibrėžtims įvertinti.

Statistinis įrankis SUSA [49], [50], sukurtas GRS, taip pat buvo pasirinktas neapibrėžtumo ir jautrumo analizei atlikti. SUSA taiko Monte Karlo simuliacijas, kurios leidžia įvertinti neapibrėžtų pradinių parametrų įtaką sunkiųjų avarijų modeliavimo rezultatams. Monte Karlo metodas grindžiamas plačiu atsitiktiniu pradinių parametrų mėginių ėmimu, kad būtų sukurtas tikimybinis modelio elgsenos supratimas. RELAP/SCDAPSIM programų paketo ir SUSA įrankio susiejimas leidžia išsamiai analizuoti neapibrėžtis bei nustatyti, kurie įėjimo parametrai turi didžiausią įtaką pasirinktiems skaičiavimo rezultatams (FOM). Be to, SUSA įrankis turi naudotojo grafinę sąsają, kuri palengvina rezultatų vizualizavimą ir interpretavimą.

Kaip buvo minėta anksčiau, naudojant GRS metodiką, neapibrėžtumams įvertinti reikalingas skaičiavimų skaičius priklauso nuo pasirinkto tikimybės ir patikimumo lygio, kuris nustatomas pagal Wilks formulę [78]. Šioje neapibrėžties analizėje pasirinktas 95 % tikimybės ir patikimumo lygis, norint jį pasiekti reikia atlikti 93 skaičiavimus naudojant RELAP/SCDAPSIM programų paketą. Gauti skaičiavimo rezultatai pateikiami SUSA įrankiui kuris analizuoja gautus skaičiavimo rezultatus ir pateikia skaičiavimo rezultatų apatinę ir viršutinę neapibrėžties ribas.

Jautrumo analizei atlikti yra daug įvairių koreliacijų, skirtų įvertinti pradinių neapibrėžtų parametrų įtaką skaičiavimo rezultatams. Branduolinėje srityje dažniausiai naudojamos šios koreliacijos: Pearson [79], Spearman reitingavimo koreliacija [79], [80], [82] ir Kendall reitingavimo koreliacija [80], [82]. Kiekvienas šių metodų turi savo privalumų, o pasirinkimas priklauso nuo duomenų pobūdžio ir analizės tikslų. Šiame darbe jautrumo analizei buvo pasirinkta Spearman reitingavimo koreliacija. Spearman koreliacijos koeficiento reikšmės gali būti nuo –1 iki +1. Artėjant koeficiento reikšmei prie +1 arba –1, stiprėja teigiama arba neigiama koreliacija tarp neapibrėžtų parametrų ir skaičiavimo rezultatų. Spearman reitingo koreliacijos koeficientas pateikiamas 4-7 lygtimi.

$$r_s(a,b) = \frac{\sum_{n=1}^{n}\left(R(x_i)-\frac{1}{2}(n+1)\right)(R(y_i)-\frac{1}{2}(n+1))}{\sum_{n=1}^{n}\left(Rx_i-\frac{1}{2}(n+1)\right)^2\left[\sum_{n=1}^{n}(R(y_i)-\frac{1}{2}(n+1))^2\right]^{0.5}}; \qquad \text{(4-7 lygtis)}$$

kur R reiškia kintamųjų X ir Y reitingą.

Kitas svarbus parametras jautrumo analizėje yra determinacijos koeficientas (R^2), kuris apibrėžiamas kaip populiacijos koreliacijos koeficiento kvadratas. Jis matuoja ryšį tarp kodo rezultato Y ir X reikšmės, gautos taikant tiesinę regresiją nuo parametrų X_1, X_2, ..., X_{npar}. Pateikti duomenys parodo, kokią dalį programų paketo apskaičiuotų rezultatų Y dispersijos galima paaiškinti nežinomais parametrais X_1, X_2, ..., X_{npar}, remiantis Y tiesine regresija nuo šių parametrų [84]. Determinacijos koeficientas (R^2) pateikiamas 4-8 lygtimi:

$$R^2 = \frac{var\ (\hat{y})}{var\ (y)}; \qquad \text{(4-8 lygtis)}$$

R^2 reikšmė naudojama Spearman koreliacijos koeficiento kokybei įvertinti. R^2 reikšmės svyruoja nuo 0 iki +1. Jei R^2 reikšmė yra mažesnė nei 0,6, jautrumo parametrų regresijos koeficientas gali būti netikslus – tai dažniausiai lemia per didelis nesuprantamų parametrų variacijų kiekis. Tokiais atvejais svarbu taikyti alternatyvias metodikas, vertinant skaičiavimo rezultatų jautrumą parametrų pokyčiams.

4.4 Asimetrinės struktūros eksperimentas

QUENCH-20 eksperimente naudojamas ketvirtis BWR kuro rinklės, kuri yra asimetrinė, kaip parodyta 75 pav. (detalus modelio aprašymas pateiktas autorės straipsnyje [25]). Bandomąją kuro rinklę sudaro dvi neutronus sugeriančios plokštės su B_4C strypais 0° ir 270° laipsnių kampuose. 90° ir 180° laipsnių kampuose yra vandens kanalas ir kampinis strypas. Dėl tokio išdėstymo, atliekant QUENCH-20 eksperimentą, temperatūra radialine kryptimi pasiskirsto netolygiai, nes šiluminių elementų imitatoriai aušinami skirtingai. Dėl QUENCH-20 bandomosios kuro rinklės charakteristikų sudėtinga modeliuoti termohidraulinius procesus, nes daugumoje programinių paketų naudojamos cilindro formos koordinatės. Be to, sudėtinga įvertinti neutronus sugeriančių B_4C plokščių oksidaciją, o ypač įvertinti oksidacijos metu susidarančias CO, CO_2 ir CH_4 dujas. QUENCH-20 eksperimente vykstantiems procesams ištirti, RELAP/SCDAPSIM programų paketui buvo sudaryti keli modeliavimo metodai ir nodalizacinės schemos. Kiekvienas metodas turi privalumų ir trūkumų, kurie aptarti kitame skyriuje.

[25] Elsalamouny N., Kaliatka T., Allison C. M.."DIFFERENT NUMERICAL MODELINGAPPROACHES APPLIED TO RELAP/SCDAPSIMCODE FOR THE SIMULATION OF QUENCH-20 TEST", The Proceedings of the International Conference on Nuclear Engineering (ICONE), 2023.

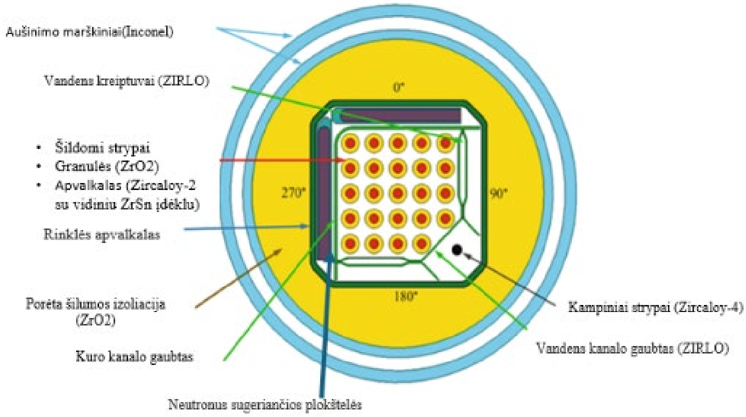

(a)

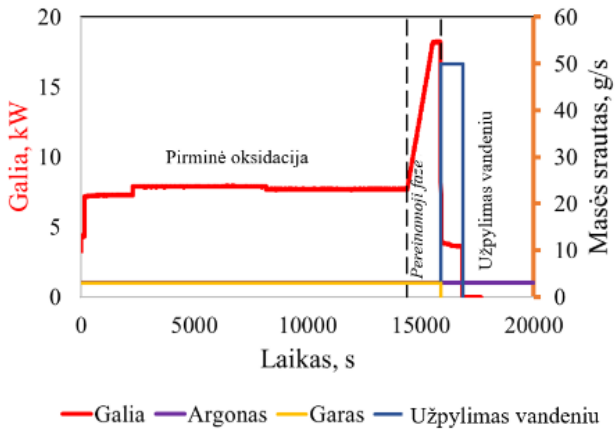

(b)

75 pav. **a)** QUENCH-20 eksperimento kuro rinklė, **b)** QUENCH-20 eksperimento metu naudojama galia bei argono, garų ir aušinimo vandens masės srautas [26]

[26] Elsalamouny N., Kaliatka T., Allison C. M.."DIFFERENT NUMERICAL MODELINGAPPROACHES APPLIED TO RELAP/SCDAPSIMCODE FOR THE SIMULATION OF QUENCH-20 TEST", The Proceedings of the International Conference on Nuclear Engineering (ICONE), 2023.

4.4.1 Pseudosimetrinis modelis

Pseudosimetrinis modelis sukurtas remiantis simetrinę struktūrą turinčių eksperimentų modeliavimo ir geriausio įverčio metodo taikymo patirtimi. QUENCH-20 ir QUENCH-06 eksperimentų kraštinės sąlygos ir eksperimentinės fazės panašios: 3 g/s debitu įleidžiamas argonas ir garas, rinklių galia nedaug skiriasi (QUENCH-06 eksperimente galia 16 kW, o QUENCH-20 eksperimente – 18 kW), užpylimo vandeniu fazėje paduodamo vandens debitas panašus (QUENCH-06 eksperimente 40 g/s, o QUENCH-20 eksperimente – 50 g/s). Tačiau reikia pažymėti, kad tarp šių dviejų eksperimentų pagrindinis skirtumas – kuro rinklės struktūra. QUENCH-20 eksperimente naudojama BWR kuro rinklė, o QUENCH-06 eksperimente – PWR kuro rinklė. Detalesnis modelio aprašymas pateiktas autorės straipsnyje [37].

Pseudosimetriniame modelyje RELAP programų paketo dalies nodalizacinė schema ta pati kaip ir QUENCH-06. Šiame modelyje minimaliai koreguotas tik 010 komponentas, kad atitiktų konkrečią QUENCH-20 eksperimentui naudotos kuro rinklės struktūrą (76 (a) pav.). SCDAP dalies nodalizacinė struktūra naudota tokia pati, kaip ir QUENCH-06 modelyje (76 (b) pav.), o geometriniai duomenys buvo atnaujinti pagal konkrečias QUENCH-20 eksperimente naudotos kuro rinklės charakteristikas. 77 pav. pavaizduotas pseudosimetrinio modelio šilumos perdavimo modeliavimas, kai šiluminių elementų imitatoriuose išskiriama šiluma perduodama tiesiogiai į aktyviosios zonos apvalkalą.

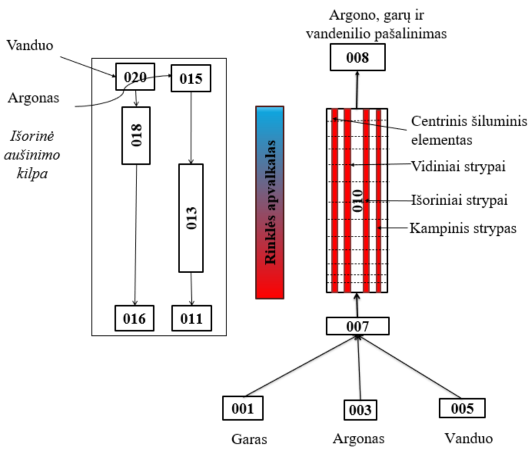

(a)

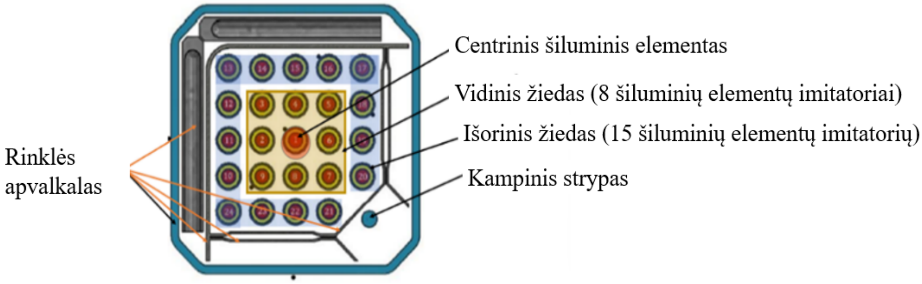

(b)

76 pav. **a)** Pseudosimetrinio modelio RELAP dalies nodalizacinė schema, **b)** pseudosimetrinio modelio SCDAP dalies nodalizacinė schema [27]

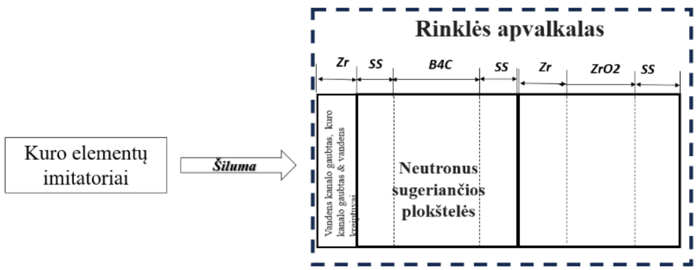

77 pav. Šilumos perdavimo modeliavimas pseudosimetriniame modelyje [28]

4.4.2 Detalus atskirų komentarų modeliavimas

Siekiant skaitiniais programų paketais tikroviškiau imituoti QUENCH-20 eksperimentą, atskiri eksperimente naudojami rinklės elementai buvo modeliuojami detaliai, sudaryti trys modeliavimo metodai (detalus sudarytų modeliavimo metodų aprašymas pateikiamas autorės straipsnyje [39]). Visuose modeliavimo metoduose naudojama ta pati RELAP nodalizacinė schema, taikomi vienodi pradiniai parametrai

[27] Elsalamouny N., Kaliatka T., Allison C. M.."DIFFERENT NUMERICAL MODELINGAPPROACHES APPLIED TO RELAP/SCDAPSIMCODE FOR THE SIMULATION OF QUENCH-20 TEST", The Proceedings of the International Conference on Nuclear Engineering (ICONE), 2023.
[28] Elsalamouny N., Kaliatka T., Kaliatka A. "QUENCH-20 test analysis using RELAP/SCDAPSIM severe accident code". Nuclear Engineering and Design. Elsevier, 2024, Vol. 419, 112995, p. 1-12. ISSN 0029-5493. https://doi.org/10.1016/j.nucengdes.2024.112995.

ir kraštinės sąlygos (78 pav.). QUENCH-20 eksperimento kuro rinklės modelio kraštines sąlygas apibrėžia nuo laiko priklausantys 001, 003, 005 ir 008 tūriai. 001, 003 ir 005 tūriai atitinka garo, argono ir aušinimo vandens parametrus. Nuo laiko priklausantis 008 tūris naudojamas kaip rinktuvas. Nuo laiko priklausomos 002, 004 ir 006 jungtys valdo garo, argono ir aušinimo vandens įleidimą į kuro rinklę. Apatinę kurio rinklės dalį atitinka 007 atšakos komponentas, o pačią rinklę atitinka 010 ir 100 vamzdžių komponentai, sujungti su apačioje esančiu 007 atšakos komponentu ir viršuje esančiu 090 atšakos komponentu, kuris atitinka viršutinę kuro rinklės dalį. 010 komponento pratekėjimo plotas 0,0046 m^2, kuriame įvertintas kuro kanalo gaubtas, vandens kreiptuvas ir vandens kanalo gaubtas. 100 komponento pratekėjimo plotas 0,000114 m^2, šiame komponente įvertintos neutronus sugeriančios plokštės. 090 šaka yra sujungta su nuo laiko priklausomu 008 tūriu per 023 jungtį.

QUENCH-20 eksperimento kuro rinklės apvalkalas aušinamas per išorinį aušinimo kontūrą. Šiam kontūrui modeliuoti buvo naudojami nuo laiko priklausantys tūriai ir vamzdžių komponentai, sujungti nuo laiko priklausančiomis ir pavienėmis jungtimis. Nuo laiko priklausantys 015 ir 020 tūriai yra argono ir aušinimo vandens šaltiniai (kraštinės sąlygos), o 011 ir 016 tūriai veikia kaip rinktuvai. Šie tūriai sujungti su 013 ir 018 vamzdžių komponentais per nuo laiko priklausančias 014 ir 019 jungtis, kurios užtikrina 16 g/s argono debitą ir 100 g/s aušinimo vandens debitą paduodamą į aušinimo kontūrą per 012 ir 017 jungtis.

Eksperimente naudotos kuro rinklės ilgis 2500 mm, o kaitinamos rinklės dalies ilgis 1024 mm. Neutronus sugeriančių plokščių ir kuro kanalo gaubto ilgis 1560 mm. Aukščio matavimai pradedami nuo 0 mm atskaitos, atitinkančios kaitinamos rinklės dalies apačią. Sukurtame modelyje kuro rinklė modeliuojama nuo –475 mm iki +1600 mm aukščio. Apatinę 175 mm kuro rinklės dalį atstoja 007 atšakos komponentas. Dalį nuo 300 mm iki +1260 mm atitinka du 010 ir 100 vamzdžių komponentai, kurių sudalinimas atitinka eksperimento metu naudotų termoporų, skirtų stebėti neutronus sugeriančių plokščių, kaitinimo elementų ir kuro kanalo gaubto išdėstymo aukščius. Kuro rinklės viršus nuo +1260 mm iki +1600 mm modeliuojamas naudojant 090 šakos komponentą. 010 ir 100 vamzdžių komponentai suskirstyti į 15 vidinių segmentų, iš kurių pirmųjų 12 segmentų aukščiai po 100 mm. 13 segmento aukštis yra 124 mm, o paskutinių dviejų segmentų aukščiai – po 118 mm. Šiluminio elemento šildoma dalis tęsiasi nuo 3 iki 13 segmento. Modelyje išorinio aušinimo kontūro ilgis atitinka kuro rinklės ilgį. Aušinimas argonu vyksta per 013 vamzdžio komponentą, kuris tęsiasi nuo –300 mm iki +1024 mm aukščio. Aušinimas vandeniu vyksta per 018 vamzdžio komponentą, kuris yra nuo +1024 mm iki +1600 mm. Vidinis 013 ir 018 vamzdžių komponentų segmentų išdėstymas toks kaip 010 ir 100 vamzdžių komponentų.

Šiluminių elementų imitatoriai, neutronus sugeriančios plokštės, kampinis strypas ir kuro rinklės apvalkalas buvo modeliuojami naudojant SCDAP komponentus, kaip parodyta 79 pav. 24 elektra kaitinamų šiluminių elementų imitatoriai modeliuoti trimis skirtingais Cora komponentais. Pirmasis Cora komponentas atitinka centrinį strypą. Antrasis komponentas atitinka vidinį žiedą, kurį sudaro centrinį strypą supantys aštuoni šiluminių elementų imitatoriai. Trečiasis komponentas atitinka išorinį žiedą, kurį sudaro 15 šiluminių elementų imitatorių. Kampinis strypas, kuris nėra kaitinamas modeliuotas kaip Fuel komponentas. Kuro rinklės apvalkalui, įskaitant jo šiluminę izoliaciją, naudojamas Shroud komponentas. Šie SCDAP komponentai sudaro QUENCH-20 eksperimentui naudotų modeliavimo metodų pagrindą ir jie nesikeitė visuose modeliavimo metoduose. Tačiau neutronus sugeriančių plokščių, kuro kanalo gaubto, vandens kanalo gaubto ir vandens kreiptuvų modeliavimas skirtingais metodais skiriasi, nes atspindi konkrečias kiekvieno modeliavimo ypatybes.

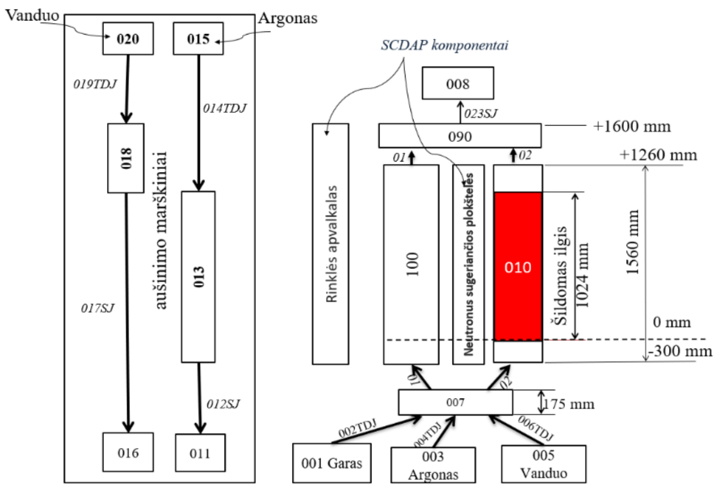

78 pav. QUENCH-020 eksperimento RELAP dalies nodalizacinė schema

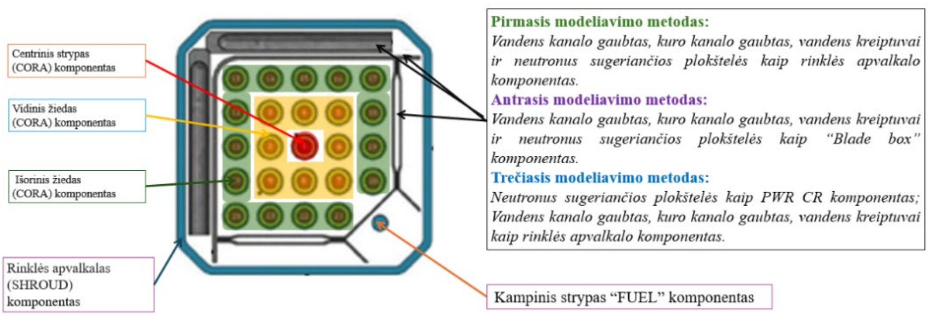

79 pav. QUENCH-20 eksperimento SCDAP dalies nodalizacinė schema

- **Pirmasis metodas atskiriems komponentams modeliuoti**

Neutronus sugeriančios plokštės, kuro kanalo gaubtas, vandens kanalo gaubtas ir vandens kreiptuvai buvo modeliuojami naudojant SCDAP Shroud komponentą, kaip parodyta 79 pav. Shroud komponentą galima apibrėžti kaip vienasluoksnę arba daugiasluoksnę struktūrą, sudarytą iš įvairių medžiagų. Taikant šį konkretų modeliavimo metodą, Shroud komponentas buvo padalintas į keturis (80 pav.) sluoksnius: 1) cirkonio, 2) nerūdijančiojo plieno, 3) boro karbido ir 4) dar vieno nerūdijančiojo plieno sluoksnį. Zr sluoksnis apskaičiuotas įvertinus Zr kiekį, esantį kuro kanalo gaubte, vandens kanalo gaubte ir vandens kreiptuvuose.

Neutronus sugeriančios plokštės modeliuojamos kaip dvi nerūdijančiojo plieno plokštelės, gaubiančios B_4C strypus. Šių sluoksnių geometriniai matmenys nustatyti pagal QUENCH-20 eksperimente naudotų medžiagų mases. Šis Shroud komponentas yra tarp išorinio šiluminių elementų imitatorių žiedo ir kito Shroud komponento, kuris šiame kontekste yra kuro rinklės apvalkalas. Į šį komponentą perduodama šiluminių elementų imitatoriuose susidariusi šiluma, o iš jo šiluma perduodama į kuro rinklės apvalkalą.

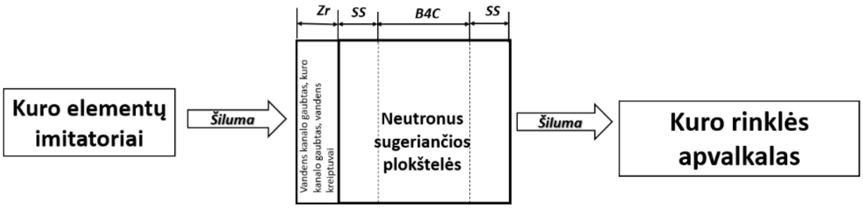

80 pav. Pirmasis metodas, šilumos perdavimas radialine kryptimi [29]

- **Antrasis metodas atskiriems komponentams modeliuoti**

Neutronus sugeriančios plokštės, kuro kanalo gaubtas, vandens kanalo gaubtas ir vandens kreiptuvai buvo modeliuojami naudojant SCDAP komponentą Blade box. Šis SCDAP komponentas yra specialiai sukurtas verdančio vandens reaktoriaus (BWR) neutronus sugeriančioms plokštėms, vandens kreiptuvams ir vandens kanalų gaubtams modeliuoti. Blade box komponentas efektyviai perteikia sudėtingą BWR vandens kreiptuvų ir vandens kanalo gaubto struktūrą ir medžiagų sudėtį. Šių elementų vidinis modeliavimas atliekamas naudojant konkrečius atskirų komponentų matmenis ir geometrinius duomenis, kurie tiksliai vaizduoja kanalo gaubto skerspjūvio dalį ir pusę vandens kreiptuvų. Šis metodas užtikrina, kad būtų realiai imituojama sudėtinga medžiagų sąveika, pavyzdžiui, šilumos perdavimas ir konstrukcinis vientisumas. Naudojant Blade box komponentą, modelis tiksliai

[29] Elsalamouny N., Kaliatka T., Kaliatka A. "QUENCH-20 test analysis using RELAP/SCDAPSIM severe accident code”. Nuclear Engineering and Design. Elsevier, 2024, Vol. 419, 112995, p. 1-12. ISSN 0029-5493. https://doi.org/10.1016/j.nucengdes.2024.112995.

atkartoja neutronus sugeriančių plokščių ir kanalo gaubto elgseną sunkios avarijos sąlygomis, todėl galima tiksliau sumodeliuoti šilumines ir mechanines reakcijas detaliai nagrinėjant BWR reaktorių aktyviąsias zonas. Tačiau reikia įvertinti reikšmingus skirtumus tarp QUENCH-20 eksperimente naudojamos rinklės ir rinklės, kuriai modeliuoti skirtas Blade box komponentas. QUENCH-20 eksperimente naudojama rinklė yra asimetrinės struktūros, todėl temperatūra pasiskirsto nevienodai. Be to, QUENCH-20 eksperimente naudojamos neutronus sugeriančios plokštės reprezentuoja tik pusę viso neutronus sugeriančio elemento (kryžiaus) skerspjūvio su horizontaliai išdėstytais B_4C strypais nerūdijančio plieno plokštelėse. Šias plokšteles gaubia apsauginis cilindras, kuris skiriasi nuo standartinio Blade box komponento konfigūracijos. QUENCH-20 eksperimente naudojamai rinklei tiksliai sumodeliuoti reikia Blade box komponentą koreguoti ir perskaičiuoti šio komponento parametrų vertes. Geometriniai parametrai, kurių reikėjo Blade box komponentui, buvo perskaičiuoti atsižvelgiant į eksperimente naudotų medžiagų masę ir tūrį, įskaitant neutronus sugeriančias plokštes, kuro kanalo gaubtą, vandens kanalo gaubtą ir vandens kreiptuvus. Buvo padidintas B_4C tūris, kad atitiktų B_4C tankį, numatytą Blade box komponente, kuriame B_4C suprantamas kaip miltelių pavidalu esanti medžiaga. QUENCH-20 eksperimente naudojamas tik vienas kanalo gaubtas, o neutronų absorberio plokštelės kraštinės ilgis beveik lygus kanalo gaubto sienelės kraštinės ilgiui. Todėl šiluminių elementų imitatorių išskiriama šiluma yra spinduliuojama į kanalo gaubtą, kuris toliau perduoda šilumą į neutronus sugeriančias plokštes, o į kitą kanalo gaubtą šiluma neperduodama. Be to, modelyje su Blade box komponentu neįvertinamas šilumos perdavimas iš neutronus sugeriančių plokščių. Todėl, kai QUENCH-20 eksperimento metu Blade box komponentas buvo naudojamas neutronus sugeriančioms plokštėms, kuro kanalo gaubtui, vandens kanalo gaubtui ir vandens kreiptuvams modeliuoti, nebuvo užfiksuotas šilumos perdavimas tarp šio komponento ir rinklės apvalkalo (81 pav.).

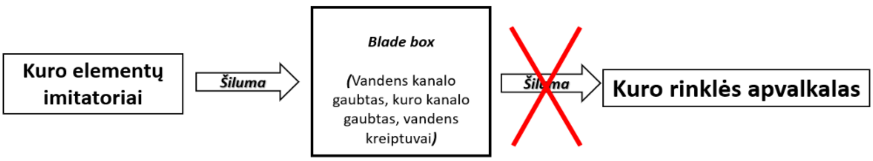

81 pav. Antrasis metodas, šilumos perdavimas radialine kryptimi [30]

[30] Elsalamouny N., Kaliatka T., Kaliatka A. "QUENCH-20 test analysis using RELAP/SCDAPSIM severe accident code”. Nuclear Engineering and Design. Elsevier, 2024, Vol. 419, 112995, p. 1-12. ISSN 0029-5493. https://doi.org/10.1016/j.nucengdes.2024.112995.

- **Trečiasis metodas atskiriems komponentams modeliuoti**

Taikant šį metodą buvo naudojami du SCDAP komponentai: PWR control rod komponentas, skirtas neutronus sugeriančioms plokštėms modeliuoti, ir Shroud komponentas, skirtas QUENCH-20 eksperimento kuro kanalo gaubtui, vandens kanalo gaubtui ir vandens kreiptuvams modeliuoti (79 pav.). PWR control rod komponentas specialiai sukurtas PWR valdymo strypų elgsenai modeliuoti. Jis apskaičiuoja valdymo strypų temperatūrą naudodamas tą patį šilumos laidumo modelį, kuris naudojamas šiluminiams elementams. Šiuose skaičiavimo modeliuose atsižvelgiama į šilumos laidumą, nerūdijančiojo plieno, cirkonio (Zr) ir boro karbido (B_4C) oksidaciją, taip pat į nerūdijančiojo plieno sąveiką su Zr ir B_4C. Be to, imituojamas nerūdijančio plieno, Zr ir B_4C lydymasis ir lydalo nutekėjimas bei vandenilio susidarymas vykstant šių medžiagų oksidacijos reakcijoms. Į modelius taip pat įtrauktas konvekcinis ir spindulinis šilumos perdavimas iš šiluminių elementų imitatorių apvalkalo ir aplink juos esančio šilumnešio.

SCDAP programų paketo PWR control rod komponento modelyje svarbu nurodyti valdymo strypų skaičių ir atstumą tarp jų, kad būtų tiksliai atspindėtas fizinis sistemos išdėstymas ir joje vykstančios sąveikos. Taikant šį metodą, neutronus sugeriančios plokštės modeliuojamos PWR control rod komponentu atsižvelgiant į eksperimente naudojamo nerūdijančiojo plieno, cirkonio (Zr) ir boro karbido (B_4C) masę ir tūrį. Šioms charakteristikoms atspindėti buvo pasirinkti šeši PWR valdymo strypai. Tarpas tarp PWR valdymo strypų buvo nustatytas taip, kad atitiktų tarpą tarp šiluminių elementų imitatorių. Be to, taikant šį metodą Shroud komponentas buvo modeliuojamas kaip vieno Zr sluoksnio elementas apskaičiuotas atsižvelgiant į eksperimente naudojamus kuro kanalo gaubto, vandens kanalo gaubto ir vandens kreiptuvų geometrinius matmenis. 82 pav. pateikiama šilumos perdavimo tarp SCDAP komponentų schema taikant šį modeliavimo metodą.

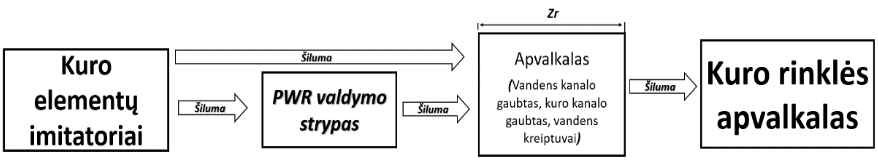

82 pav. Trečiasis metodas, šilumos perdavimas radialine kryptimi [31]

[31] Elsalamouny N., Kaliatka T., Kaliatka A. "QUENCH-20 test analysis using RELAP/SCDAPSIM severe accident code". Nuclear Engineering and Design. Elsevier, 2024, Vol. 419, 112995, p. 1-12. ISSN 0029-5493. https://doi.org/10.1016/j.nucengdes.2024.112995.

4.5 Rezultatai ir jų aptarimas

Šioje dalyje pristatomi sukurtų modelių simetriniams ir asimetriniams eksperimentams skaičiavimo rezultatai.

4.5.1 PHEBUS FPT-1 eksperimentas

Tyrimui buvo atrinkti svarbiausi parametrai, kurie analizuojami šiame darbe: bendras susidariusio vandenilio kiekis, apvalkalo temperatūra ir išsiskyrusi Cs/I frakcija. Susidariusio vandenilio kiekio skaičiavimo rezultatai pateikiami 83 pav. Modeliuojant gautos 10, 6, 9 ir 5 gramais didesnės vertės, lyginant su eksperimentiniais duomenimis, pirminės oksidacijos, oksidacijos, pastovios galios ir įkaitimo fazėse. Tačiau eksperimento pabaigoje gautas vandenilio kiekis atitinka skaičiavimo rezultatus, buvo gautas toks pat susidariusio vandenilio kiekis (96 g). 84 pav. pateikti apvalkalo temperatūros modeliavimo rezultatai atitinka eksperimentinius duomenis, gautus galios didinimo ir įkaitimo fazėse. Pastovios galios ir įkaitimo fazėse modeliavimo vertės yra 50 laipsnių aukštesnės. 85 pav. pateikti išsiskyrusios Cs ir I skilimo frakcijos modeliavimo rezultatai. Gautos vertės visose fazėse gerokai mažesnės lyginant su eksperimentiniais duomenimis. Eksperimento pabaigoje išsiskyrusi skilimo produktų dalis, gauta modeliuojant, yra ~0,65, o pagal eksperimentinius duomenis, Cs dalis yra 0,87, o jodo 0,85. Šis rezultatas rodo, kad siūlomas CORSOR-M modelis yra tinkamas įvertinti Cs/I išsiskyrimo dalį ankstyvosiose degradacijos fazėse, tačiau vėlesnėse fazėse reikėtų peržiūrėti modelyje naudojamus koeficientus arba taikyti kitus modeliavimo metodus, kurie atsižvelgia ne tik į temperatūra pagrįstą skilimo produktų išsiskyrimo eigą.

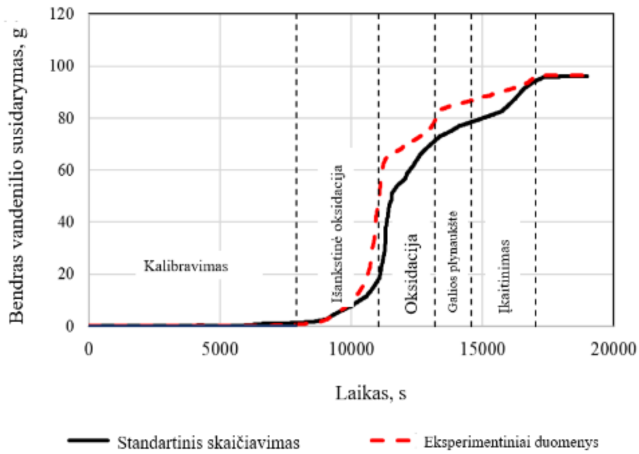

83 pav. Susidariusio vandenilio palyginamųjų skaičiavimų su eksperimentiniais duomenimis rezultatai

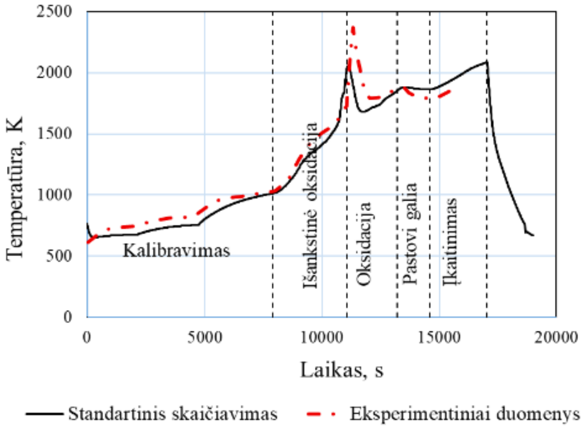

84 pav. Apvalkalo temperatūros palyginamųjų skaičiavimų su eksperimentiniais duomenimis rezultatai

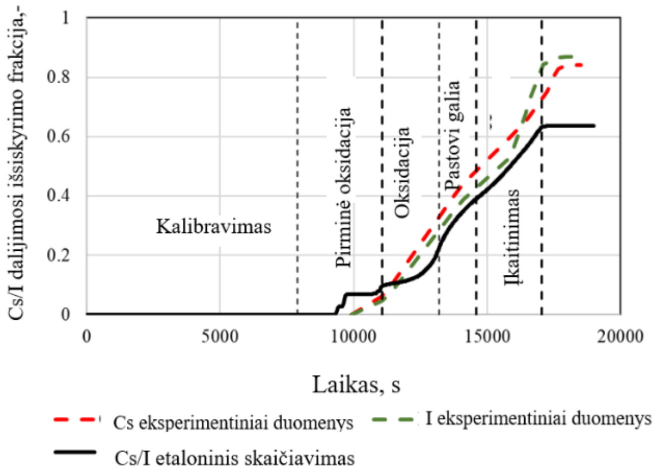

85 pav. Išsiskyrusios Cs/I skilimo frakcijos palyginamųjų skaičiavimų su eksperimentiniais duomenimis rezultatai

4.5.2 QUENCH-06 eksperimentas

Tyrimui buvo atrinkti svarbiausi parametrai, kurie analizuojami šiame darbe: susidariusio vandenilio kiekis, apvalkalo temperatūra 950 mm aukštyje (karščiausia vieta) ir oksido sluoksnio storis prieš ir po užpilant vandeniu. Susidariusio vandenilio kiekio modeliavimo rezultatai pateikiami 86 pav. Modeliavimo rezultatai atitinka eksperimentinius duomenis pirminės oksidacijos fazėje.

Pereinamojoje fazėje modeliuojant gautos vertės yra 5 % aukštesnės lyginant su eksperimentiniais duomenimis. Bandymo pabaigoje modeliuojant gautos vertės yra 15 % žemesnės už eksperimentinius duomenis. 87 pav. parodyti apvalkalo temperatūros 950 mm aukštyje modeliavimo rezultatai, kurie labai panašūs į eksperimentinius duomenis. Oksido sluoksnio storio prieš ir po užpylimo vandeniu modeliavimo vertės mažesniame aukštyje buvo aukštesnės lyginant su eksperimentiniais duomenimis, tačiau didesniame aukštyje jos panašios į eksperimentinius duomenis. Oksido sluoksnio storis po vandens užpylimo buvo gerokai mažesnis lyginant su eksperimentiniais duomenimis. Šis rezultatas rodo, kad RELAP/SCDAPSIM programų pakete įdiegtas oksidacijos modelis neteisingai įvertino oksidaciją vandens užpylimo fazės metu. Ši problema buvo pateikta programų paketo kūrėjams, modelio atnaujinimai yra planuojami būsimoje jo versijoje. Nepaisant šių neatitikimų, skaičiavimo rezultatai kiekybiškai sutampa su eksperimentiniais duomenimis.

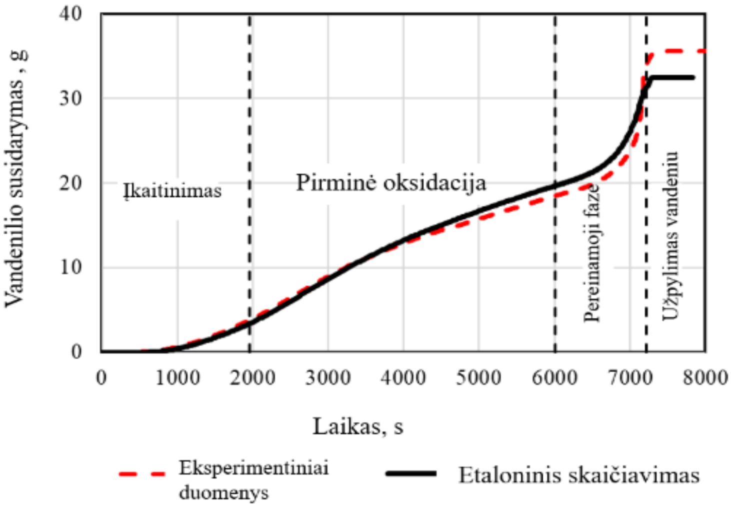

86 pav. Susidariusio vandenilio palyginamųjų skaičiavimų su eksperimentiniais duomenimis rezultatai

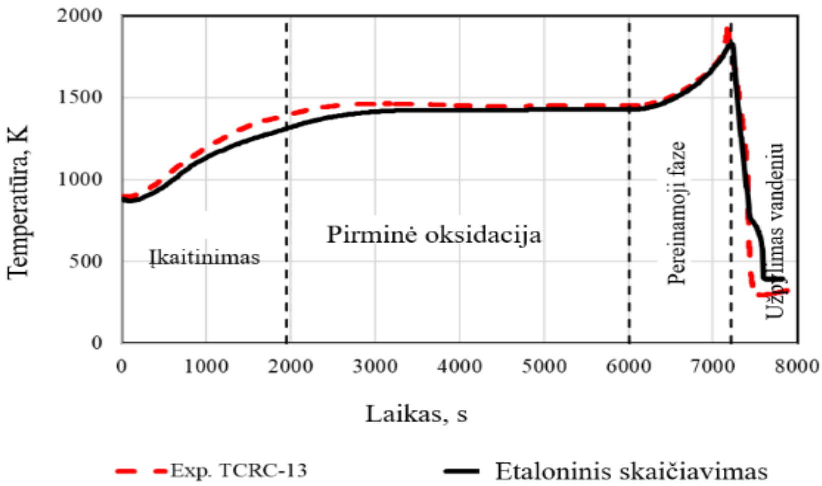

87 pav. Apvalkalo temperatūros 950 mm aukštyje palyginamųjų skaičiavimų su eksperimentiniais duomenimis rezultatai

4.5.3 BEPU metodo naudojimas

Atsižvelgiant į 72 pav. pateiktą tyrimų metodologiją, BEPU metodas pritaikytas sunkiųjų avarijų su daliniu kuro išsilydymu skaičiavimo rezultatų neapibrėžtims įvertinti ir atlikti rezultatų jautrumo analizę. Skaičiavimo neapibrėžtumams įvertinti buvo pasirinkta daugybė neapibrėžtų parametrų (kraštinės sąlygos, apvalkalo medžiagų šiluminės savybės, geometrijos ir SCDAP modeliavimo parametrai) kartu su jų neapibrėžties intervalais ir jų tikimybių pasiskirstymo funkcija.

PHEBUS FPT-1 eksperimentas

Iš anksčiau aptartų BE metodų buvo pasirinktas GRS (vok. Gesellschaft für Anlagen- und Reaktorsicherheit) metodas. Pirmajame šio metodo etape parengiama neapibrėžties parametrų (etaloninės reikšmės, jų neapibrėžčių intervalai ir tikimybių pasiskirstymo funkcijos) specifikacija. Neapibrėžties intervalai ir skirstinys nustatyti vadovaujantis inžinerine praktika ir patirtimi. Kai kurių SCDAP parametrų neapibrėžties intervalai pasirinkti 50 % nuo pradinės vertės. Taip pasirinkta todėl, kad nežinoma, kokią įtaką šios neapibrėžtys turės skaičiavimo rezultatams sunkiosios avarijos atveju. Parametrams su žinomomis charakteristikomis taikomas normalusis skirstinys. Situacijose, kuriose nėra aiškus parametro verčių pasiskirstymas, paprastai naudojamas tolygusis skirstinys.

Eksperimentinis neapibrėžtumas Cs ir I frakcijai atitinka maždaug 14 % apskaičiuotos visos susidariusio vandenilio masės vertės. 88 pav. pateiktos susidariusio vandenilio kiekio viršutinė ir apatinė neapibrėžties ribos. Susidariusio vandenilio kiekio neapibrėžties viršutinė ir apatinė ribos gaubia eksperimentinius duomenis beveik visą eksperimento laiko intervalą. Lyginant galutines apskaičiuotas susidariusio vandenilio vertes, eksperimente gautos neapibrėžtys viršija viršutinę ir apatinę neapibrėžties ribas. 89 pav. pateikiamos šiluminio elemento apvalkalo temperatūros neapibrėžties ribos. Eksperimentinius duomenis apgaubia viršutinė ir apatinė neapibrėžties ribos. Tačiau aukščiausios temperatūros oksidacijos fazėje viršutinė neapibrėžties riba nesutampa su eksperimentiniais duomenimis. Oksidacijos fazėje eksperimentinių duomenų vertės didesnės, už viršutinę neapibrėžties ribą, taip pat eksperimento metu gautas temperatūros pikas yra ~100 s vėliau. Išsiskyrusios Cs ir I frakcijos neapibrėžties viršutinė ir apatinė ribos pateiktos 90 pav. Eksperimentiniai duomenys iki įkaitimo fazės vidurio išlieka tarp viršutinės ir apatinės neapibrėžties ribų. Tačiau bandymo pabaigoje apskaičiuota viršutinė neapibrėžties riba yra 20 % mažesnė už eksperimentinius duomenis. Šis rezultatas rodo, kad net atsižvelgiant į pateiktas neapibrėžtis, CORSOR-M modelio apskaičiuotos Cs ir I vertės vėlesnėje kuro strypo degradacijos fazėje (kai kuro strypo temperatūra aukšta) neatitiko eksperimentinių duomenų. Reikia peržiūrėti šiame modelyje naudojamus koeficientus arba taikyti kitus modeliavimo metodus, kurie vertina ne vien temperatūra grįstą skilimo produktų išsiskyrimo sklaidą.

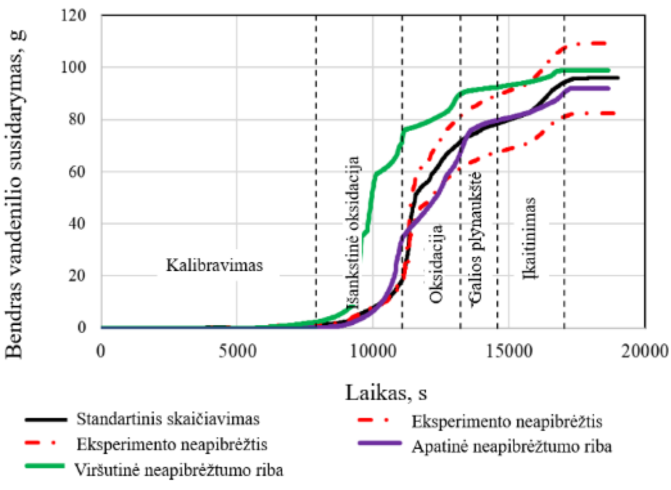

88 pav. Susidariusio vandenilio kiekio neapibrėžties ribos

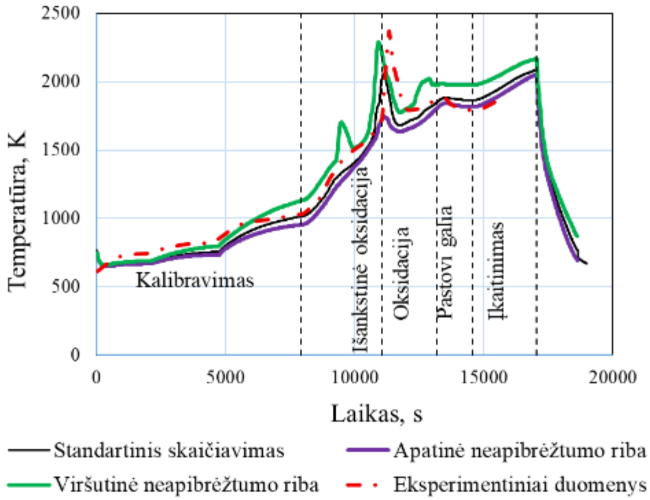

89 pav. Apvalkalo temperatūros neapibrėžties ribos

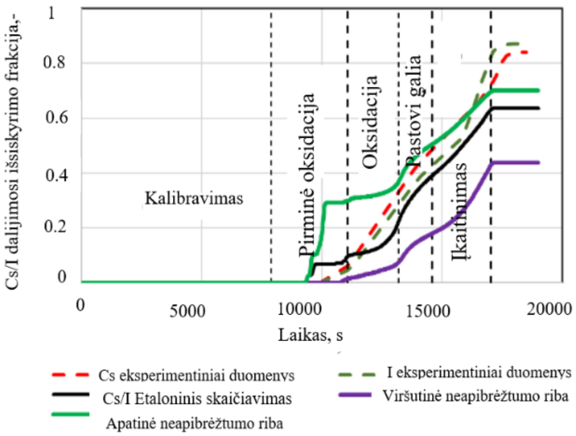

90 pav. Išsiskyrusios Cs ir I skilimo dalies neapibrėžties ribos

Jautrumo analizės rezultatai parodė, kad ZrO_2 šilumos laidumas ir kraštinė sąlygos, apibūdinančios šilumos perdavimą iš branduolinio kuro rinklės į ją supančias konstrukcijas, turi didžiausią įtaką visiems (susidariusio vandenilio kiekiui, apvalkalo temperatūrai ir išsiskyrusiai Cs ir I frakcijai) skaičiavimo rezultatams visuose eksperimento etapuose. Detaliau pristatyta autorės straipsnyje [32].

[32] Elsalamouny N., Kaliatka T. "Uncertainty Quantification of the PHEBUS FPT-1 Test Modelling Results". Energies. Basel: MDPI, 2021, Vol. 14, 7320, p. 1-17. ISSN 1996-1073. https://doi.org/10.3390/en14217320.

QUENCH-06 eksperimentas

QUENCH-06 skaičiavimo rezultatams gauti buvo atlikti tokie patys neapibrėžties įvertinimo žingsniai, kaip ir PHEBUS FPT-1 atveju. Buvo nuspręsta vertinti vandenilio susidarymą, temperatūros kitimą bandymo metu bei oksido sluoksnio storį prieš ir po gesinimo fazės. Toks sprendimas priimtas todėl, kad šie rezultatai atspindi kuro rinklės degradaciją sunkiųjų avarijų metu, taip pat šie duomenys paremti plačia eksperimentine duomenų baze, kurią pateikė KIT.

Atsižvelgiant į pasirinktus tyrimo parametrus, parengta neapibrėžtų parametrų lentelė, kurioje pateikiamos parametrų neapibrėžties ribos ir tikimybių pasiskirstymo funkcijos. Iš viso buvo pasirinkta 19 parametrų, susijusių su eksperimento geometrinę struktūrą, kraštinėmis sąlygomis, apvalkalo vientisumo ir konvekcinio šilumos perdavimo modeliavimu. 91 pav. pateikiamas viršutinės ir apatinės neapibrėžties ribų palyginimas su eksperimentiniais duomenimis ir susidariusio vandenilio kiekio standartinio skaičiavimo rezultatu. QUENCH-6 eksperimento pabaigoje skirtumas tarp mažiausių ir didžiausių modeliavimo rezultatų yra 14,2 %. Tačiau eksperimentiniai duomenys gauti viso eksperimento metu yra tarp apskaičiuotų viršutinės ir apatinės neapibrėžties ribų. Kitokia situacija buvo modeliuojant centrinio šiluminio elemento temperatūrą 950 mm aukštyje. Apskaičiuotas skirtumas tarp žemiausios ir aukščiausios temperatūros pirminės oksidacijos fazėje yra tik ~50 K (~2,5 % skirtumas nuo aukščiausios apskaičiuotos temperatūros). Taigi, 92 pav. matome, kad modelyje apskaičiuotos viršutinė ir apatinė neapibrėžties ribos sklaida yra nedidelė, o apskaičiuotos vertės labai panašios į eksperimentinius duomenis.

Atliekant QUENCH-06 eksperimentą, po 6620 sek. buvo išimtas vienas iš kampinių strypų tam, kad būtų išmatuotas oksido sluoksnio storis prieš vandens užpylimo fazę. Prieš vandens užpylimą išmatuotas oksido sluoksnio storis palygintas su RELAP/SCDAPSIM skaičiavimo rezultatų viršutine ir apatine ribomis. Palyginimo rezultatai rodo, kad apskaičiuotos vertės šiek tiek didesnės nei gautos atliekant eksperimentinius matavimus. Išmatuotas ir apskaičiuotas oksido sluoksnio storis QUENCH-06 eksperimento pabaigoje buvo palygintas. Mažesniame aukštyje (iki 850 mm) apskaičiuotos vertės yra didesnės, tačiau nuo 850 mm iki 1000 mm aukštyje gautos daug didesnės eksperimentinių matavimų vertės. Šis rezultatas rodo, kad eksperimento metu (greito aušinimo fazė) 850–1000 mm aukštyje cirkonio lydinio dangos oksidacija buvo daug intensyvesnė, palyginti su RELAP/SCDAPSIM programų paketo pateiktais rezultatais. Šis rezultatas rodo, kad oksidacijos modelis, įdiegtas RELAP/SCDAPSIM programų pakete, neteisingai įvertino oksidaciją užpylimo fazės metu. Ši problema buvo pateikta programų paketo kūrėjams, modelio patobulinimai planuojami kitoje versijoje. Nepaisant šių neatitikimų, programų paketu atlikti skaičiavimai kiekybiškai atitinka eksperimentinius duomenis.

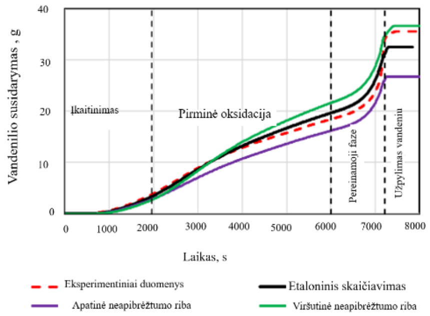

91 pav. Susidariusio vandenilio kiekio apskaičiuotos neapibrėžties ribos

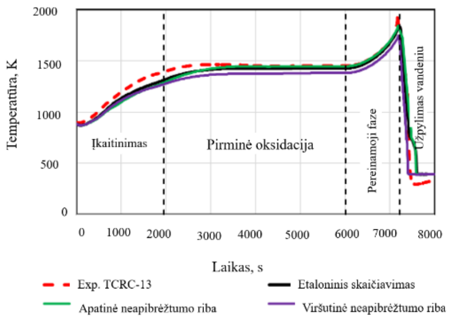

92 pav. Apvalkalo temperatūros 950 mm aukštyje apskaičiuotos neapibrėžties ribos

Atlikta jautrumo analizė parodė, kad įkaitinimo fazėje apskaičiuotam susidariusio vandenilio kiekiui didžiausią įtaką turėjo pradinis apvalkalo storis. Tačiau visose kitose eksperimento fazėse didžiausią įtaką skaičiavimo neapibrėžtims turėjo šiluminiams elementų imitatoriams tiekiama elektros galia. Į kuro rinklę įleidžiamo garo debitas taip pat turi reikšmingą įtaką visose eksperimento fazėse. Centrinio šiluminio elemento temperatūros 950 mm aukštyje, pirminės oksidacijos ir pereinamojoje fazėse didžiausią įtaką skaičiavimo rezultatams taip pat turi elektros galia. Vandens užpylimo fazėje didžiausią įtaką turėjo įleidžiamo aušinimo vandens debitas. Analizuojant oksido sluoksnio storį, nustatyta, kad didžiausią įtaką rezultatams darė elektros galia ir įleidžiamo garo debitas, ypač eksperimento pereinamojoje ir vandens užpylimo fazėse.

Detaliau pristatyta autorės straipsnyje [33].

4.5.4 Eksperimento su asimetrine struktūra skaičiavimų rezultatai

Susidariusio vandenilio kiekio, apskaičiuoto taikant pseudosimetrinį modelį ir detalius atskirų komponentų modelius (aptartus 4.4.2 skyriuje), palyginimas su eksperimentiniais duomenimis pavaizduotas 93 pav.

Naudojant pseudosimetrinį modelį apskaičiuotas vandenilio susidarymas prasideda maždaug 3000 sekundžių vėliau, nei nustatyta eksperimentiniu būdu, dėl vėluojančio Zr oksidacijos proceso pradžios. Susidariusio vandenilio kiekis išlieka maždaug 30 % mažesnis lyginant su eksperimentiniais duomenimis iki 15000 s nuo

[33] IAEA, Advancing the State of the Practice in Uncertainty and Sensitivity Methodologies for Severe Accident Analysis in Water Cooled Reactors in the QUENCH-06 Experiment. IAEA-TECDOC-2045, 2024.

eksperimento pradžios. Vėliau pereinamosios fazės pabaigoje ir vandens užpylimo fazės pradžioje stebimas staigesnis vandenilio susidarymas, tačiau eksperimento pabaigoje visas apskaičiuotas susidariusio vandenilio kiekis yra 30 g, t. y. maždaug 50 % mažesnis už eksperimentinius rezultatus.

Taikant pirmąjį detalaus atskirų komponentų modeliavimo metodą (nuoroda 4.4.2.1), vandenilio susidarymas prasidėjo maždaug 1500 s vėliau nei eksperimento metu dėl vėlesnės Zr oksidacijos pradžios. Iš pradžių apskaičiuotas susidariusio vandenilio kiekis buvo mažesnis už eksperimentines vertes iki 8000 sekundžių. Tačiau vėliau skaičiavimai, pademonstravo spartesnį vandenilio susidarymą, todėl iki pirminės oksidacijos fazės pabaigos apskaičiuotos vertės buvo beveik 20 % didesnės už eksperimentinius duomenis. Šis neatitikimas matomas visos pereinamosios fazės metu, o vandens užpylimo fazės pabaigoje apskaičiuotas susidariusio vandenilio kiekis buvo 47 g, t. y. apie 18 % mažesnis už eksperimentinius duomenis.

Vandenilio susidarymo kreivė gauta taikant antrąjį detalaus atskirų komponentų modeliavimo metodą (nuoroda 4.4.2.2) pirminės oksidacijos ir pereinamojoje fazėse tiksliai atitiko eksperimento metu stebimą tendenciją, o apskaičiuotos vertės buvo tik 3 % mažesnės už eksperimentinius duomenis. Tačiau šiame modelyje nebuvo užfiksuotas vandenilio susidarymo pikas, kuris turėjo būti vandens užpylimo fazėje. Todėl vandens užpylimo fazės pabaigoje visas susidariusio vandenilio kiekis buvo maždaug 27 g, t. y. apie 50 % mažesnis lyginant su eksperimentiniais duomenimis.

Taikant trečiąjį detalaus atskirų komponentų modeliavimo metodą (nuoroda 4.4.2.2), vandenilio susidarymas prasidėjo maždaug 3000 s vėliau nei bandymo metu, panašiai kaip ir taikant pirmąjį metodą, dėl vėlai prasidėjusios Zr oksidacijos. Apskaičiuotos vertės buvo mažesnės už eksperimentinius duomenis iki 8000 s. Išankstinės oksidacijos ir pereinamojoje fazėse apskaičiuotas susidariusio vandenilio kiekis buvo tik 2 % didesnis už eksperimentines vertes. Pagal šį metodą apskaičiuotas vandenilio susidarymas vandens užpylimo fazėje buvo didžiausias palyginti su visais kitais metodais: iš viso susidarė 52 g vandenilio, nors ši vertė vis tiek buvo 10 % mažesnė už eksperimento metu nustatytą susidariusio vandenilio kiekį.

94 pav. pateikiamas apskaičiuotų apvalkalo temperatūros verčių palyginimas su termoporų rodmenimis. Atliekant QUENCH-20 eksperimentą, prie šiluminių elementų imitatorių apvalkalų buvo pritvirtintos termoporos temperatūros pokyčiams eksperimento metu registruoti. 950 mm aukštyje nuo kaitinamo šiluminio elemento imitatoriaus apačios uždėtos trys termoporos: TFS1/13, TFS9/13 ir TFS16/13. Eksperimente TFS reiškia termoporą, pritvirtintą prie šiluminio elemento apvalkalo išorinio paviršiaus. Du pasvyruoju brūkšiu atskirti skaitmenys žymi šiluminio elemento imitatoriaus numerį ir aukštį. Šiuo atveju termoporos buvo pritvirtintos prie šiluminių elementų imitatorių, esančių kuro rinklės centre, vidinio žiedo kampe ir išorinio žiedo viršutiniame kampe. Šių termoporų rodmenyse pastebėtas temperatūros verčių pasiskirstymas ~150 laipsnių. Taip yra dėl eksperimento struktūros asimetrijos

ir nevienodo temperatūros pasiskirstymo (skirtingo aušinimo sąlygų) atliekant QUENCH-20 eksperimentą. Naudojant pseudosimetrinį modelį apskaičiuotos apvalkalo temperatūros vertės iki ~12000 s yra 5 % žemesnės už TSF16/13 termoporos išmatuotą temperatūrą. Vėliau apskaičiuoti rezultatai sutampa su eksperimentiniais TSF16/13 duomenimis. Pirminės oksidacijos ir pereinamojoje fazėse apvalkalo temperatūra, apskaičiuota taikant pirmąjį detalaus atskirų komponentų modeliavimo metodą, yra tarp TSF9/13 ir TFS16/13 termoporų rodmenų. Su šiuo modeliavimo metodu vandens užpylimo fazėje gautas didžiausias temperatūros pikas lyginant su visais kitais modeliavimo metodais. Šis temperatūros pikas yra 6 % (150 K) žemesnis už TSF1/13 termoporos rodmenis. Apvalkalo temperatūra 950 mm aukštyje apskaičiuota antruoju detaliu atskirų komponentų modeliavimo metodu pirminės oksidacijos ir pereinamojoje fazėse yra tarp TSF9/13 ir TFS16/13 termoporų rodmenų, kaip ir skaičiuojant pirmuoju metodu. Vandens užpylimo fazėje taikant šį modeliavimo metodą nustatytas žemiausias temperatūros pikas, palyginti su kitais modeliavimo metodais. Skaičiavimo rezultatus palyginus su TFS1/13 termoporos rodmenimis, maksimali apskaičiuota temperatūra yra 15 % (315 K) žemesnė. Taikant trečiąjį detalaus atskirų komponentų modeliavimo metodą, gautos 6 % (95 K) mažesnės vertės, lyginant su visais termoporų rodmenimis pirminės oksidacijos ir pereinamojoje fazėse. Vandens užpylimo fazėje apskaičiuotos apvalkalo temperatūros 950 mm aukštyje pikas yra 12 % (250 K) žemesnis lyginant su eksperimentiniais duomenimis.

95 pav. pateikiamas rinklės apvalkalo temperatūros 950 mm aukštyje verčių, apskaičiuotų taikant pseudosimetrinį ir detalaus atskirų komponentų modeliavimo metodus, ir termoporų rodmenų palyginimas. Šiame aukštyje yra dvi termoporos: TSH13/180 ir TSH13/270. Šios termoporos (TSH) pritvirtintos prie išorinio rinklės apvalkalo paviršiaus. Termoporų žymėjime pirmasis skaitmuo nurodo aukštį (šiuo atveju 950 mm), o antrasis – termoporos padėties kampą rinklėje. Bandymo metu šias termoporas veikia mechaninės apkrovos, todėl šios termoporos gali turėti pažeidimų kurie gali turėti įtakos termoporų rodmenims. Pasitarus su eksperimento vykdytojais (KIT), buvo sutarta, kad TSH13/270 rodmenis reikėtų vertinti atsargiai, nes ši termopora registravo aukštesnę temperatūrą nuo pat bandymo pradžios. Dėl šios priežasties skaičiavimo rezultatai buvo lyginami tik su TSH13/180 termoporos rodmenimis. Pagal pseudosimetrinį modelį apskaičiuota rinklės apvalkalo temperatūra sutampa su eksperimentiniais duomenimis, užfiksuotais termoporos. Rinklės apvalkalo temperatūra, apskaičiuota taikant pirmąjį detalaus atskirų komponentų modeliavimo metodą, yra iki 3 % (35 K) aukštesnė lyginant su eksperimentiniais duomenimis pirminės oksidacijos fazėje. Tačiau pereinamojoje fazėje apskaičiuotos temperatūros vertės yra 10 % (130 K) žemesnės nei išmatuotos eksperimento metu. Vandens užpylimo fazėje apskaičiuota rinklės apvalkalo maksimali temperatūra 950 mm aukštyje yra 8 % (130 K) aukštesnė už termoporos rodmenis. Skaičiavimo pagal antrąjį detalaus atskirų komponentų modeliavimo metodą rezultatai yra 40 % (450 K) žemesni už termoporos rodmenis pirminės oksidacijos ir pereinamojoje fazėse. Be to, vandens užpylimo fazėje apskaičiuota

aukščiausia rinklės apvalkalo temperatūra 950 mm aukštyje yra 50 % (800 K) žemesnė už termoporos rodmenis. Tračiuoju detalaus atskirų komponentų modeliavimo metodu apskaičiuota apsauginio cilindro temperatūra 950 mm aukštyje buvo ~ 6 % (65 K) žemesnė už eksperimentinius duomenis pirminės oksidacijos ir pereinamojoje fazėse. Vandens užpylimo fazėje apskaičiuota rinklės apvalkalo maksimali temperatūrą buvo 5 % (90 K) aukštesnė, palyginti su termoporos rodmenimis.

Trečiuoju detalaus atskirų komponentų modeliavimo metodu buvo galima įvertinti B_4C oksidacijos procesą ir sumodeliuoti CO, CO_2, CH_4 ir H_2 susidarymą (žr. 96 pav.), tačiau apskaičiuotos CO, CO_2, CH_4 ir H_2 vertės yra žemesnės už eksperimentinius duomenis. Tikėtina, kad skirtumą nulėmė skirtingu metu prasidėjusios reakcijos. Eksperimente B_4C oksidacija prasideda 500 s anksčiau nei taikomame skaičiavimo modelyje. Eksperimente B_4C oksidacija garo aplinkoje prasideda prie ~ 1600 K temperatūros, o skaičiavimuose prie ~1719 K.

Detaliau pristatyta autorės straipsnyje [34].

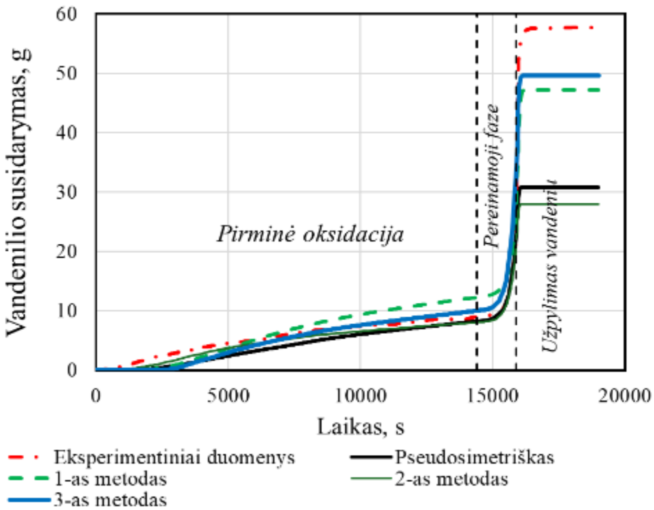

93 pav. Vandenilio susidarymas

[34] Elsalamouny N., Kaliatka T., Kaliatka A. "QUENCH-20 test analysis using RELAP/SCDAPSIM severe accident code". Nuclear Engineering and Design. Elsevier, 2024, Vol. 419, 112995, p. 1-12. ISSN 0029-5493. https://doi.org/10.1016/j.nucengdes.2024.112995.

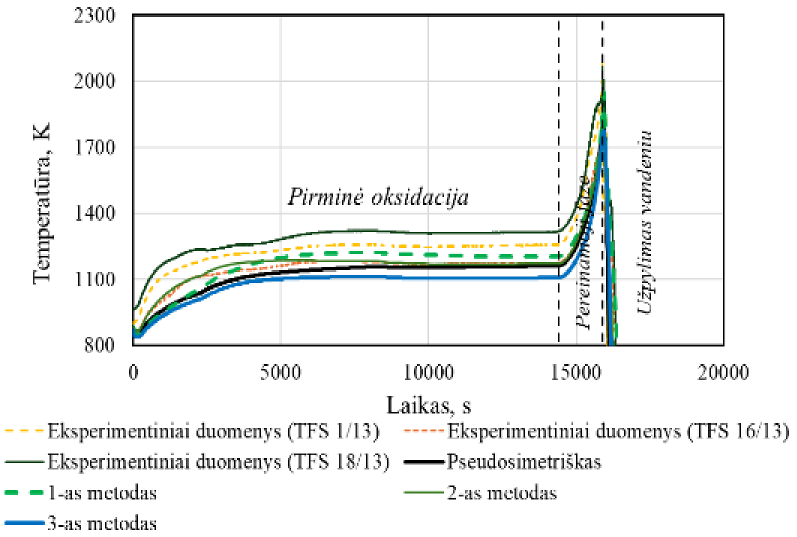

94 pav. Apvalkalo temperatūra 950 mm aukštyje

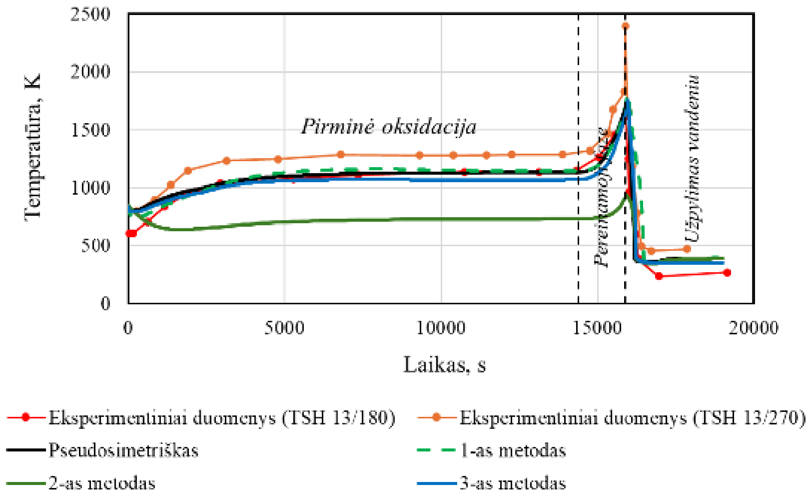

95 pav. Rinklės apvalkalo temperatūra 950 mm aukštyje

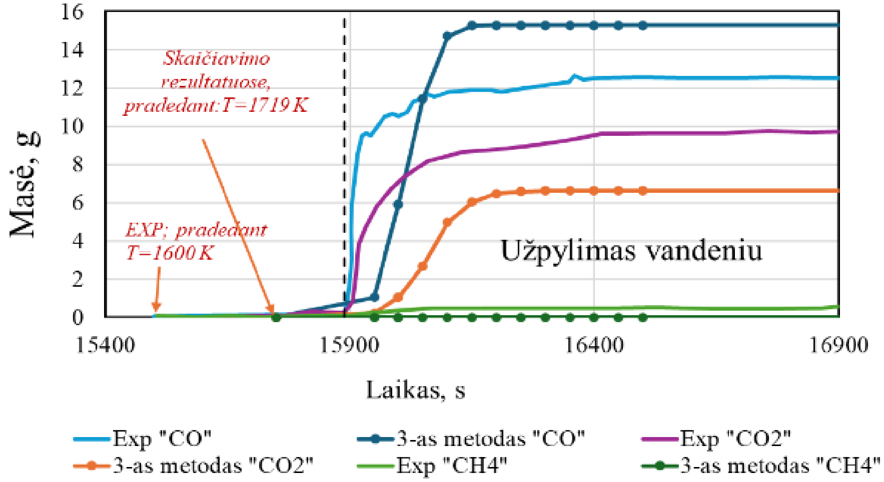

96 pav. B_4C oksidacijos metu išsiskyrusios dujos

IŠVADOS IR REKOMENDACIJOS

Siekdami sukurti metodiką fizinių procesų tyrimui branduoliniuose įrenginiuose su simetrine ir asimetrine struktūra, buvo atlikti sunkiųjų avarijų eksperimentų, kuriuose tiriamas dalinis branduolio išsilydymas, skaitiniai tyrimai. Tyrimai, atlikti taikant BEPU metodiką ir sunkiųjų avarijų programų paketą RELAP/SCDAPSIM kartu su statistiniu įrankiu SUSA. Tyrimo rezultatai leido suformuluoti šias išvadas:

1. CORSOR-M modelis veiksmingai įvertina Cs/I išsiskyrimą ankstyvose rinklės degradacijos fazėse. Tačiau vėlesnėse fazėse būtini modeliai, apimantys daugiau nei vien temperatūra pagrįstą skilimo produktų išsiskyrimą.
2. BEPU metodu atlikta neapibrėžčių analizė <u>įrenginiams su simetrine struktūra</u> patvirtina modeliavimo rezultatų patikimumą – daugumoje analizuotų atvejų apskaičiuoti intervalai aprėpė eksperimentinius duomenis. Jautrumo analizė parodė:
    - Medžiagų savybės ir kraštinės sąlygos stipriai lemia skaičiavimo rezultatus (Spearmano koreliacijos koeficientas >0,78).
    - SCDAP programų paketo dalies parametrai, susiję su apvalkalo plyšimu ir oksidacija, turi reikšmingą įtaką skaičiavimo rezultatams vėlyvosios degradacijos fazės metu (Spearmano koeficientas >0,4).
3. Remiantis ankstesnių eksperimentinių tyrimų turinčių simetrines struktūros (PHEBUS FPT-1 ir QUENCH-06) patirtimi, sukurta metodika pritaikyta eksperimentui, turinčiam asimetrinę struktūrą (QUENCH-20). Buvo sukurti ir įvertinti pseudosimetrinis bei dar trys detalūs atskirų komponentų modeliavimo metodai, skirti modeliuoti QUENCH-20 eksperimentą:
    - <u>Pseudosimetrinis:</u> šis metodas leidžia tiksliai atkartoti eksperimento rezultatus prieš vandens užpylimą, tačiau susidariusio vandenilio kiekis vandens užpylimo fazės pabaigoje yra ~30 % mažesnis.
    - <u>SCDAP Shroud komponentas:</u> šiuo metodu gauti rezultatai gerai atitinka eksperimento metu išmatuotą temperatūrą, apskaičiuotas susidariusio vandenilio kiekis yra ~18 % arba ~10 g mažesnis dėl trūkstamo B_4C oksidacijos modelio.
    - <u>SCDAP Blade box komponentas:</u> šis metodas leidžia gerai atkartoti apvalkalo temperatūrą, tačiau dėl netikslaus šilumos perdavimo modeliavimo nepakankamai įvertinama oksidacija ir susidariusio vandenilio kiekis (~50 % mažesnis).
    - <u>SCDAP PWR control rod + Shroud komponentai</u>: šis metodas leidžia pasiekti geriausią atitiktį eksperimentiniams duomenims, apskaičiuotas vandenilio kiekis yra tik ~12 % mažesnis, bei šis modelis įvertina B_4C oksidaciją.

REFERENCES

[1] D. Elliott and T. Cook, Symbolic power: The future of nuclear energy in Lithuania, *Sci Cult (Lond)*, vol. 13, no. 3, pp. 373–400, 2004, doi: 10.1080/0950543042000262431.

[2] World Nuclear Association, World Nuclear Performance Report 2024, 2024.

[3] Oxford Institute for energy studies, NUCLEAR ENERGY IN THE GLOBAL ENERGY LANDSCAPE: ADVANCING SUSTAINABILITY AND ENSURING ENERGY SECURITY ?, 2024.

[4] IAEA, Outlook for Global Nuclear Power Development Energy, Electricity and Nuclear Power: Developments and Projections, 2007.

[5] M. J. Skolds, SUBJECT: THREE MILE ISLAND STATION, UNIT 1 NRC INSPECTION REPORT 05000289/2003007 Dear Mr. Skolds: On July 11, 2003, the US Nuclear Regulatory Commission (NRC) completed an engineering team inspection at the Three Mile Station (TMI), Unit 1. The enclosed report presents the, 2003.

[6] N. Muellner[1], Three Decades after Chernobyl: Technical or Human Causes?, *The Technological and Economic Future of Nuclear Power*, p. 323, 2019.

[7] IAEA, The Fukushima Daiichi Accident, International Atomic Energy Agency, 2015.

[8] IAEA, IAEA Safety Standards Severe Accident Management Programmes for Nuclear Power Plants for protecting people and the environment No. NS-G-2.15 Safety Guide, 2009. [Online]. Available: http://www-ns.iaea.org/standards/feedback.htm

[9] B. R. Sehgal, *Nuclear safety in light water reactors: severe accident phenomenology*. Academic Press, 2011.

[10] M. Schwarz, G. Hache, and P. Von der Hardt, PHEBUS FP: a severe accident research programme for current and advanced light water reactors, *Nuclear Engineering and Design*, vol. 187, no. 1, pp. 47–69, 1999.

[11] KIT, QUENCH Program, https://quench.forschung.kit.edu/24.php.

[12] F. S. D'Auria, H. Glaeser, S. Lee, J. Miák, M. Modro, and R. R. Schultz, *Best Estimate Safety Analysis for Nuclear Power Plants: Uncertainty Evaluation. IAEA Safety Report Series*, vol. 52. IAEA, 2008.

[13] IAEA, *IAEA Safety Glossary: 2018 Edition*, 2018th ed. Vienna: IAEA, 2019. Accessed: Jul. 20, 2025. [Online]. Available: https://www.iaea.org/publications/11098/iaea-safety-glossary-2018-edition

[14] M. R. Galetti and F. S. D'Auria, Questions arising from the application of Best-Estimate Methods to the Angra-2 NPP Licensing Process in Brasil, in *Int. Meet. on Best-Estimate Methods in Nuclear Installation Safety Analysis (BE-2000) IX*, 2000.

[15] L. E. Herranz *et al.*, Overview of key thermal–hydraulic phenomena in severe accident unfolding: Current knowledge and further needs, *Nuclear Engineering and Design*, vol. 407, p. 112256, 2023.

[16] L. E. Herranz *et al.*, MUSA–Management and Uncertainties of Severe Accidents, in *Proceedings of 2nd RCM on IAEA CRP on on Advancing the State of Practice in Uncertainty and Sensitivity Methodologies for SA Analysis in WCRs*, IAEA, 2020.
[17] F. Gabrielli, A. Stakhanova, and V. H. Sanchez-Espinoza, Uncertainty and Sensitivity Analysis of the QUENCH-06 Experiment by Means of Severe Accident Codes in the Framework of the IAEA CRP I31033 on Advancing the State-of-Practice in Uncertainty and Sensitivity Methodologies for Severe Accident Analysis in Water Cooled Reactors, in *International Conference on Topical Issues in Nuclear Installation Safety: Strengthening Safety of Evolutionary and Innovative Reactor Designs. Book of Abstracts*, 2022, pp. 33–34.
[18] P. Hofmann, Current knowledge on core degradation phenomena, a review, *Journal of nuclear materials*, vol. 270, no. 1–2, pp. 194–211, 1999.
[19] Richard S, Severe accidents in light water reactors, Risk-Informed Methods and Applications, *Nuclear and Energy Engineering*, Chapter 3, Pages 29-42, 2024.
[20] I. A. E. Agency, *Fuel failure in water reactors: causes and mitigation*. International Atomic Energy Agency, 2003.
[21] X. Shi, X. Cao, and Z. Liu, Oxidation behavior analysis of cladding during severe accidents with combined codes for Qinshan Phase II Nuclear Power Plant, *Ann Nucl Energy*, vol. 58, pp. 246–254, 2013.
[22] J. L. Vandegrift *et al.*, Oxidation behavior of Zirconium, Zircaloy-3, Zircaloy-4, Zr-1Nb, and Zr-2.5 Nb in air and oxygen, *Nuclear Materials and Energy*, vol. 20, p. 100692, 2019.
[23] G. Repetto *et al.*, B4C oxidation modelling in severe accident codes: Applications to PHEBUS and QUENCH experiments, *Progress in Nuclear Energy*, vol. 52, no. 1, pp. 37–45, 2010.
[24] M. Steinbrück, M. S. Veshchunov, A. V Boldyrev, and V. E. Shestak, Oxidation of B4C by steam at high temperatures: New experiments and modelling, *Nuclear Engineering and Design*, vol. 237, no. 2, pp. 161–181, 2007.
[25] P. Chatelard *et al.*, ASTEC V2 severe accident integral code main features, current V2. 0 modelling status, perspectives, *Nuclear Engineering and Design*, vol. 272, pp. 119–135, 2014.
[26] NRC, Pressurized Water Reactor (PWR) Systems, *Reactor Concepts Manual, US NRC Technical Training Center*, vol. 603, 2015.
[27] V. Mokhov and N. Trunov, VVER reactors: clean and reliable source of energy in the past and in the future, in *International conference on opportunities and challenges for water cooled reactors in the 21. century. PowerPoint presentations*, 2009, p. 42.
[28] S. Bozzola, Fundamentals of boiling water reactor (BWR), *Iaea-Smr--68/2*, pp. 71–130, 1982.

[29] J. Griffiths, Reactor Physics and Economic Aspects of the CANDU Reactor System, Atomic Energy of Canada Ltd., Chalk River, Ontario. Chalk River Nuclear Labs, 1983.

[30] Y. Zvonarev, A. Volchek, V. Kobzar, P. Chatelard, and J. P. Van Dorsselaere, ASTEC and ICARE/CATHARE modelling improvement for VVERs, *Nuclear Engineering and Design*, vol. 241, no. 4, pp. 1055–1062, 2011.

[31] C. M. Allison *et al.*, SCDAP/RELAP5/Mod2 Code Manual, Nuclear Regulatory Commission, Washington, DC (USA). Div. of Systems …, 1989.

[32] L. J. Siefken, E. W. Coryell, E. A. Harvego, and J. K. Hohorst, SCDAP/RELAP5/Mod3. 3 Code Manual: User's Guide and Input Manual, *Idaho National Engineering and Enviromental Laboratory, Idaho Falls) NUREG/CR*, vol. 6150, no. 3, 2001.

[33] R. O. Gauntt *et al.*, MELCOR computer code manuals, *Sandia National Laboratories, NUREG/CR*, vol. 6119, p. 785, 2000.

[34] P. Chatelard, J. lle Fleurot, O. Marchand, and P. Drai, Assessment of ICARE/CATHARE V1 severe accident code, in *International Conference on Nuclear Engineering*, 2006, pp. 145–154.

[35] I. Sato, S. Yoshikawa, T. Yamashita, M. Cibula, and S. Mizokami, MAAP code analysis focusing on the fuel debris condition in the lower head of the pressure vessel in Fukushima-Daiichi Nuclear Power Station Unit 2, *Nuclear Engineering and Design*, vol. 404, p. 112205, 2023.

[36] S. Hagen, P. Hofmann, V. Noack, G. Schanz, G. Schumacher, and L. Sepold, Results of SFD Experiment CORA-13 (OECD International Standard Problem 31), 1993.

[37] K. Obaidurrahman, et al. Chapter 8 - Nuclear reactor safety, *Physics of Nuclear Reactors*, Pages 449-510, 2021.

[38] M. Sánchez-Castillo *et al.*, CODEX: a next-generation sequencing experiment database for the haematopoietic and embryonic stem cell communities, *Nucleic Acids Res*, vol. 43, no. D1, pp. D1117–D1123, 2015.

[39] International Atomic Energy Agency, IAEA-TECDOC-1332: Safety Margins of Operating Reactors-Analysis of Uncertainties and Implications for Decision Making, International Atomic Energy Agency, Vienna, Austria, Jan. 2003. Accessed: Jul. 20, 2025. [Online]. Available: https://www.iaea.org/publications/6533/safety-margins-of-operating-reactors-analysis-of-uncertainties-and-implications-for-decision-making

[40] F. D'Auria, Best estimate plus uncertainty (BEPU): status and perspectives, *Nuclear Engineering and Design*, vol. 352, p. 110190, 2019.

[41] M. Y. Young, S. M. Bajorek, M. E. Nissley, and L. E. Hochreiter, Application of code scaling applicability and uncertainty methodology to the large break loss of coolant, *Nuclear Engineering and Design*, vol. 186, no. 1–2, pp. 39–52, 1998.

[42] L. Uusitalo, A. Lehikoinen, I. Helle, and K. Myrberg, An overview of methods to evaluate uncertainty of deterministic models in decision support, *Environmental Modelling & Software*, vol. 63, pp. 24–31, 2015.

[43] A. E. R. Board, Probabilistic safety assessment for nuclear power plants and research reactors, *AERB, Mumbai, IN*, 2008.
[44] F. S. D'Auria, H. Glaeser, S. Lee, J. Miák, M. Modro, and R. R. Schultz, *Best Estimate Safety Analysis for Nuclear Power Plants: Uncertainty Evaluation. IAEA Safety Report Series*, vol. 52. IAEA, 2008.
[45] B. E. Boyack *et al.*, Quantifying reactor safety margins part 1: an overview of the code scaling, applicability, and uncertainty evaluation methodology, *Nuclear Engineering and Design*, vol. 119, no. 1, pp. 1–15, 1990.
[46] A. Peregudov, O. Andrianova, K. Raskach, and A. Tsibulya, GRS Method for Uncertainties Evaluation of Parameters in a Prospective Fast Reactor, *Nuclear Data Sheets*, vol. 118, pp. 548–550, 2014.
[47] H. Glaeser, GRS method for uncertainty and sensitivity evaluation of code results and applications, *Science and Technology of Nuclear Installations*, vol. 2008, no. 1, p. 798901, 2008.
[48] A. Peregudov, O. Andrianova, K. Raskach, and A. Tsibulya, Application of GRS method to evaluation of uncertainties of calculation parameters of perspective sodium-cooled fast reactor, in *EPJ Web of Conferences*, EDP Sciences, 2013, p. 07002.
[49] Q. Xiong, J. Gou, J. Shan, and Y. Hui, Improvement of the uncertainty method with model treatment and optimized global sensitivity analysis and its application to pressurized water reactor, *Ann Nucl Energy*, vol. 149, p. 107794, 2020.
[50] K.-I. Ahn and S.-Y. Park, Best-practice severe accident uncertainty and sensitivity analysis for a short-term SBO sequence of a reference PWR using MAAP5, *Ann Nucl Energy*, vol. 170, p. 108981, 2022.
[51] M. Kloos and N. Berner, SUSA. Software for uncertainty and sensitivity analyses. Classical methods, Gesellschaft fuer Anlagen-und Reaktorsicherheit (GRS) gGmbH, Köln (Germany), 2021.
[52] M. Kloos, The tool SUSA 4 for probabilistic uncertainty and sensitivity analyses, *Proceedings of the Uncecomp*, 2015.
[53] M. Kloos, Main features of the tool SUSA 4.0 for uncertainty and sensitivity analyses, *Safety and Reliability of Complex Engineered Systems, edited by L. Podofillini, B. Sudret, B. Stojadinovic, E. Zio, W. Kröger (CRC Press, London, UK, 2015)*, pp. 107–132, 2015.
[54] M. D'Onorio *et al.*, Nuclear safety Enhanced: A Deep dive into current and future RAVEN applications, *Nuclear Engineering and Design*, vol. 427, p. 113422, 2024.
[55] M. D'Onorio, F. Giannetti, F. Mascari, and G. Caruso, Uncertainty analyses using the RAVEN software tool coupled with MELCOR severe accident code, in *Proceedings of the ANS Best Estimate Plus Uncertainty International Conference (BEPU 2018)*, 2018.
[56] K. Chevalier-Jabet, F. Cousin, L. Cantrel, and C. Séropian, Source term assessment with ASTEC and associated uncertainty analysis using SUNSET tool, *Nuclear Engineering and Design*, vol. 272, pp. 207–218, 2014.

[57] R. Gencheva, A. Stefanova, and P. Groudev, ASTECV2. 2b and SUNSET uncertainty and sensitivity analyses on IVMR WWER1000 Test Case, 2022.

[58] B. M. Adams, P. D. Hough, and J. A. Stephens, Dakota Software Training: Uncertainty Quantification., Sandia National Lab.(SNL-NM), Albuquerque, NM (United States); Sandia …, 2016.

[59] A. Stephens and L. Swiler, Dakota sensitivity analysis and uncertainty quantification, with examples, *SAND2014-5015*, 2014.

[60] R. Schow, D. Kim, and T. Jevremovic, DACOS: DAKOTA-AGENT neutronics computational optimization system, *Ann Nucl Energy*, vol. 112, pp. 245–256, 2018.

[61] V. Vileiniskis and A. Kaliatka, Best estimate analysis of PHEBUS FPT1 experiment bundle phase using ASTEC code ICARE module, *Kerntechnik*, vol. 76, no. 4, pp. 254–260, 2011.

[62] J. Wang *et al.*, Simulation of the PHEBUS FPT-1 experiment using MELCOR and exploration of the primary core degradation mechanism, *Ann Nucl Energy*, vol. 85, pp. 193–204, 2015.

[63] S. Šadek, Analysis of Phebus FPT1 Experiment with RELAP5/SCDAPSIM Computer Code, 2004.

[64] T. Kaliatka, E. Ušpuras, and V. Vileiniškis, Best Estimate Analysis of PHEBUS FPT1 Test Using RELAP/SCDAPSIM Code, in *International Conference on Nuclear Engineering*, American Society of Mechanical Engineers, 2012, pp. 411–418.

[65] L. Sepold *et al.*, *Experimental and computational results of the QUENCH-06 test (OECD ISP-45)*. Forschungszentrum Karlsruhe in der Helmholtz-Gemeinschaft, 2004.

[66] T. Kaliatka, A. Kaliatka, and V. Vileiniskis, Application of best estimate approach for modelling of QUENCH-03 and QUENCH-06 experiments, *Nuclear Engineering and Technology*, vol. 48, no. 2, pp. 419–433, 2016.

[67] M. Garbarini, G. Agnello, A. Bersano, F. Gabrielli, L. Luzzi, and F. Mascari, Simulation of QUENCH-06 experiment by MELCOR v2. 2 with Uncertainty Analysis, *Nucl Technol*, pp. 1–20, 2025.

[68] H. Madokoro, K. Okamoto, C. Allison, L. Siefken, J. Hohorst, and S. Hagen, Assessment of RELAP/SCDAPSIM/MOD3. 5 against the BWR core degradation experiment CORA-17, in *10th International Topical Meeting on Nuclear Thermal-Hydraulics, Operation and Safety (NUTHOS-10), Japan*, 2014.

[69] G. Gerova, I. Spasov, C. Allison, and M. Steinbrück, Modeling and simulation of the QUENCH 12 experiment with the RELAP/SCDAPSIM/MOD3. 5 code, in *AIP Conference Proceedings*, AIP Publishing LLC, 2018, p. 020019.

[70] O. Dutkiewicz, K. M. Marcinkiewicz, H. Madokoro, S. Shumski, C. M. Allison, and J. K. Hohorst, RELAP/SCDAPSIM/MOD3. 5 analysis of KIT's QUENCH-14 experiment, *EPJ Nuclear Sciences & Technologies*, vol. 3, p. 25, 2017.

[71] T. Kaliatka, Implementation of QUENCH-10 experiment modelling experience for the modelling of severe accidents in spent fuel pools, in *Proceedings 23rd International QUENCH Workshop Karlsruhe Institute of Technology, Germany (doi: 10.5445/IR/1000076201) October*, 2017, pp. 17–19.
[72] T. Kaliatka, E. Uspuras, and C. M. Allison, Modeling of QUENCH 10 experiment on air ingress using RELAP/SCDAPSIM MOD 3.5, in *International Conference on Nuclear Engineering*, American Society of Mechanical Engineers, 2017, p. V004T06A007.
[73] T. Hollands *et al.*, Pre-and Post-Test Simulations of the QUENCH-18 Bundle Experiment in the frame of the NUGENIA QUESA Project, in *The 9TH European Review Meeting on Severe Accident Research (ERMSAR2019), Czech Republic, March 18-20, 2019*, 2019, p. 76.
[74] J. Stuckert, S. Bechta, T. Hollands, P. Isaksson, and M. Steinbrueck, Experimental and modelling results of the QUENCH-20 experiment with BWR test bundle, *Nuclear Engineering and Design*, vol. 410, p. 112391, 2023.
[75] O. Murat, V. Sanchez-Espinoza, S. Wang, and J. Stuckert, Preliminary validation of ASTEC V2. 2. b with the QUENCH-20 BWR bundle experiment, *Nuclear Engineering and Design*, vol. 370, p. 110931, 2020.
[76] A. Vasiliev and J. Stuckert, Application of thermal hydraulic and severe accident code SOCRAT/V3 to bottom water reflood experiment QUENCH-LOCA-1, *Journal of Nuclear Engineering and Radiation Science*, vol. 2, no. 2, p. 021024, 2016.
[77] B. Clément and T. Haste, Comparison Report on International Standard Problem ISP-46 (PHEBUS FPT1), *Note Technique Semar*, vol. 3, p. 021, 2003.
[78] M. R. Kuhlman, D. J. Lehmicke, and R. O. Meyer, CORSOR user's manual, Battelle Columbus Labs., OH (United States), 1985.
[79] T. Kaliatka, A. Kaliatka, V. Vileiniškis, and E. Ušpuras, Modelling of QUENCH-03 and QUENCH-06 Experiments Using RELAP/SCDAPSIM and ASTEC Codes, *Science and Technology of Nuclear Installations*, vol. 2014, no. 1, p. 849480, 2014.
[80] N. W. Porter, Wilks' formula applied to computational tools: A practical discussion and verification, *Ann Nucl Energy*, vol. 133, pp. 129–137, 2019.
[81] M.-T. Puth, M. Neuhäuser, and G. D. Ruxton, Effective use of Spearman's and Kendall's correlation coefficients for association between two measured traits, *Anim Behav*, vol. 102, pp. 77–84, 2015.
[82] E. Szmidt and J. Kacprzyk, The Spearman and Kendall rank correlation coefficients between intuitionistic fuzzy sets, in *Proceedings of the 7th Conference of the European Society for Fuzzy Logic and Technology*, Atlantis Press, 2011, pp. 521–528.
[83] C. Spearman, Demonstration of formulae for true measurement of correlation, *Am J Psychol*, pp. 161–169, 1907.

[84] M. G. Kendall, A new measure of rank correlation, *Biometrika*, vol. 30, no. 1–2, pp. 81–93, 1938.
[85] K. M. Ramachandran and C. P. Tsokos, *Mathematical statistics with applications in R*. Academic Press, 2020.
[86] S. M. Ross, *Introductory statistics*. Academic Press, 2017.
[87] G. Glen and K. Isaacs, Estimating Sobol sensitivity indices using correlations, *Environmental Modelling & Software*, vol. 37, pp. 157–166, 2012.
[88] B.-S. Ju, H.-Y. Son, and J. Lee, Advanced Sobol sensitivity analysis of a 1: 4-scale prestressed concrete containment vessel using an ANN-based surrogate model, *Nuclear Engineering and Technology*, vol. 57, no. 3, p. 103259, 2025.
[89] K. P. Singh, N. Basant, and S. Gupta, Support vector machines in water quality management, *Anal Chim Acta*, vol. 703, no. 2, pp. 152–162, 2011.
[90] D. G. Rossiter, Co-kriging with the gstat package of the R environment for statistical computing, *Web: http://www. itc. nl/rossiter/teach/R/R ck. pdf*, 2007.
[91] T. Hollands, Experimental investigation of QUENCH-20 and simulation with AC2/ATHLET-CD, in *ERMSAR Conf. Proceed.*, 2022.
[92] F. P. Griffin, BWR control blade/channel box interaction models for SCDAP/RELAP5, Oak Ridge National Lab., TN (United States), 1993.
[93] A. I. Oludare, M. N. Agu, A. M. Umar, S. O. Adedayo, O. E. Omolara, and L. N. Okafor, Control rods drop failure on reactors stability and safety, *Advances in Physics Theories and Applications*, vol. 27, pp. 58–73, 2014.
[94] F. Mascari *et al.*, Main outcomes of the Phebus FPT1 uncertainty and sensitivity analysis in the EU-MUSA project, *Ann Nucl Energy*, vol. 196, p. 110205, 2024.
[95] S. Brumm *et al.*, Uncertainty quantification for severe-accident reactor modelling: Results and conclusions of the MUSA reactor applications work package, *Ann Nucl Energy*, vol. 211, p. 110962, 2025.
[96] O. Coindreau *et al.*, Uncertainty quantification for a severe accident sequence in a SFP in the frame of the H-2020 project MUSA: First outcomes, *Ann Nucl Energy*, vol. 188, p. 109796, 2023.

CURRICULUM VITAE

Name: Noura

Last Name: Elsalamouny

Place of birth: Cairo, Egypt

Email: nourarelsalamouny@gmail.com

Education:

- 2015: Alexandria University, Bachelor of Nuclear Engineering
- 2019: National Institute for Nuclear Research, Master of Nuclear Engineering and Thermal Physics
- 2020–2024: Lithuanian Energy Institute, Doctoral Studies in Technological Sciences (Energy and Thermal Engineering, T 006)

PUBLICATIONS RELATED TO THE DISSERTATION

List of scientific articles on the dissertation topic Clarivate Analytics Web of Science databases

1- Elsalamouny N. [LEI] , Kaliatka T. [LEI] . Uncertainty Quantification of the PHEBUS FPT-1 Test Modelling Results In: *Energies.* Basel: MDPI, 2021, Vol. 14, 7320, p. 1-17. ISSN 1996-1073.

2- Elsalamouny N. [LEI] , Kaliatka T. [LEI] , Kaliatka A. [LEI] . QUENCH-20 test analysis using RELAP/SCDAPSIM severe accident code In: *Nuclear Engineering and Design.* Lausanne: Elsevier, 2024, Vol. 419, 112995, p. 1-12. ISSN 0029-5493.

List of scientific conferences

1- Elsalamouny N. [LEI] , Kaliatka T. [LEI] . Uncertainty and sensitivity analysis of the phebus fpt1 test simulation results In: *The 17th International Conference of Young Scientists on Energy and Natural Sciences Issues (CYSENI 2021) Kaunas, Lithuania, May 24-28, 2021.* Kaunas: Lithuanian Energy Institute, 2021, p. 448-449. ISSN 1822-7554.

2- Elsalamouny N. [LEI] , Kaliatka T. [LEI] . Development of a numerical model of quench-20 test based on lei experience on modeling of quench tests In: *CYSENI 2022: 18th international conference of young scientists on energy and natural sciences issues, 24-27 May 2022, Kaunas, Lithuania.* Kaunas: Lithuanian Energy Institute, 2022, p. 257-260. ISSN 2783-6339.

3- Elsalamouny N. [LEI] , Kaliatka T. [LEI] , Kaliatka A. [LEI] . Lei quench tests modeling experience and the preliminary modeling results of quench-20 test using relap/scdapsim In: *Proceedings 16th International conference on heat transfer, fluid mechanics and thermodynamics.* Stellenbosch: Stellenbosch University, 2022, p. 606-611. ISBN 978-0-7972-1886-4.

4- Elsalamouny N. [LEI] , Kaliatka T. [LEI] , Allison CM. Different numerical modeling approaches applied to relap/scdapsim code for the simulation of quench-20 test In: *Proceedings of the 2023 30th International Conference on Nuclear Engineering ICONE30.* Kyoto: The Japan Society of Mechanical Engineers, 2023, p. 1-9.

5- Elsalamouny N. [LEI] , Kaliatka T. [LEI] . Parametric sensitivity studies for RELAP/SCDAPSIM model of QUECH-20 test In: *Proceedings of the 11th European Review Meeting on Severe Accidents Research (ERMSAR2024).* Stockholm: Publisher Royal Institute of Technology Stockholm (KTH), 2024, Log Number 095, p. 1-1.

Other publications

1- IAEA, Advancing the State of the Practice in Uncertainty and Sensitivity Methodologies for Severe Accident Analysis in Water Cooled Reactors in the QUENCH-06 Experiment. *IAEA-TECDOC-2045*, 2024.

UDK 621.039+621.039.588+519.242] (043.3) SL344.

2021-*-*, * leidyb. apsk. l. Tiražas 14 egz. Užsakymas *.

Išleido Kauno technologijos universitetas, K. Donelaičio g. 73, 44249 Kaunas

Spausdino leidyklos „Technologija spaustuvė, Studentų g. 54, 51424 Kaunas